Physics of laser-driven plasma-based electron accelerators

E. Esarey, C. B. Schroeder, and W. P. Leemans

Lawrence Berkeley National Laboratory, Berkeley, California 94720, USA

(Published 27 August 2009)

Laser-driven plasma-based accelerators, which are capable of supporting fields in excess of 100 GV/m, are reviewed. This includes the laser wakefield accelerator, the plasma beat wave accelerator, the self-modulated laser wakefield accelerator, plasma waves driven by multiple laser pulses, and highly nonlinear regimes. The properties of linear and nonlinear plasma waves are discussed, as well as electron acceleration in plasma waves. Methods for injecting and trapping plasma electrons in plasma waves are also discussed. Limits to the electron energy gain are summarized, including laser pulse diffraction, electron dephasing, laser pulse energy depletion, and beam loading limitations. The basic physics of laser pulse evolution in underdense plasmas is also reviewed. This includes the propagation, self-focusing, and guiding of laser pulses in uniform plasmas and with preformed density channels. Instabilities relevant to intense short-pulse laser-plasma interactions, such as Raman, self-modulation, and hose instabilities, are discussed. Experiments demonstrating key physics, such as the production of high-quality electron bunches at energies of 0.1–1 GeV, are summarized.

DOI: 10.1103/RevModPhys.81.1229 PACS number(s): 52.38.Kd, 41.75.Lx, 52.40.Mj

CONTENTS

I. INTRODUCTION

Laser-driven plasma-based accelerators were originally proposed three decades ago by Tajima and Dawson (1979). Dawson, who passed away in 2001, was responsible for many of the early developments in this field, including the plasma beat wave accelerator, the laser wakefield accelerator, and the photon accelerator (Tajima and Dawson, 1979; Joshi *et al.*, 1984; Wilks *et al.*, 1989). In addition, he was one of the early pioneers of particle-in-cell (PIC) simulation of plasmas (Dawson, 1983; Mori *et al.*, 1988; Birdsall *et al.*, 1991), which is now a widely used tool in the study of plasma-based accelerators. During his lifetime, the field of plasma-based accelerators has grown into a world-wide research effort with ongoing experimental programs in France, Germany, Korea, Japan, Taiwan, the UK, and the United States, to name a few (see, e.g., Schroeder *et al.*, 2009). Much of this growth is due to the rapid development of chirped-pulse amplification (CPA) laser technology, pioneered by Mourou and colleagues (Strickland and Mourou, 1985; Maine *et al.*, 1988; Mourou and Umstadter, 1992; Perry and Mourou, 1994), making readily available compact sources of intense, high-power, ultrashort laser pulses.

Laser-plasma accelerator (LPA) experiments prior to 2004 have demonstrated acceleration gradients >100 GV/m, accelerated electron energies >100 MeV, and accelerated charge >1 nC (Modena *et al.*, 1995; Nakajima *et al.*, 1995; Umstadter, Chen, *et al.*, 1996; Ting *et al.*, 1997; Gahn *et al.*, 1999; Leemans *et al.*, 2002; Malka *et al.*, 2002). However, the quality of the accelerated electron bunch was less than desired. Typically, the accelerated bunch was characterized by an exponential energy distribution, with most of the electrons at low energy (<10 MeV) and a long exponentially small tail extending out to high energy (>100 MeV). This dramatically changed in 2004 when three groups (Faure *et al.*, 2004; Geddes *et al.*, 2004; Mangles *et al.*, 2004) reported the production of high-quality electron bunches characterized by significant charge ($\gtrsim$100 pC) at high mean energy ($\sim$100 MeV) with small energy spread (approximately few percent) and low divergence (approximately a few milliradians). These high-quality electron bunches were a result of a higher degree of control of the laser and plasma parameters, an improvement of diagnostic techniques, an extension of the laser propagation distance through the plasma, and a greater understanding of the underlying physics, in particular, the importance of matching the acceleration length to the dephasing length. Using a plasma-channel-guided laser, high-quality electron bunches up to 1 GeV have been experimentally demonstrated (Leemans, Nagler, *et al.*, 2006). Methods for controlled injection of electrons into plasma wakefields using colliding laser pulses have also been demonstrated (Faure, Rechatin, *et al.*, 2006), as well as production of stable bunches using negative plasma density gradients (Geddes *et al.*, 2008). High-quality GeV-class electron bunches will enable a variety of applications of LPAs, such as front-end injectors for conventional accelerators and drivers for compact, short-pulse radiation sources.

This review provides an overview of the physics and issues relevant to LPAs, in which charged particles are accelerated by plasma waves excited by short-pulse, high-intensity lasers. The remainder of the Introduction discusses a few of the basic features of plasma accelerators and the basic principles and limitations of laser-driven acceleration in vacuum and gases. Section II discusses the basic models used to describe plasma wave generation. Included is a discussion of nonlinear plasma waves, wave breaking, plasma wave phase velocity, and the acceleration of electrons by the plasma wave. Section III describes the various LPA configurations, specifically the laser wakefield accelerator (LWFA), the plasma beat wave accelerator (PBWA), the self-modulated LWFA, wakefields driven by multiple pulses, and the highly nonlinear regime of electron cavitation. Some of these configurations are shown schematically in Fig. 1. Included is a discussion of diffraction, dephasing, pump depletion, and beam loading, which can limit the single-stage energy gain. Self-trapping and the injection of ultrashort electron bunches into plasma waves using laser triggered injection or density gradients are discussed in Sec. IV. Methods for optically guiding laser pulses in plasmas are discussed in Sec. V, including relativistic self-focusing, preformed density channels, ponderomotive self-channel, and plasma wave effects. Section VI describes a few of the more relevant laser-plasma instabilities, including backward and forward Raman scattering, self-modulation, and laser hosing. Section VII discusses several methods for producing high-quality electron bunches. Throughout this review experimental results are mentioned. A summary is presented in Sec. VIII, as well as a discussion of future prospects for LPAs.

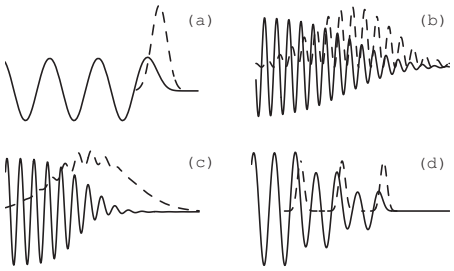

FIG. 1. Schematic of LPAs: (a) LWFA, (b) PBWA, (c) self-modulated (SM) LWFA, and (d) resonant laser pulse train. Shown are the excited plasma wave potentials (solid lines) and right-moving laser intensity envelopes (dashed lines).

A. Acceleration in plasma

Plasma-based accelerators are of great interest because of their ability to sustain extremely large acceleration gradients. The accelerating gradients in conventional radio-frequency (rf) linear accelerators (linacs) are currently limited to $\sim$100 MV/m, partly due to breakdown that occurs on the walls of the structure. Ionized plasmas, however, can sustain electron plasma waves with electric fields in excess of $E_0 = cm_e\omega_p/e$ or

$$E_0(\mathrm{V/m}) \simeq 96\sqrt{n_0(\mathrm{cm}^{-3})}, \tag{1}$$

where $\omega_p = (4\pi n_0 e^2/m_e)^{1/2}$ is the electron plasma frequency, n_0 is the ambient electron number density, m_e and e are the electron rest mass and charge, respectively, and c is the speed of light in vacuum. Equation (1) is referred to as the cold nonrelativistic wave breaking field (Dawson, 1959). For example, a plasma density of $n_0 = 10^{18}$ cm^{-3} yields $E_0 \simeq 96$ GV/m, which is approximately three orders of magnitude greater than that obtained in conventional linacs. Accelerating gradients on the order of 100 GV/m have been inferred in plasma-based accelerator experiments (Gordon *et al.*, 1998; Malka *et al.*, 2002).

In addition to extremely large accelerating gradients, plasma-based accelerators have the potential to produce extremely short electron bunches. The length of the accelerating wave in a plasma-based accelerator is approximately the plasma wavelength $\lambda_p = 2\pi c/\omega_p = 2\pi/k_p$ or

$$\lambda_p(\mu\mathrm{m}) \simeq 3.3 \times 10^{10}/\sqrt{n_0(\mathrm{cm}^{-3})}, \quad (2)$$

e.g., $\lambda_p \simeq 33$ μm for $n_0 = 10^{18}$ cm^{-3}. A high-quality electron bunch produced by a plasma-based accelerator would have a bunch duration $\tau_b < \lambda_p/c$, i.e., a duration $\tau_b < 100$ fs for $n_0 = 10^{18}$ cm^{-3}. Measurements of coherent transition radiation produced by electron bunches generated in LPAs indicated <50 fs bunch durations (Leemans *et al.*, 2004; van Tilborg *et al.*, 2006, 2007). LPAs, which are typically driven by femtosecond laser pulses, are intrinsically sources of femtosecond electron bunches. Furthermore, the electron bunches are intrinsically synchronized to the laser pulses, enabling a wide variation of pump-probe applications.

An important parameter in the discussion of intense laser-plasma interactions is the laser strength parameter a_0, defined as the peak amplitude of the normalized vector potential of the laser field $\boldsymbol{a} = e\boldsymbol{A}/m_e c^2$. The laser strength parameter is related to the peak laser intensity I_0 and power $P = \pi r_0^2 I_0/2$ by $I_0 = (\pi c/2)(m_e c^2 a_0/e\lambda)^2$, which yields

$$a_0^2 \simeq 7.3 \times 10^{-19}[\lambda(\mu\mathrm{m})]^2 I_0(\mathrm{W/cm}^2) \quad (3)$$

and $P(\mathrm{GW}) \simeq 21.5(a_0 r_0/\lambda)^2$, where a linearly polarized laser field with a Gaussian radial profile is assumed, e.g., $\boldsymbol{a} = a_0 \exp(-r^2/r_0^2)\cos(kz - \omega t)\boldsymbol{e}_x$ with r_0 the laser spot size at focus, $\lambda = 2\pi/k$ the laser wavelength, and $\omega = ck$ the laser frequency in vacuum. Furthermore, the peak laser electric field amplitude is $E_L = m_e c\omega a_0/e$, i.e., $E_L(\mathrm{TV/m}) \simeq 3.21 a_0/\lambda(\mu\mathrm{m})$. Physically, $\boldsymbol{a} = \boldsymbol{p}_\perp/m_e c$ is the normalized transverse "quiver" momentum of a plasma electron in the laser field, as indicated by conservation of transverse canonical momentum in the broad laser pulse [or one-dimensional (1D)] limit ($r_0 \gg \lambda$). When $a_0 \gtrsim 1$, the electron quiver motion is relativistic and the laser-plasma interaction is nonlinear. Relativistic electron motion ($a_0 \gtrsim 1$) requires laser intensities $I \gtrsim 10^{18}$ W/cm^2 for wavelengths of $\lambda \simeq 1$ μm. Such intensities are routinely produced by compact, solid-state laser systems based on the CPA technique.

B. Acceleration in vacuum and gases

The laser acceleration of electrons in vacuum and gases is intrinsically limited by diffraction, electron slippage, ionization, and the smallness of the laser wavelength (Esarey *et al.*, 1995; Sprangle *et al.*, 1996a). In vacuum, the motion of an electron in a laser field is determined by the Lorentz force equation

$$d\tilde{\boldsymbol{p}}/dct = \partial \boldsymbol{a}/\partial ct - (\tilde{\boldsymbol{p}}/\tilde{\gamma}) \times (\nabla \times \boldsymbol{a}), \quad (4)$$

where $\tilde{\boldsymbol{p}}$ is the electron momentum normalized to $m_e c$ and $\tilde{\gamma} = (1 + \tilde{p}^2)^{1/2}$ is the relativistic Lorentz factor. Roughly speaking, the first term on the right-hand side of Eq. (4) describes the linear response of the electron to the electric field $\boldsymbol{E}$ of the laser and is responsible for "direct" laser acceleration, whereas the second term describes the nonlinear response to the $\boldsymbol{v} \times \boldsymbol{B}$ force and is responsible for "ponderomotive" laser acceleration. The axial (in the z direction of laser propagation) ponderomotive force is $F_{pz} \simeq -(m_e c^2/\tilde{\gamma})(\partial/\partial z)a^2/2$, assuming $\tilde{\boldsymbol{p}}_\perp = \boldsymbol{a}_\perp$, which is exact in one dimension (i.e., valid for $r_0 \gg \lambda$).

When a laser field propagating along the z axis is focused in vacuum, the laser spot size and intensity evolve via $r_s = r_0(1 + z^2/Z_R^2)^{1/2}$ and $I = I_0(r_0^2/r_s^2)\exp(-2r^2/r_s^2)$, respectively, where $Z_R = kr_0^2/2$ is the Rayleigh length, and a fundamental Gaussian mode is assumed. The finite laser spot size implies the existence of an axial component of the electric field of the laser via $\nabla \cdot \boldsymbol{E} = 0$, i.e., $E_z \sim (1/kr_0)E_\perp$. The amplitude of this axial field can be very large, which suggests using the axial field directly for laser acceleration, with an energy gain for a relativistic ($\tilde{\gamma} \gg 1$) electron propagating along the axis scaling as $\int dz(v_z E_z)$. The phase velocity, however, of the optical field along the axis is greater than c and is $v_{\mathrm{ph}}/c \simeq 1 + 1/kZ_R$ near the focus. Since $v_{\mathrm{ph}} > c$, electrons with $v_z \lesssim c$ will phase slip with respect to the accelerating field and decelerate. This will occur over a dephasing length, which for highly relativistic electrons is $\sim Z_R$, i.e., the dephasing length is on order of the diffraction length. Higher-order laser modes have also been considered for vacuum laser acceleration (Hafizi *et al.*, 1997; Varin and Piché, 2002; Karmakar and Pukhov, 2007), as well as exploiting subluminal phase regions in the three-dimensional (3D) laser focal volume (Pang *et al.*, 2002; Popov *et al.*, 2008).

This phase slippage argument forms the basis for the so-called Lawson-Woodward theorem (Woodward 1947; Lawson, 1979; Palmer, 1980), which states that under certain restrictive conditions no net electron energy gain is possible using laser fields. The Lawson-Woodward theorem assumes (i) the region of interaction is infinite, (ii) the laser fields are in vacuum with no walls or boundaries present, (iii) the electron is highly relativistic ($v_z \simeq c$) along the acceleration path, (iv) no static electric or magnetic fields are present, and (v) nonlinear effects (e.g., ponderomotive and radiation reaction forces) are neglected.

One or more of the assumptions of Lawson-Woodward theorem must be violated in order to achieve a nonzero net energy gain. For example, one can introduce optics to limit the laser-electron interaction to approximately a region of length $2Z_R$ about the focus, such that minimal phase slippage occurs (Esarey *et al.*, 1995; Huang and Byer, 1996; Plettner *et al.*, 2005). The maximum energy gain due to laser acceleration by the E_z field is then $\Delta W(\mathrm{MeV}) \simeq 31\sqrt{P(\mathrm{TW})}$, where a first-order Laguerre-Gaussian mode has been assumed (Esarey *et al.*, 1995). Although substantial energy gains are possible with high laser power, this is problematic in practice since this method requires that optics be placed near the focus and are susceptible to laser damage at high intensity. Furthermore, the electron bunch must pass through a small aperture in the optics, which can limit the amount of charge that can be accelerated (Sprangle *et al.*, 1996a). Experiments demonstrated a 30 keV energy modulation on a 30 MeV electron beam from the inter-

action with a 0.5 mJ, 4 ps laser pulse in a semi-infinite vacuum region, i.e., the interaction was terminated by an 8 μm thick gold-coated Kapton tape near focus (Plettner *et al.*, 2005).

Alternatively, finite energy gains can be achieved by introducing a background of gas into the interaction region, as in the inverse Cherenkov accelerator (Kimura *et al.*, 1995). The gas can reduce the phase velocity of the laser field to less than c, reducing the slippage. Furthermore, in principle, diffraction can be overcome by relying on optical guiding (self-focusing) in the gas (Sprangle *et al.*, 1996b). Nevertheless, ionization of the gas, which occurs at a relatively low laser intensity $\sim 10^{14}$ W/cm^2 (for $\lambda \approx 1$ μm) and increases the phase velocity, remains a fundamental limitation to the accelerating field in gas-filled devices. Experiments demonstrated a 3.7 MeV modulation on a 40 MeV electron beam using a 580 MW CO_2 laser pulse interacting with a 12 cm gas-filled cell (Kimura *et al.*, 1995). Another method to reduce the phase velocity is to propagate the laser in a plasma channel with an axially modulated density, which supports laser modes with subluminal spatial harmonics (York *et al.*, 2008).

In addition to direct laser acceleration, finite energy gains can also result from the nonlinear or ponderomotive force. Since the ponderomotive force scales inversely with electron energy and proportional to the laser intensity, $F_p \sim (1/\tilde{\gamma})\nabla a^2$, this mechanism is most efficient at low electron energies and high laser intensities. Simulations (Quesnel and Mora, 1998) and experiments (Malka *et al.*, 1997) have shown that by focusing a high-intensity laser pulse onto a source of electrons (experimentally created by a preexploded thin foil), ponderomotive acceleration can result in the production of electrons with energies in the range of a few MeV with a large energy spread and a high degree of scattering. In principle the scattering can be reduced using high-order laser modes (Stupakov and Zolotorev, 2001). Simulations (Pang *et al.*, 2002; Popov *et al.*, 2008) indicated that when a moderate energy electron bunch intersects with a very intense laser pulse at a small angle, a signification fraction of the electrons can be accelerated to energies in excess of 100 MeV (for $a \sim 10$) through a combination of direct and ponderomotive acceleration. Other ponderomotive acceleration schemes include the vacuum beat wave accelerator (Esarey *et al.*, 1995), which relies on the ponderomotive force of the beat wave produced by two copropagating laser pulses, and the inverse free-electron laser (Liu *et al.*, 1998; Kimura *et al.*, 2001; Musumeci *et al.*, 2005), which relies on the beat wave produced by a laser pulse propagating through a magnetic wiggler field. Again, a major limitation to these schemes is the $1/\tilde{\gamma}$ scaling of the ponderomotive force.

A fundamental limitation to all concepts that rely on electron acceleration through the direct interaction (linear or nonlinear) with the laser field is the smallness of the laser wavelength, typically on the order of a micron. For example, a first-order Laguerre-Gaussian mode has a quarter wavelength phase region for which the laser field is both accelerating and focusing. To accelerate an electron bunch while maintaining a small energy spread and emittance, it is desirable that a high-quality bunch be injected into the proper phase region of the laser field with a bunch length small compared to a $\lambda/4$ (corresponding to 0.8 fs for $\lambda = 1$ μm). Conventional accelerators typically produce electron bunches with durations $\gtrsim 1$ ps. One possibility may be to prebunch a conventional electron bunch at the laser wavelength using an inverse free-electron laser, as has been experimentally demonstrated (Liu *et al.*, 1998), and use this as an injector into a second stage of a laser accelerator (Kimura *et al.*, 2001, 2004).

Plasma-based accelerators can overcome many of the fundamental limitations that restrict laser acceleration in vacuum and gases. For example, ionization and breakdown are not limitations since the plasma can be fully preionized. Diffraction can be overcome through self-focusing and with preformed plasma channels. In plasma-based accelerators, acceleration is the result of the axial field of the plasma wave and not the laser field directly. The phase velocity of the plasma wave is typically equal to the group velocity of the laser pulse and is less than c. Although the plasma wave is excited by the ponderomotive force of the laser field, the $1/\tilde{\gamma}$ scaling of the ponderomotive force is not a limitation since $\tilde{\gamma} \sim 1$ for the plasma electrons. In effect, the plasma acts as a transformer, converting the transverse laser field into the axial electric field of the plasma wave. Furthermore, the accelerating wavelength is the plasma wavelength λ_p, which is typically 10–1000 times larger than the laser wavelength, and in many cases approximately equal to the laser pulse length. The injection of ultrashort electron bunches into a single period of a plasma wave is possible using self-injection or laser injection methods (see Sec. IV). Plasma-based acceleration methods are, however, subject to their own intrinsic limitations, such as restrictions arising from electron dephasing, pump depletion, and, in some cases, laser-plasma instabilities.

II. PLASMA WAVES AND ACCELERATION

Calculation of the plasma wakefields (driven electron plasma waves) generated by nonevolving drive laser pulses is straightforward. Analytical solutions exist in the 3D linear regime and in the 1D nonlinear regime. In the 3D nonlinear regime, the use of numerical codes is usually required. The full problem, which includes the self-consistent evolution of the drive laser pulses, is sufficiently complicated to require numerical calculation. Various aspects of the propagation and transport of the drive beams will be discussed in subsequent sections. Before discussing specific LPA configurations (e.g., PBWA, LWFA, self-modulated LWFA, etc.), the physical forces that drive wakefields (i.e., space charge and ponderomotive forces) and the mathematical models used to describe wakefield generation will be briefly discussed. In the following, it is convenient to use the

normalized electrostatic $\phi = e\Phi/m_e c^2$ and vector $\boldsymbol{a} = e\boldsymbol{A}/m_e c^2$ potentials.

A. Ponderomotive force

In LPAs, wakefields are driven via the ponderomotive force. The ponderomotive force (Kruer, 1988) can be derived by considering the electron fluid momentum equation in the cold fluid limit,

$$d\boldsymbol{p}/dt = -e[\boldsymbol{E} + (\boldsymbol{v}\times\boldsymbol{B})/c], \tag{5}$$

where $\boldsymbol{p}$ and $\boldsymbol{v}$ are the plasma fluid element momentum and velocity, respectively, and $d/dt = \partial/\partial t + (\boldsymbol{v}\cdot\nabla)$. The electric and magnetic fields of the laser can be written as $\boldsymbol{E} = -\partial\boldsymbol{A}/\partial ct$ and $\boldsymbol{B} = \nabla\times\boldsymbol{A}$, where the vector potential of the laser is polarized predominately in the transverse direction, e.g., $\boldsymbol{A} = A_0\cos(kz-\omega t)\mathbf{e}_\perp$. In the linear limit $|a| = e|A|/m_e c^2 \ll 1$, the leading-order electron fluid motion is the quiver momentum $\boldsymbol{p}_q = m_e c\boldsymbol{a}$, as indicated by $\partial\boldsymbol{p}_q/\partial t = -e\boldsymbol{E}$. Letting $\boldsymbol{p} = \boldsymbol{p}_q + \delta\boldsymbol{p}$, the second-order motion is

$$\begin{aligned} d\,\delta\boldsymbol{p}/dt &= -[(\boldsymbol{p}_q/m_e)\cdot\nabla]\boldsymbol{p}_q - \boldsymbol{p}_q\times(c\nabla\times\boldsymbol{a}) \\ &= -m_e c^2\nabla(a^2/2). \end{aligned} \tag{6}$$

Hence, $\boldsymbol{F}_p = -m_e c^2\nabla(a^2/2)$ is the 3D ponderomotive force in the linear limit ($a^2 \ll 1$). The ponderomotive force can also be viewed as the radiation pressure (i.e., the gradient of the electromagnetic energy density).

In the 1D nonlinear regime, conservation of canonical momentum implies $\boldsymbol{u}_\perp = \boldsymbol{p}_\perp/m_e c = \mathbf{a}_\perp$, i.e., $\boldsymbol{a}_\perp$ is the normalized quiver momentum. Hence, in one dimension, the nonlinear ponderomotive force is $F_{pz} = -(m_e c^2/2\gamma)\partial a_\perp^2/\partial z$. In the 3D nonlinear regime, the leading-order transverse motion of the electron fluid is still the quiver motion, $\boldsymbol{u}_\perp \simeq \boldsymbol{a}_\perp$, provided that the laser pulse is propagating in an underdense plasma and has a sufficiently broad spot size, $r_0 \gtrsim \lambda_p \gg \lambda$. Defining $\delta\boldsymbol{u} = \boldsymbol{u} - \boldsymbol{a}$, the fluid momentum equation can be written as (Sprangle *et al.*, 1992; Chen and Sudan, 1993; Esarey, Sprangle, *et al.*, 1993)

$$\partial\delta\boldsymbol{u}/\partial ct = \nabla(\phi - \gamma), \tag{7}$$

which is exact under the assumption that the vorticity $\nabla\times\delta\boldsymbol{u}$ is initially (prior to the passage of the laser pulse) zero. Here $\nabla\phi$ is the space-charge force and $\nabla\gamma$ represents the generalized nonlinear ponderomotive force $\boldsymbol{F}_{pN} = -m_e c^2\nabla\gamma$.

B. Linear plasma waves

In the linear ($a \ll 1$) 3D regime, wakefield generation can be examined using the cold fluid equations, i.e., the Poisson equation, the continuity equation, and the fluid momentum equation. For example, the plasma wave generated in an initially uniform plasma is described by (Gorbunov and Kirsanov, 1987; Sprangle *et al.*, 1988; Esarey *et al.*, 1989)

$$(\partial^2/\partial t^2 + \omega_p^2)\,\delta n/n_0 = c^2\nabla^2 a^2/2, \tag{8}$$

$$(\partial^2/\partial t^2 + \omega_p^2)\,\phi = \omega_p^2 a^2/2, \tag{9}$$

where $\delta n/n_0 = (n-n_0)/n_0$ is the normalized density perturbation associated with the electrostatic wake ϕ in the limit $a^2 \ll 1$. The solutions for the density perturbation ($|\delta n/n_0| \ll 1$) and electric field of the wake are

$$\delta n/n_0 = (c^2/\omega_p)\int_0^t dt'\sin[\omega_p(t-t')]\nabla^2 a^2(\boldsymbol{r},t')/2 \tag{10}$$

and

$$\boldsymbol{E}/E_0 = -c\int_0^t dt'\sin[\omega_p(t-t')]\,\nabla\, a^2(\boldsymbol{r},t')/2, \tag{11}$$

respectively. Equations (10) and (11) describe plasma waves generated at the frequency ω_p and are valid for $E \ll E_0$, where $E_0 = m_e c\omega_p/e$ is the cold nonrelativistic wave breaking field [Eq. (1)]. Solutions to Eqs. (10) and (11) indicate that wakefields will be generated most efficiently when the envelope scale length, which characterizes the axial gradient in the normalized laser intensity a^2, is on the order of the plasma wavelength $\lambda_p = 2\pi c/\omega_p$. The radial extent of the wake is on the order of the laser spot size r_s.

In addition to the axial wakefield E_z, transverse wakefields E_r and B_θ will be generated. For $a^2 \ll 1$, $E_z \sim E_r \sim a^2$ and $B_\theta \sim a^4$. The transverse wakefields are related to the axial wakefield by the Panofsky-Wenzel theorem (Panofsky and Wenzel, 1956; Keinigs and Jones, 1987), $\partial E_z/\partial r = \partial(E_r - B_\theta)/\partial(z-ct)$. A relativistic particle with axial velocity $v_z \simeq c$ that is being accelerated by a wakefield with phase velocity $v_p \simeq c$ will experience a radial force proportional to $E_r - B_\theta$. Notice that if the axial field is $E_z \sim \exp(-2r^2/r_s^2)\cos[k_p(z-ct)]$, then $E_r - B_\theta \sim (4r/k_p r_s^2)\exp(-2r^2/r_s^2)\sin[k_p(z-ct)]$ and the radial force is zero along the axis. For $a^2 \ll 1$, there is a phase region of the wake of width $k_p|\Delta(z-ct)| = \pi/4$ for which a relativistic electron will experience simultaneous axial accelerating and radial focusing forces.

Equations (8)–(11) are valid to $\sim O(a^2)$ assuming $a^2 \ll 1$. Applying a perturbation expansion of the fluid quantities in powers of a, higher-order corrections to the density and field may be computed (Gorbunov *et al.* 1997). In particular a quasistatic (varying on the time scale $\sim\omega_p^{-1}$) magnetic field that scales as $\sim O(a^4)$ is generated in an initially uniform plasma, given by (Gorbunov, *et al.*, 1996, 1997)

$$(\partial_{ct}^2 - \nabla^2 + k_p^2)\boldsymbol{B}/E_0 = -k_p^{-3}\nabla\times[(\nabla\partial_{ct}\phi)\nabla^2\phi]/4, \tag{12}$$

behind the drive laser, where ϕ is given by Eq. (9).

The linear response of plasma wave excitation in a plasma channel (transverse plasma inhomogeneity), $n = n(r)$, has been investigated by Andreev *et al.* (1997). The channel results in increasing curvature of the plasma wave fronts with increasing distance behind the drive laser. As a consequence, the plasma wave phase region where simultaneous acceleration and focusing oc-

cur increases. Wake excitation in a plasma channel also leads to damping of the plasma wave (Andreev *et al.*, 1997; Shvets and Li, 1999). For a wide ($k_p r_{ch} \gg 1$) parabolic, $n = n_0(1 + r^2/r_{ch}^2)$, plasma channel the amplitude of the plasma wave on axis decreases as $\delta n(\zeta)/\delta n(0) = 1 - 2\zeta^2/k_p^2 r_{ch}^4$, where $\zeta = z - ct$ is the distance behind the laser pulse (Andreev *et al.*, 1997).

C. Nonlinear plasma waves

In the linear regime, $E \ll E_0$, the plasma wave is a simple sinusoidal oscillation with frequency ω_p and a wave phase velocity v_p (the phase velocity is determined by the driver), e.g., $\phi = \phi_0 \cos[\omega_p(z/v_p - t)]$. When $E \gtrsim E_0$, the plasma wave becomes highly nonlinear. Wakefield generation in the nonlinear 1D regime can be examined by assuming that the drive beam is nonevolving, i.e., the drive beam is a function of only the coordinate $\xi = z - v_p t$, where $v_p \leqslant c$ is the phase velocity of the plasma wave. For laser drivers, $v_p \simeq v_g$, where v_g is the laser pulse group velocity. The quasistatic approximation (Sprangle *et al.*, 1990a, 1990b) can be applied such that the plasma fluid quantities are also assumed to be functions only of the comoving variable ξ. The 1D limit applies to broad drivers, $k_p r_\perp \gg 1$, where $r_\perp$ is the characteristic radial dimension of the drive beam. The 1D quasistatic fluid momentum and continuity equations give

$$\boldsymbol{u}_\perp - \boldsymbol{a}_\perp = 0, \tag{13}$$

$$\gamma - \beta_p u_z - \phi = 1, \tag{14}$$

$$n(\beta_p - \beta_z) = \beta_p n_0. \tag{15}$$

The Poisson equation $\partial^2\phi/\partial\xi^2 = k_p^2(n/n_0 - 1)$ can be written as (Berezhiani and Murusidze 1992; Esarey, Ting, *et al.*, 1993; Teychenné *et al.*, 1993)

$$k_p^{-2}\frac{\partial^2\phi}{\partial\xi^2} = \gamma_p^2\left\{\beta_p\left[1 - \frac{\gamma_\perp^2}{\gamma_p^2(1+\phi)^2}\right]^{-1/2} - 1\right\}, \tag{16}$$

where $\gamma_\perp^2 = 1 + u_\perp^2 = 1 + a^2$, $\gamma_p = (1 - \beta_p^2)^{-1/2}$, and $\beta_p = v_p/c$. The axial electric field of the wake is $E_z = -E_0\partial\phi/\partial\xi$ and the plasma fluid quantities are

$$n/n_0 = \gamma_p^2\beta_p\left[\left(1 - \frac{\gamma_\perp^2}{\gamma_p^2(1+\phi)^2}\right)^{-1/2} - \beta_p\right], \tag{17}$$

$$u_z = \gamma_p^2(1+\phi)\left[\beta_p - \left(1 - \frac{\gamma_\perp^2}{\gamma_p^2(1+\phi)^2}\right)^{1/2}\right], \tag{18}$$

$$\gamma = \gamma_p^2(1+\phi)\left[1 - \beta_p\left(1 - \frac{\gamma_\perp^2}{\gamma_p^2(1+\phi)^2}\right)^{1/2}\right]. \tag{19}$$

In the limit $\gamma_p^2 \gg 1$, Eq. (16) simplifies to (Bulanov *et al.*, 1989; Berezhiani and Murusidze, 1990; Sprangle *et al.*, 1990a, 1990b)

$$k_p^{-2}\frac{\partial^2\phi}{\partial\xi^2} = \frac{(1+a^2)}{2(1+\phi)^2} - \frac{1}{2}, \tag{20}$$

and the plasma fluid quantities are

$$n/n_0 = \frac{\gamma_\perp^2 + (1+\phi)^2}{2(1+\phi)^2}, \tag{21}$$

$$u_z = \frac{\gamma_\perp^2 - (1+\phi)^2}{2(1+\phi)}, \tag{22}$$

$$\gamma = \frac{\gamma_\perp^2 + (1+\phi)^2}{2(1+\phi)}. \tag{23}$$

The above expressions for the cold fluid motion $\boldsymbol{u}$ and γ also describe the single particle motion of an electron ($\tilde{\boldsymbol{p}}$ and $\tilde{\gamma}$, initially at rest) in the potentials $\boldsymbol{a}(\xi)$ and $\phi(\xi)$.

Analytical solutions to Eq. (20) in terms of elliptic integrals can be found for square laser pulse profiles (Bulanov *et al.*, 1989; Berezhiani and Murusidze 1990; Sprangle *et al.*, 1990a, 1990b). As the plasma wave amplitude becomes nonlinear, the plasma wave steepens and its period lengthens.

In the region behind the drive beam, $a^2 = 0$, an analysis of Eq. (16) indicates that the electrostatic potential oscillates in the range $\phi_{min} \leqslant \phi \leqslant \phi_{max}$ and the axial electric field oscillates in the range $-E_{max} \leqslant E \leqslant E_{max}$. The values ϕ_{min} and ϕ_{max}, denoted by ϕ_m, are (Esarey and Pilloff, 1995)

$$\phi_m = \hat{E}_{max}^2/2 \pm \beta_p[(1 + \hat{E}_{max}^2/2)^2 - 1]^{1/2}, \tag{24}$$

where $\hat{E}_{max} = E_{max}/E_0$ and the $\pm$ give ϕ_{max} and ϕ_{min}, respectively. For $E_{max}/E_0 \gtrsim 1$, Eq. (16) indicates that the electric field departs from a simple sinusoidal form (Akhiezer and Polovin, 1956; Bulanov *et al.*, 1989; Berezhiani and Murusidze, 1990; Sprangle *et al.*, 1990a, 1990b). In particular, the electric field exhibits the characteristic "sawtooth" profile associated with wave steepening and the density oscillations become highly peaked (as illustrated in Fig. 8 in Sec. III.A). Furthermore, the period of the nonlinear plasma wave increases as the amplitude increases. The nonlinear plasma wavelength in the limit $\gamma_p \gg 1$ is (Bulanov *et al.*, 1989; Berezhiani and Murusidze, 1990; Sprangle *et al.*, 1990a, 1990b) $\lambda_{Np} = (2/\pi)\lambda_p(1+\phi_{max})^{1/2}E_2(\varrho)$, where $E_2(\varrho) = \int_0^{\pi/2} d\theta(1 - \varrho^2\sin^2\theta)^{1/2}$ is the complete elliptic integral of the second kind with argument $\varrho^2 = 1 - (1+\phi_{max})^{-2}$ or

$$\lambda_{Np} = \lambda_p\begin{cases} 1 + 3(E_{max}/E_0)^2/16, & E_{max}/E_0 \ll 1 \\ (2/\pi)(E_{max}/E_0 + E_0/E_{max}), & E_{max}/E_0 \gg 1, \end{cases} \tag{25}$$

where E_{max} is the peak electric field of the plasma wave and $\lambda_p = 2\pi/k_p = 2\pi c/\omega_p$. For a square laser pulse profile, with optimal length for plasma wave excitation ($L \simeq \lambda_{Np}/2$), $E_{max}/E_0 = (a^2/2)(1 + a^2/2)^{-1/2}$ for a linearly polarized laser.

The lengthening of the plasma wave period can be important in plasma-based accelerators. For example, in

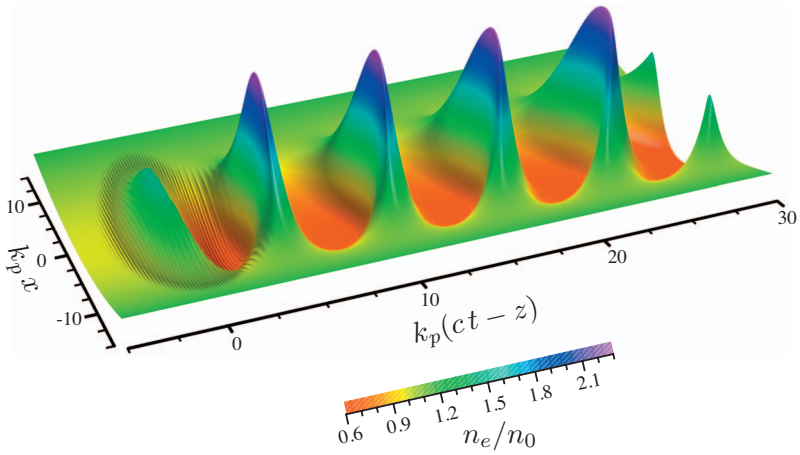

FIG. 2. (Color) Plasma density perturbation excited by Gaussian laser pulse with $a_0=1.5$, $k_0/k_p=20$, $k_pL_{\rm rms}=1$, and $k_pr_0=8$. Laser pulse is traveling to the left.

the PBWA, the plasma wave is driven at a constant beat frequency $\Delta\omega=\omega_1-\omega_2\simeq\omega_p$. As the wave grows, however, the effective plasma frequency decreases, $\omega_{p,\rm eff}=2\pi c/\lambda_{Np}$. Hence, the driver (i.e., the laser beat wave) becomes out of phase with the nonlinear plasma wave. This leads to saturation of the plasma wave amplitude in the PBWA (Rosenbluth and Liu, 1972; Tang *et al.*, 1985). Alternatively, if the plasma wave is to be driven to large amplitudes by a series of individual laser pulses, the change in the nonlinear plasma period can affect the optimal spacing between pulses as well as the optimal duration of the pulses (Umstadter *et al.*, 1994).

In the 3D nonlinear regime, numerical calculations are usually required. One possible approach is to use a full nonlinear plasma fluid model (Shadwick *et al.*, 2002) or a nonlinear quasistatic fluid model (Sprangle *et al.*, 1992; Esarey, Sprangle *et al.* 1993), which is discussed in Sec. V. An alternative (more computationally expensive) approach for wakefield calculation is to use particle simulations (Pukhov and Meyer-ter-Vehn, 1996; Tzeng *et al.*, 1996; More and Antonsen, 1997; Ren *et al.*, 2000). An example of a nonlinear plasma wave in two dimensions, as computed using a fluid model (Shadwick *et al.*, 2002), is shown in Fig. 2. Figure 2 shows the density perturbation excited by a Gaussian laser pulse with $a_0=1.5$, $k/k_p=20$, $k_pr_0=8$, and $k_pL_{\rm rms}=1$, where $L_{\rm rms}$ is the root-mean-square (rms) length of the laser intensity profile. The short wavelength oscillations observed at the front of the plasma wave are at half the laser wavelength and result from the linear polarization of the pulse.

The increase in the plasma wavelength with increasing wave amplitude has an additional effect on nonlinear 3D plasma waves. Consider a plasma wave that is driven more strongly on axis than off axis, e.g., a laser-driven accelerator, where the laser intensity peaks on axis and typically has a Gaussian radial profile. On axis, the plasma wave amplitude is maximum and, in the nonlinear regime, the plasma wavelength on axis is larger than off axis. Thus the plasma wavelength varies as a function of radius $\lambda_{Np}(r)$. This causes the wave fronts of the plasma wave to become curved and take on a "horseshoe" shape. For a plasma wave of fixed amplitude, the farther back within the plasma wave train, the more curved the plasma wave front, i.e., after ℓ periods, the phase front at large radii is located at $\ell\lambda_p$, whereas on axis, the phase front is located at $\ell\lambda_{Np}(r=0)$. This effect has been observed in two-dimensional (2D) nonlinear quasistatic fluid simulations (Sprangle *et al.*, 1992; Krall *et al.*, 1993; Esarey, Sprangle, *et al.*, 1993), 2D particle simulations (Decker *et al.*, 1994; Bulanov *et al.*, 1995, 1997), and 2D full fluid simulations (e.g., see Fig. 2). Curvature of the plasma wave fronts can lead to transverse wave breaking, as discussed in Sec. II.D.

D. Wave breaking

Plasmas are capable of supporting large amplitude electrostatic waves with phase velocities near the speed of light. In the linear regime, the electric field of a plasma wave in a plasma-based accelerator has the form $E_z=E_{\rm max}\sin[\omega_p(z/v_p-t)]$, where $v_p\simeq c$ is the phase velocity. The peak field amplitude $E_{\rm max}$ of the plasma wave can be estimated from the Poisson equation $\boldsymbol{\nabla}\cdot\boldsymbol{E}=4\pi e(n_0-n_e)$. A simple estimate for the maximum field amplitude is given by assuming all plasma electrons are oscillating with a wave number $k_p=\omega_p/c$. This gives $(\omega_p/c)E_{\rm max}=4\pi en_0$ or $E_{\rm max}=E_0$, where $E_0=cm_e\omega_p/e$ is the cold nonrelativistic wave breaking field (Dawdson, 1959).

It is possible for the maximum amplitude of a nonlinear plasma wave to exceed the value E_0. Using the nonlinear, relativistic, cold fluid equations in one dimension, the maximum amplitude of a periodic plasma wave is (Akhiezer and Polovin, 1956; Esarey and Pilloff, 1995)

$$E_{\rm WB}=\sqrt{2}(\gamma_p-1)^{1/2}E_0, \tag{26}$$

which is referred to as the cold relativistic wave breaking field, where $\gamma_p=(1-v_p^2/c^2)^{-1/2}$ is the relativistic Lorentz factor associated with the phase velocity of the plasma wave. The plasma wave phase velocity is approximately the group velocity of the laser, which in the 1D low-intensity limit is $\gamma_p\simeq\omega/\omega_p$, where ω is the frequency of the laser. As an example, consider an LPA with a plasma density of $n_0\simeq10^{17}$ cm^{-3}. For a laser wavelength of 1 μm, $\gamma_p\simeq100$ and $E_{\rm WB}\simeq14E_0$. Note that when the

plasma wave field amplitude approaches E_{WB}, Eq. (24) implies $(1+\phi)\rightarrow 1/\gamma_p$, and the cold plasma density [Eq. (17)] becomes singular, $n\rightarrow\infty$. This singularity indicates a breakdown of the cold fluid equations. Cold fluid theory will be a good approximation near the wave breaking field in the limit $\gamma_p\beta_{th}\ll\beta_p$, where $c\beta_{th}=(k_BT_0/m)^{1/2}$ is the thermal velocity spread of the plasma electrons, with T_0 the initial electron plasma temperature and k_B the Boltzmann constant. In a warm plasma, the electron distribution has a thermal spread about its mean fluid velocity, and thermal effects (i.e., pressure) will reduce the maximum plasma wave amplitude or wave breaking field.

In the limit of slow phase velocity waves, $\beta_{th}\ll\beta_p\ll 1$, corrections to the cold nonrelativistic wave breaking field E_0 have been calculated using a warm fluid model by Coffey (1971). In the ultrarelativistic phase velocity $\beta_p=1$ limit, the warm wave breaking field was found (Rosenzweig, 1988; Katsouleas and Mori, 1989) to be $E_{WB}\sim E_0/\beta_{th}^{1/2}$. This expression for E_{WB} is valid for $\gamma_p\beta_{th}\gg 1$, e.g., for an ultrarelativistic ($\beta_p=1$) particle beam driver. For laser-driven plasma waves, however, typically plasma wave phase velocities are $\gamma_p\sim 10-100$ and initial (photoionized) plasma temperatures are $\beta_{th}^2mc^2\sim 10$ eV (Durfee *et al.*, 1995; Volfbeyn *et al.*, 1999). Therefore, an LPA typically satisfies $\gamma_p\beta_{th}\lesssim 1$, and, hence, the above expression for E_{WB} does not apply.

A warm relativistic fluid theory can be used to describe wave breaking in the regime of laser-driven plasma waves (Schroeder *et al.*, 2005). This theory assumes $k_BT<mc^2$ (i.e., nonrelativistic plasma temperatures). Using the 1D quasistatic warm fluid momentum and continuity equations, the Poisson equation can be written as (Schroeder *et al.*, 2005)

$$\frac{\partial^2}{\partial\xi^2}\left[\frac{\gamma_\perp(1-\beta_pw_z)}{(1-w_z^2)^{1/2}}+\frac{3}{2}\beta_{th}^2\frac{(1-\beta_pw_z)(1-w_z^2)^{1/2}}{\gamma_\perp(1-\beta_p^{-1}w_z)^2}\right]=\frac{k_p^2w_z}{\beta_p-w_z},\tag{27}$$

where w_z is the warm fluid axial velocity. For example, Fig. 3 plots the plasma density n/n_0 (dotted curve), plasma wave electric field E_z/E_0 (solid curve), and plasma temperature T/T_0 (dashed curve) as a function of $\xi=z-v_pt$ excited by a Gaussian laser pulse $a=a_0\exp(-\xi^2/4L_{rms}^2)$ with $a_0=2$ and $k_pL_{rms}=1$ for $\gamma_p=10$. The plasma temperature undergoes periodic oscillations in the wake owing to compression of the plasma density (Shadwick *et al.*, 2004, 2005; Schroeder *et al.*, 2005; Esarey *et al.*, 2007). The temperature evolution behind the laser pulse (to lowest order in the small parameter $k_BT/mc^2<1$) is given by $T=[(n/n_0)^2(1-w_z^2)]T_0$.

The wave breaking limit, defined as the maximum amplitude of an electrostatic standing wave (a function of only $\xi=z-v_pt$) allowed within the fluid model, can be calculated using Eq. (27). For example, the lowest-order corrections (in the limit $\gamma_p\beta_{th}<\beta_p$) to the cold relativistic wave breaking field [Eq. (26)] are (Schroeder *et al.*, 2005)

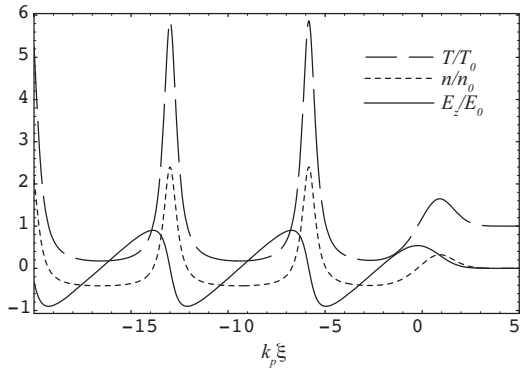

FIG. 3. Time-averaged plasma density perturbation n/n_0-1 (dotted curve), plasma wave electric field E_z/E_0 (solid curve), and plasma temperature T/T_0 (dashed curve) excited by a Gaussian laser pulse with normalized intensity $a=2$ and rms length $k_pL_{rms}=1$ (centered at $k_p\xi=0$).

$$(E_{WB}/E_0)^2\simeq 2\gamma_\perp(\gamma_p-1)-\beta_p^2\gamma_p\gamma_\perp(8\delta_{th}/3-2\delta_{th}^2),\tag{28}$$

where $\delta_{th}=(3\beta_{th}^2\gamma_p^2/\gamma_\perp^2\beta_p^2)^{1/4}$. Equation (28) includes the possible presence of an intense laser field (e.g., the self-modulated LWFA), with $\gamma_\perp^2=1+a^2$. The wave breaking field is larger in the presence of a laser field. For a plasma wave behind the drive laser pulse, $\gamma_\perp=1$. In the warm fluid theory of wave breaking there is no shock formation (i.e., the density remains finite) at the wave breaking limit. For fields larger than Eq. (28) no traveling wave solutions exist. Figure 4 shows the wave breaking field, E_{WB}/E_0 (solid curve), versus initial temperature β_{th}^2 with $\gamma_p=10$ and $\gamma_\perp=1$. The dotted curve is the ultrarelativistic result ($\beta_p=1$) and the dashed line is the cold limit ($\beta_{th}=0$). Note that for typical short-pulse laser-plasma interactions, $\beta_{th}^2\sim 10^{-4}$.

The above expressions for the wave breaking field were based on 1D theories. Wave breaking in three dimensions has not been thoroughly investigated and gen-

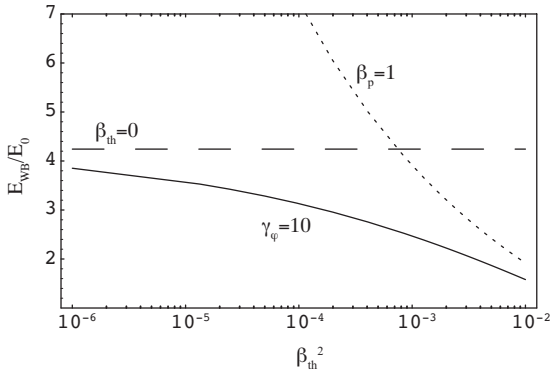

FIG. 4. Maximum plasma wave electric field amplitude E_{WB}/E_0 [Eq. (28)] vs initial temperature β_{th}^2 with $\gamma_p=10$ and $\gamma_\perp=1$. The dotted curve is the ultrarelativistic result $\beta_p=1$ and the dashed line is the cold limit.

eral expressions for the maximum field amplitude are not known. PIC simulations (Decker *et al.*, 1994; Bulanov *et al.*, 1995; Pukhov and Meyer-ter-Vehn, 2002; Tsung *et al.*, 2004) in two and three dimensions in the highly nonlinear cavitated regime have demonstrated the generation of plasma waves with amplitudes in excess of E_0. The wake generation in the blow-out regime is discussed in Sec. III.E. Simulations (Krall *et al.*, 1993; Shadwick *et al.*, 2002) based on nonlinear 2D fluid equations have shown wave amplitudes in excess of E_0.

The transverse structure of the plasma wave and curvature of the wake phase fronts, as described in Sec. II.C, can lead to "2D wave breaking" (Bulanov *et al.*, 1997). Specifically, when the curvature radius of the phase front is on the order of the electron fluid displacement, the regular structure of the plasma wave is destroyed and particle trapping may occur. For a fixed amplitude nonlinear 2D wake (i.e., neglecting wake damping), 2D wave breaking will always occur at a sufficiently long distance behind the driver. The larger the wake amplitude, the shorter the distance behind the driver is the onset point of 2D wave breaking. A similar effect can occur for linear (or nonlinear) plasma waves in a plasma channel. In a plasma channel, the plasma density is minimum on axis; hence the plasma wavelength is longer on axis than off axis. This leads to wake wave front curvature, and the curvature increases with distance behind the driver until the point of 2D wave breaking is reached.

E. Electron acceleration and dephasing

Consider an electron accelerated along the z axis (laser-propagation axis) by a linear electrostatic plasma wave of the form $E_z = E_{\max}\sin[\omega_p(z/v_p - t)]$. As the electron is accelerated, its velocity will increase and approach the speed of light, $v_z \to c$. If the phase velocity of the plasma wave is constant with $v_p < c$, the electrons will eventually outrun the plasma wave and move into a phase region of the plasma wave that is decelerating. This limits the energy gain of the electron in the plasma wave and is commonly referred to as electron dephasing. The dephasing length L_d is defined as the length the electron must travel before it phase slips by one-half of a period with respect to the plasma wave. For a highly relativistic electron, $v_z \simeq c$, the linear dephasing length L_d is given by $(1-v_p/c)L_d = \lambda_p/2$, i.e., $L_d \simeq \gamma_p^2\lambda_p$, assuming $\gamma_p = \omega/\omega_p \gg 1$. The maximum energy gain after a dephasing length (Tajima and Dawson, 1979; Joshi *et al.*, 1984) is roughly $W_{\max} \simeq eE_{\max}L_d \simeq 2\pi\gamma_p^2(E_{\max}/E_0)m_ec^2$, assuming $E_{\max} < E_0$.

In a 1D plasma wave, electron trapping, acceleration, and dephasing can be studied by examining the electron orbits in phase space $(\tilde{p}, \psi)$, where $\tilde{p}$ is the normalized electron momentum and $\psi = k_p\xi = k_p(z - v_p t)$ is the phase. In the linear regime, the plasma wave is described by a sinusoidal electrostatic potential $\phi = \phi_0 \cos\psi$, where $\phi_0 = E_{\max}/E_0$ is the amplitude. The phase region $-\pi < \psi < 0$ is accelerating. Consider an electron injected into the plasma wave with $v_z < v_p$ at $\psi = 0$. Initially, the electron is slipping backward with respect to the plasma wave. If the initial electron velocity is too low, the electron does not gain sufficient energy and $v_z < v_p$ at $\psi = -\pi$. Hence, the electron would be untrapped and would continue to slip backward through the plasma wave. If, however, the electron has a sufficiently high initial velocity such that $v_z > v_p$ as the electron approaches $\psi \to -\pi$, the electron will be trapped and execute closed orbits in the $-\pi < \psi < \pi$ phase region. The separatrix, which separates the region of trapped and untrapped orbits in phase space, is shown in Fig. 5 for $\gamma_p = 10$ and $\phi_0 = 0.1$.

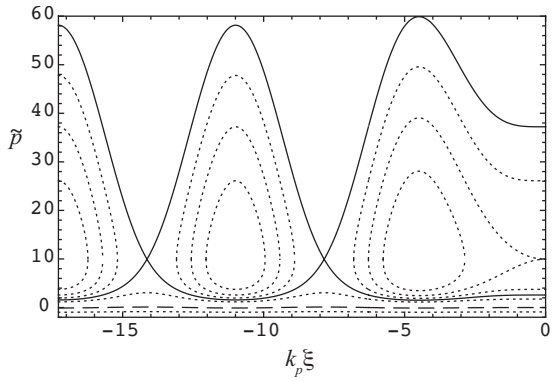

FIG. 5. Single particle orbits in phase space $(\tilde{p}, k_p\xi)$ for an electron in a small amplitude sinusoidal plasma wave with a normalized potential given by $\phi = \phi_0 \cos\psi$, with $\gamma_p = 10$ and $\phi_0 = 0.1$. Solid curve is separatrix. Dashed curve is the cold fluid orbit. Excitation of the plasma wave by a laser pulse with a half-sine envelope of length $\lambda_p/2$ (head at $k_p\zeta = 0$) is assumed.

The motion of a test electron in a 1D nonlinear plasma wave is described by the Hamiltonian (Esarey and Pilloff, 1995)

$$H(\tilde{p}, \psi) = \tilde{\gamma} - \beta_p\tilde{p} - \phi(\psi), \tag{29}$$

where $H(\tilde{p}, \psi) = \text{const}$ along a given electron orbit and $\phi = \phi(\psi)$ is the solution to Eq. (16), which oscillates in the range $\phi_{\min} \leqslant \phi \leqslant \phi_{\max}$ and is related to $E_{\max}$ by Eq. (24). In particular, the separatrix $\tilde{\gamma}_s(\psi)$ characterizing the test electron orbits in $(\tilde{\gamma}, \psi)$ phase space is given by $H(\tilde{\gamma}_s, \psi) = H(\gamma_p, \psi_{\min})$, where $\phi(\psi_{\min}) = \phi_{\min}$.

Figure 6 shows several separatrices for $\gamma_p = 20$ and for different values of the plasma wave amplitude, given by $E_{\max}/E_0 = 0.18$, 0.47, 1.5, 3.2, and 5.8. The value $E_{\max}/E_0 = 0.18$ corresponds to the innermost curve and $E_{\max}/E_0 = 5.8$ corresponds to the outermost curve. These curves were obtained (Esarey and Pilloff, 1995) by plotting $H(\tilde{\gamma}_s, \psi) = H(\gamma_p, \psi_{\min})$ after numerically solving Eq. (16) for $\phi = \phi(\psi)$ with the initial conditions $\partial\phi/\partial\xi = 0$ and $\phi = \phi_{\max}$ at $\psi = 0$. The width of the separatrix $\Delta\psi_s$ corresponds to the nonlinear plasma wavelength, $\lambda_{Np} = \Delta\psi_s/k_p$, given by Eq. (25). As the plasma wave amplitude increases, the nonlinear wavelength increases.

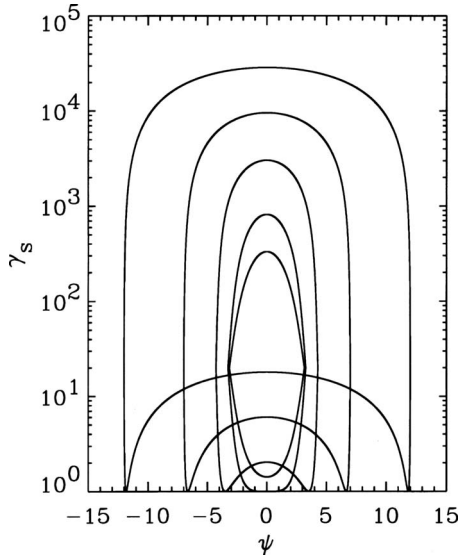

FIG. 6. Phase-space separatrix $\gamma_s(\psi)$ plotted for several values of the plasma wave amplitude $E_{max}/E_0=0.18$, 0.47, 1.5, 3.2, and 5.8, with $\gamma_p=20$. The value $E_{max}/E_0=0.18$ corresponds to the innermost curve and $E_{max}/E_0=5.8$ corresponds to the outermost curve. From Esarey and Pilloff, 1995.

The maximum momentum $\tilde{p}_{max}$ and minimum momentum $\tilde{p}_{min}$, denoted by $\tilde{p}_m$, for an electron on the separatrix are (Esarey and Pilloff, 1995)

$$\tilde{p}_m = \beta_p\gamma_p(1+\gamma_p\Delta\phi) \pm \gamma_p[(1+\gamma_p\Delta\phi)^2-1]^{1/2}, \quad (30)$$

where $\Delta\phi=\phi_{max}-\phi_{min}$, i.e., $\Delta\phi=2\beta_p[(1+\hat{E}_{max}^2/2)^2-1]^{1/2}$, as indicated by Eq. (24). In the limits $\gamma_p\Delta\phi\gg1$ and $\gamma_p^2\gg1$, $\tilde{p}_{max}\simeq2\gamma_p^2\Delta\phi$ and $\tilde{p}_{min}\simeq-\Delta\phi/2+1/(2\Delta\phi)$. In particular, the maximum energy of a trapped electron is (Esarey and Pilloff, 1995)

$$\tilde{\gamma}_{max} \simeq 2\gamma_p^2 \times \begin{cases} 2\hat{E}_{max} & \text{for } 2 \gg \hat{E}_{max}^2 \gg 1/4\gamma_p^2 \\ \hat{E}_{max}^2 & \text{for } \hat{E}_{max}^2 \gg 2, \end{cases} \quad (31)$$

where $\hat{E}_{max}=E_{max}/E_0$. The limit $\hat{E}_{max}^2\ll2$ corresponds to the well-known limit for linear sinusoidal plasma waves (Tajima and Dawson, 1979; Joshi *et al.*, 1984; Mora, 1992). When $\hat{E}_{max}^2\gg2$, however, $\tilde{\gamma}_{max}\simeq2\gamma_p^2\hat{E}_{max}^2$, which implies that higher electron energies can be obtained for electrons trapped in nonlinear plasma waves. The nonlinear regime where $\hat{E}_{max}>1$ has been observed in simulations of the self-modulated LWFA (Krall *et al.*, 1993; Decker *et al.*, 1994; Bulanov *et al.*, 1995) and laser wakefields driven by multiple pulses (Nakajima, 1992; Bonnaud *et al.*, 1994; Umstadter *et al.*, 1994). For the maximum field in a cold plasma ($E_{max}=E_{WB}$), Eq. (30) indicates that (Esarey and Pilloff, 1995) $\tilde{\gamma}_{max}=4\gamma_p^3-3\gamma_p$.

An estimate for the dephasing length is given by $W_{max}=m_ec^2\tilde{\gamma}_{max}=eE_{max}L_d$. This yields

$$L_d = \gamma_p^2\lambda_{Np} \times \begin{cases} 2/\pi, & \hat{E}_{max} \ll 1 \\ 1/2, & \hat{E}_{max} \gg 1, \end{cases} \quad (32)$$

where λ_{Np} is given by Eq. (25). The actual dephasing length (Teychenné *et al.*, 1994b) requires the simultaneous solution of the equation of motion and Eq. (16).

As an example, consider an LWFA with $n_0=2.8\times10^{18}$ cm^{-3} and $\lambda=1$ μm, i.e., $\gamma_g\simeq\gamma_p\simeq20$ and $E_0\simeq160$ GV/m. In the limit $\hat{E}_{max}^2\gg2$, Eq. (31) yields $W_{max}\simeq400\hat{E}_{max}^2$, where $W_{max}\simeq m_ec^2\tilde{\gamma}_{max}$. At the maximum field in a cold plasma, $E_{WB}\simeq6.2E_0$ and $W_{max}\simeq16$ GeV. Notice that $\tilde{\gamma}_{max}\simeq4\gamma_p^3E_{max}/E_{WB}$, assuming $\gamma_p^2\gg1$ and $\gamma_p(E_{max}/E_{WB})^2\gg1$. Hence, for a fixed value of E_{max}/E_{WB}, $\tilde{\gamma}_{max}\propto n_0^{-3/2}$ and substantially higher single-stage energy gains can be achieved by operating at lower densities, albeit with longer acceleration stages.

Note that the above results are obtained from 1D theory and assume a constant amplitude plasma wave. An evolving plasma wave amplitude and 3D effects alter these results. For example, Mora (1992) showed that the effects of laser diffraction can lead to a more restrictive trapping condition for linear plasma waves.

F. Plasma wave phase velocity

The phase velocity of the plasma wave is important for determining the minimum injection energy, the maximum energy gain, the maximum plasma wave amplitude, and the dephasing length. Neglecting the evolution of the drive beam as it propagates, the phase velocity of the plasma wave is equal to the group velocity of the drive laser.

In the linear regime, the group velocity of a laser pulse in a plasma can be determined from the 1D dispersion relation, $\omega^2=c^2k^2+\omega_p^2$. This yields $v_g=c(1-\omega_p^2/\omega^2)^{1/2}$ and $\gamma_g=(1-v_g^2/c^2)^{-1/2}=\omega/\omega_p$. Nonlinear corrections to the group velocity in one dimension have been analyzed by Decker and Mori (1994). Note that, in the nonlinear regime the linear relation $v_g=c^2k/\omega$ is no longer valid. In the long pulse, underdense $\omega_p/\omega\ll1$ limit, the nonlinear group velocity was found by Decker and Mori (1994) to be $\gamma_g=(\omega/\omega_p)[(\gamma_\perp+1)/2]^{1/2}$, which in the limit $a^2\ll1$ gives $\gamma_g\simeq(\omega/\omega_p)(1+a^2/8)$. A calculation based on the intensity transport velocity yields $\gamma_g\simeq(\omega/\omega_p)(1+3a^2/8)$ (Esarey *et al.*, 2000).

The group velocity of a laser pulse is also reduced by 3D effects. For example, consider a laser pulse in vacuum undergoing Rayleigh diffraction. The evolution of the spot size (or radius) of a Gaussian laser pulse evolves according to $r_s=r_0(1+z^2/Z_R^2)^{1/2}$, where r_0 is the minimum spot size at the focal point $z=0$ and $Z_R=kr_0^2/2$ is the Rayleigh length. In effect, the photons are traveling at approximately a diffraction angle $\theta_d=r_0/Z_R$ with respect to the z axis. Hence, the axial group velocity is reduced by $v_g\simeq c\cos\theta_d\simeq c(1-\theta_d^2/2)$. A more detailed calculation indicates that, in the linear regime, the

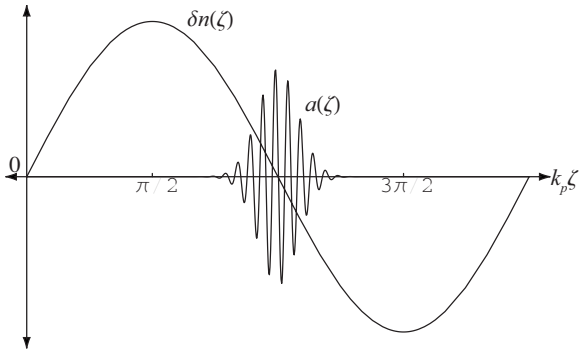

FIG. 7. Schematic of laser pulse frequency upshifting by a plasma wave with $v_p \simeq v_g \simeq c$ (pulse moving to the right). Positive frequency shifts require the laser pulse a to be centered about regions of the plasma wave ($\delta n = n - n_0$) with a decreasing density.

3D group velocity is given by (Esarey and Leemans, 1999)

$$\gamma_g \simeq (\omega_p^2/\omega^2 + 2c^2/\omega^2 r_0^2)^{-1/2}. \tag{33}$$

In effect, the linear 3D dispersion relation is $\omega^2 - c^2k^2 = \omega_p^2 + 2c^2/r_0^2$ (for a matched laser pulse in a parabolic plasma channel, $\omega^2 - c^2k^2 = \omega_p^2 + 4c^2/r_0^2$). For tightly focused laser pulses, this 3D correction can significantly limit the group velocity. As an example, consider a laser pulse with a $\lambda = 1$ μm wavelength and $r_0 = 10$ μm spot size, propagating in a plasma of density $n_0 = 10^{16}$ cm^{-3}; in one dimension, $\gamma_g \simeq 330$, however, the finite spot size reduces the group velocity such that $\gamma_g \simeq 44$.

Distortions of the pulse driving the plasma wave can also affect the plasma wave phase velocity. In the LWFA in the 1D limit, it has been shown that the wake phase velocity is approximately equal to the group velocity associated with the position of the peak of intensity profile (Decker and Mori, 1994). Furthermore, the plasma wave can lead to locally enhanced diffraction and focusing, which distorts the pulse profile and reduces the plasma wave phase velocity (Leemans *et al.*, 1996).

G. Photon acceleration

In addition to accelerating electrons, a plasma wave can be used to upshift the frequency (often referred to as photon acceleration) of a properly phased, low intensity, short laser pulse, as shown in Fig. 7 (Wilks *et al.*, 1989; Esarey *et al.*, 1990). Consider a plasma wave with an electron density perturbation of the form $\delta n = -\delta n_0 \sin k_p\zeta$, where $\zeta = z - ct$, and a low intensity "witness" laser pulse centered about $\zeta = 0$ with a pulse length $L \ll \lambda_p$. The local density at the front of the pulse, $n(\zeta = L/2)$, will be less than that at the back of the pulse, $n(\zeta = -L/2)$. Since the local phase velocity of the laser pulse is $\beta_{\rm ph} = v_{\rm ph}/c \simeq 1 + \omega_p^2(\zeta)/2\omega^2$, where $\omega_p^2(\zeta) \propto n(\zeta)$, the phase velocity at the pulse front is less than that at the back of the pulse, i.e., $v_{\rm ph}(L/2) < v_{\rm ph}(-L/2)$. Hence, the phase peaks at the back move faster than those at the front and the pulse wavelength decreases (the pulse frequency increases). For small shifts, the laser wavelength will evolve according to $\lambda \simeq \lambda_0 + z\Delta\beta_{\rm ph}$, where $\Delta\beta_{\rm ph} = \lambda_0 d\beta_{\rm ph}/d\zeta < 0$ is the difference in phase velocity between adjacent phase peaks, z is the propagation distance, and $\lambda_0 = 2\pi c/\omega_0$ is the initial laser wavelength. Hence, the frequency shift is $\omega/\omega_0 \simeq 1 - z d\beta_{\rm ph}/d\zeta$, where $d\beta_{\rm ph}/d\zeta \simeq (\omega_p^2/2\omega_0^2) d(\delta n/n_0)/d\zeta$. A more detailed calculation indicates that the frequency will be upshifted according to (Esarey *et al.*, 1990)

$$\frac{\omega}{\omega_0} \simeq \left(1 + \frac{\omega_p^2}{\omega_0^2}\frac{\delta n_0}{n_0} k_p z \cos k_p\zeta\right)^{1/2}, \tag{34}$$

where nonlinear effects and phase slippage between the laser pulse and plasma wave have been neglected.

Typically, the plasma wave induced frequency shifts are small. For example, consider a laser with $\lambda = 1$ μm and $r_0 = 30$ μm, propagating in a plasma of density $n_0 = 10^{18}$ cm^{-3} ($\lambda_p = 30$ μm). After propagating one Rayleigh length $z = Z_R$, $\omega/\omega_0 \simeq 1 + \delta n_0/3n_0$. Small frequency shifts, however, can be detected and this process can be useful for diagnosing the wakefield (Marquès *et al.*, 1996; Siders *et al.*, 1996; Matlis *et al.*, 2006). Large frequency shifts require long propagation distances and large plasma wave amplitudes. For example, after one electron dephasing length $L_d = \lambda_p\omega^2/\omega_p^2$, $\omega/\omega_0 = (1 + 2\pi\delta n_0/n_0)^{1/2}$. Laser redshifting and blueshifting of a drive pulse by its plasma wakefield have also been observed (Geddes *et al.*, 2005a; Faure, Glinec, *et al.*, 2006; Murphy *et al.*, 2006; Rowlands-Rees *et al.*, 2008).

III. LASER-PLASMA ACCELERATORS

A. Laser wakefield accelerator

In the laser wakefield accelerator (LWFA) (Tajima and Dawson, 1979; Gorbunov and Kirsanov, 1987; Sprangle *et al.*, 1988), a single, short ($\lesssim 1$ ps), high-intensity ($\gtrsim 10^{17}$ W/cm^2) laser pulse drives a plasma wave. The wakefield is driven most efficiently when the laser pulse length is on the order of the plasma period $L \sim \lambda_p$. The LWFA was first proposed by Tajima and Dawson (1979). Prior to 1985, the technology for generating ultraintense picosecond laser pulses did not exist and only the PBWA concept, described in Sec. III.B, appeared feasible (the PBWA concept relied on long pulses of modest intensity). The LWFA was later reinvented independently by Gorbunov and Kirsanov (1987) and by Sprangle *et al.* (1988). This roughly coincides to the time when CPA was applied to compact solid-state lasers and a table-top terawatt laser system was first demonstrated by Mourou and co-workers (Maine *et al.*, 1988). The nonlinear theory of the LWFA in one dimension was developed by Bulanov *et al.* (1989), Berezhiani and Murusidze (1990), and Sprangle *et al.* (1990a, 1990b). The nonlinear theory of the LWFA in two dimensions, including the self-consistent evolution of the laser pulse, was analyzed by Sprangle *et al.* (1992) and Esarey, Sprangle, *et al.* (1993).

As an intense laser pulse propagates through an underdense plasma, $(\lambda/\lambda_p)^2 \ll 1$, the ponderomotive force associated with the laser pulse envelope, $F_p \sim \nabla a^2$, expels electrons from the region of the laser pulse. If the length scale L_z of the axial gradient in the pulse profile is approximately equal to the plasma wavelength, $L_z \sim \lambda_p$, the ponderomotive force excites large amplitude plasma waves (wakefields) with phase velocities approximately equal to the laser pulse group velocity [see Fig. 1(a)]. For a typical axially symmetric laser pulse (e.g., a Gaussian profile), the wakefield amplitude will be maximum when $L_{\rm rms} \simeq \lambda_p/(2\pi)$. The precise value of L that maximizes the wake amplitude will depend on the shape of the axial pulse profile. Following are some examples.

Linear regime sine pulse. Consider an LWFA driven by a circularly polarized laser pulse with a normalized intensity $a^2 = a_0^2 \exp(-2r^2/r_s^2)\sin^2(\pi\zeta/L)$ for $0 < \zeta < L$, where $\zeta = z - ct$ and $a_0^2 \ll 1$. Solutions to Eq. (11) indicate that the wakefield amplitude is maximum for pulse lengths $L \simeq \lambda_p$. Behind the pulse, $\zeta < 0$, the axial electric field and density perturbation of the wake are (Esarey *et al.*, 1989)

$$\frac{E_z}{E_0} = -\frac{\pi}{4} a_0^2 \exp\left(-\frac{2r^2}{r_s^2}\right)\cos k_p\zeta \tag{35}$$

and

$$\frac{\delta n}{n_0} = -\frac{\pi}{4} a_0^2 \left[1 + \frac{8}{k_p^2 r_s^2}\left(1 - \frac{2r^2}{r_s^2}\right)\right]\exp\left(-\frac{2r^2}{r_s^2}\right)\sin k_p\zeta \tag{36}$$

for $L = \lambda_p$. For linear polarization, averaging over the fast oscillation yields Eqs. (35) and (36) with a_0^2 replaced with $a_0^2/2$. Notice that a tightly focused laser pulse with $k_p^2 r_s^2/8 < 1$ will result in a larger density perturbation $\delta n/n_0$ on axis, whereas the axial electric field E_z on axis is unchanged in comparison to the 1D values.

Linear regime Gaussian pulse. For a circularly polarized Gaussian pulse profile, $a^2 = a_0^2 \exp(-\zeta^2/L^2)$, the wakefield amplitude behind the pulse ($\zeta^2 \gg L^2$) is (Gorbunov and Kirsanov, 1987)

$$E_{\rm max}/E_0 = (\sqrt{\pi} a_0^2/2) k_p L \exp(-k_p^2 L^2/4), \tag{37}$$

assuming $a_0^2 \ll 1$. Equation (37) explicitly shows the dependence of the wake amplitude on the pulse length L. In particular, the wake amplitude achieves a maximum value of $E_{\rm max}/E_0 = a_0^2(\pi/2e)^{1/2} \simeq 0.76 a_0^2$ when $L = \lambda_p/\pi\sqrt{2}$.

Nonlinear regime square pulse. Consider a circularly polarized laser pulse with a square axial profile in the 1D limit $r_0^2 \gg \lambda_p^2$. The wakefield amplitude is maximum when $L \simeq \lambda_{Np}/2$, where λ_{Np} is the nonlinear plasma wavelength [Eq. (25)] and is (Bulanov *et al.*, 1989; Berezhiani and Murusidze, 1990; Sprangle *et al.*, 1990a, 1990b)

$$E_{\rm max}/E_0 = a_0^2(1 + a_0^2)^{-1/2}, \tag{38}$$

where $a_0^2 = 3.6 \times 10^{-19} \lambda^2(\mu{\rm m}) I_0({\rm W/cm^2})$ (for linear polarization, replace a_0^2 with $a_0^2/2$). Notice that $E_{\rm max} \propto \lambda_p^{-1} \sim L^{-1}$. Hence, the wakefield amplitude can be increased by operating at high densities and shorter pulse lengths. At high densities, however, the laser pulse group velocity is reduced and electron dephasing can limit the energy gain, as discussed in Secs. II.E and III.G.

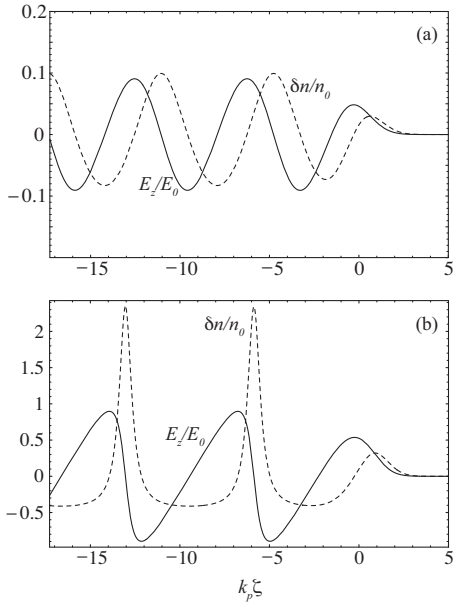

FIG. 8. Time-averaged density variation $\delta n/n_0$ (dashed curve) and axial electric field E_z/E_0 (solid curve) in an LWFA driven by a Gaussian laser pulse (pulse is moving to the right, centered at $k_p\zeta = 0$ with rms intensity length $L_{\rm rms} = k_p^{-1}$) for (a) $a_0 = 0.5$ and (b) $a_0 = 2.0$.

Nonlinear regime Gaussian pulse. Equation (16) can be solved numerically for the plasma wave excitation in the nonlinear regime. In Fig. 8 a plasma wave is driven by a linearly polarized Gaussian laser pulse of the form $a = a_0 \exp(-\zeta^2/4L_{\rm rms}^2)\cos(k\zeta)$ with pulse (rms laser intensity profile) length $k_p L_{\rm rms} = 1$. A mildly relativistic case $a_0 = 0.5$ is shown in Fig. 8(a) and a highly relativistic case $a_0 = 2$ is shown in Fig. 8(b). Figure 8 shows the normalized density perturbation $\delta n/n_0 = n/n_0 - 1$ and the normalized axial electric field E_z/E_0. The nonlinear effects of wave steepening and period lengthening are evident in Fig. 8(b).

Because the plasma wave is driven by a single laser pulse with $L \sim \lambda_p$, the wakefield amplitude is relatively insensitive to uncertainties in the pulse duration and the plasma uniformity. This is shown in Fig. 9, where the peak wakefield amplitude $E_{\rm max}$ is shown as a function of the normalized pulse length $k_p L_{\rm rms}$ at fixed laser intensity ($a_0 = 0.5$ and 2). Plotted in Fig. 9 is the wakefield amplitude normalized to $E_0(a_0^2/2)(1 + a_0^2/2)^{-1/2}$, which is the maximum wakefield amplitude for a square pulse profile. Notice that the electric field amplitude is maximum for $k_p L_{\rm rms} \approx 1$ and is fairly insensitive to changes in the pulse length. The (dashed) curve for the $a_0 = 2$ case is also broader because of an increase in the nonlinear plasma wavelength.

The optimal pulse length conditions for the square, sine, and Gaussian pulse profiles discussed above may

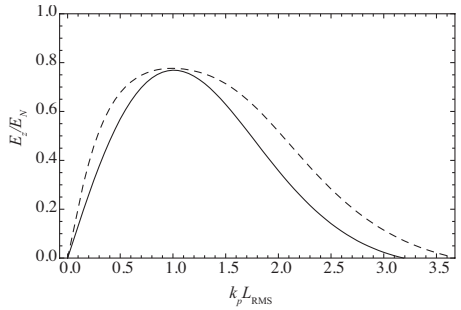

FIG. 9. Amplitude of axial electric field E_z [normalized to the maximum amplitude of a flat-top pulse $E_N=(a_0^2/2)/(1+a_0^2/2)^{1/2}$] plotted as a function of laser pulse length $k_pL_{\rm rms}$ for the LWFA examples shown in Fig. 8: $a_0=0.5$ (solid curve) and $a_0=2.0$ (dashed curve). The laser pulse envelope is $a=a_0\exp(-\zeta^2/4L_{\rm rms}^2)$.

be summarized as follows. For the square pulse, the wakefield is maximum $E_{\max}=a_0^2E_0$ when $L_{\rm FWHM}=0.5\lambda_p$ ($k_pL_{\rm rms}=0.91$). For the sine pulse, the wakefield is maximum $E_{\max}=0.82a_0^2E_0$ when $L_{\rm FWHM}=0.42\lambda_p$ ($k_pL_{\rm rms}=0.95$). For the Gaussian pulse, the wakefield is maximum $E_{\max}=0.76a_0^2E_0$ when $L_{\rm FWHM}=0.37\lambda_p$ ($k_pL_{\rm rms}=1$). Here the pulse length is expressed in terms of the full width at half maximum (FWHM) length $L_{\rm FWHM}$ and the root-mean-square (rms) length $L_{\rm rms}$ of the pulse intensity profile. These results assume $a_0^2\ll1$ and circular polarization (Leemans *et al.*, 1996).

Furthermore, since the laser pulse in the LWFA is of short duration, $L\sim\lambda_p$, various instabilities that can be detrimental to the propagation of long pulses can be reduced. Schemes that use long laser pulses, $L\gg\lambda_p$, such as the PBWA and the self-modulated LWFA, are subject to various laser-plasma instabilities, some of which are discussed in Sec. VI.

Perhaps the first experimental evidence for plasma wave generation by the LWFA mechanism was obtained by Hamster *et al.* (1993). In these experiments, the emission of terahertz radiation at the plasma frequency was observed when the plasma was driven by a laser pulse of length $L\simeq\lambda_p$. Specifically, $\omega_p/2\pi=4.6$ THz radiation was observed for a 0.1 ps laser pulse propagating in a plasma of density 2×10^{17} cm^{-3}. This radiation is emitted presumably by the radial electron plasma currents of the laser-induced wakefield. Direct measurement of plasma wave generated in the LWFA has been reported by researchers at Ecole Polytechnique (Marquès *et al.*, 1996) and at the University of Texas at Austin (Siders *et al.*, 1996) using probe pulses and time-resolved frequency-domain-interferometry techniques. In the Ecole Polytechnique experiments (Marquès *et al.*, 1996) a 120 fs duration, 800 nm wavelength laser pulse with a maximum energy of 40 mJ was focused to a maximum intensity of 3×10^{17} W/cm^2 in a plasma of density 10^{17} cm^{-3}. A pair of probe pulses, separated from each other by $1.5\lambda_p$, were used to map out the wakefield by adjusting the delay between the pump and probe pulses. A plasma wave with a perturbed density of 30–100 % was measured over several plasma periods behind the probe pulse. At the University of Texas (Siders *et al.*, 1996), three probe pulses were used to measure the density perturbation at a fixed delay behind the pump pulse. By varying the ambient plasma density, the plasma wave amplitude was observed to vary in good agreement with theory. Kotaki *et al.* (2002) measured the laser-driven coherent wakefield excitation (up to 20 GeV/m) in a gas jet with a plasma density on the order of 10^{18} cm^{-3} using a time-resolved frequency domain interferometer. Single-shot visualization of laser-wakefield structures was achieved using frequency-domain holography (Matlis *et al.*, 2006), a technique designed to image structures propagating near luminal velocities. The frequency-domain holography technique uses a copropagating chirped probe pulse to encode the plasma density variations excited by the drive laser; interference of the probe with a reference pulse allows holographic images of the wake structure to be reconstrusted.

Dewa *et al.* (1998) reported the observation of electron acceleration in LFWA experiments, although with some controversy (Bernard *et al.*, 1999), with energies of 100 MeV (17 MeV injected from a linac) with a 2 TW laser system. Amiranoff *et al.* (1998) observed LWFA accelerated electrons with an energy gain of 1.6 MeV (3 MeV injected) using a 3.5 TW laser system. The peak longitudinal electric field was estimated to be 1.5 GV/m. Kitagawa *et al.* (2004) observed electron acceleration using a 1 μm, $\sim$0.5 ps duration laser exciting a plasma wave in a glass capillary with plasma density (plasma electrons created via ablation) of 10^{16} cm^{-3}.

B. Plasma beat wave accelerator

In the plasma beat wave accelerator (PBWA) (Rosenbluth and Liu, 1972; Tajima and Dawson, 1979; Joshi *et al.*, 1984; Kitagawa *et al.*, 1992; Clayton *et al.*, 1993; Everett *et al.*, 1994), two long laser pulses of frequencies ω_1 and ω_2 are used to resonantly excite a plasma wave. This is done by appropriately adjusting the laser frequencies and plasma density to satisfy the resonance condition $\Delta\omega\equiv\omega_1-\omega_2\simeq\omega_p$. When this is satisfied, large amplitude plasma waves can be generated. The PBWA was first proposed by Tajima and Dawson (1979) as an alternative to the laser wakefield accelerator since compact, ultrashort pulse, ultrahigh power laser technology (Mourou and Umstadter, 1992; Perry and Mourou, 1994) was not available in 1979. Resonant excitation of a plasma wave using two laser pulses had been previously analyzed by Rosenbluth and Liu (1972) for plasma heating applications. The PBWA was subsequently analyzed by various researchers (Joshi *et al.*, 1984; Tang *et al.*, 1985; Horton and Tajima, 1986; McKinstrie and Forslund, 1987; Esarey *et al.*, 1988; Gibbon and Bell, 1988; Mori *et al.*, 1988). To overcome the problem of dephasing between the accelerated electrons and the plasma wave, Katsouleas and Dawson (1983) proposed the use of a transverse magnetic field. Tang *et al.* (1985) described how the plasma wave amplitude could be in-

creased by operating at an optimal frequency mismatch $\Delta\omega_{\rm opt}$, such that $\omega_1-\omega_2=\Delta\omega_{\rm opt}$. Various aspects of the PBWA have been analyzed and simulated, such as the self-focusing of the laser pulses by relativistic, plasma wave, cascading effects (Esarey *et al.*, 1988; Gibbon and Bell, 1988; Mori *et al.*, 1988; Esarey and Ting, 1990) and the chaotic behavior of beat waves in the presence of an ion wave (Leemans *et al.*, 1992b).

Consider two laser pulses with combined normalized vector potentials given by $a=a_1\cos(k_1z-\omega_1t)+a_2\cos(k_2z-\omega_2t)$, where $k_{1,2}$ are the laser wave numbers. The ponderomotive force $\nabla a^2/2$ will have a resonant beat term $(a^2)_{\rm res}=a_1a_2\cos(\Delta kz-\Delta\omega t)$, where $\Delta k\equiv k_1-k_2$. In the linear regime, plasma wave generation is described by $(\partial^2/\partial t^2+\omega_p^2)\phi=\omega_p^2(a^2/2)_{\rm res}$, and the ponderomotive beat term can resonantly drive a plasma wave when $\Delta\omega\simeq\omega_p$. When the resonance condition is exactly satisfied, $\Delta\omega=\omega_p$, secular growth of the plasma wave results, $\phi=-\phi_s\sin(\Delta kz-\Delta\omega t)$, where $\phi_s=a_1a_2k_p|\zeta|/4$ and $|\zeta|=|z-ct|$ is the distance behind the front of the laser pulses. Hence, the amplitude of the plasma wave within the laser pulse is (Rosenbluth and Liu, 1972)

$$E_{\rm max}/E_0=a_1a_2k_p|\zeta|/4. \tag{39}$$

Furthermore, notice that the phase velocity of the plasma wave, $v_p=\Delta\omega/\Delta k$, is given by $v_p/c\simeq1-\omega_p^2/(2\omega_1\omega_2)$ in the limit $\omega_p^2/\omega_1^2\sim\omega_p^2/\omega_2^2\ll1$, i.e., the phase velocity of the plasma wave is approximately equal to the group velocity of the driving lasers.

In effect, the laser beat wave acts as a series of laser pulses, each of amplitude a_1a_2 and of duration $\Delta\tau=2\pi/\Delta\omega$. Each of these pulses generates a wake of amplitude $E_{\rm max}/E_0=\pi a_1a_2/2$. The total plasma wave amplitude generated by a laser beat wave of length $L=N\lambda_p$ is $E_{\rm max}/E_0=N\pi a_1a_2/2$, where N is the number of laser beat periods within the pulse.

The result given by Eq. (39) was based on linear plasma theory, $|\phi|\ll1$. Various nonlinear effects were neglected. In particular, as discussed in Sec. II.C, as the plasma wave amplitude increases the plasma wave period increases. Since the period of the beat wave is fixed, whereas the period of the plasma wave is increasing, the plasma wave will eventually become out of phase with the laser beat wave. This resonant detuning of the plasma wave from the beat wave will limit the amplitude of the plasma wave (Rosenbluth and Liu, 1972).

The nonlinear dynamics of the beat wave generation in one dimension with $\omega_p^2/\omega^2\ll1$ can be examined using the nonlinear Poisson equation [Eq. (20)]. Analysis of Eq. (20) indicates that the nonlinear plasma wavelength is $\lambda_{Np}=(4/k_p)(1+\phi_s)^{1/2}E_2(\varrho)$, where ϕ_s is the maximum amplitude of the plasma wave, $\varrho^2=1-(1+\phi_s)^{-2}$, and E_2 is the complete elliptic integral of the second kind. In the limit $\phi_s^2\ll1$, $\lambda_{Np}\simeq\lambda_p(1+3\phi_s^2/16)$, which indicates that the nonlinear plasma wavelength increases as the plasma wave amplitude increases. Hence, in the limit $\phi_s^2\ll1$, the nonlinear plasma wave number is

$$k_{Np}\simeq k_p(1-3\phi_s^2/16). \tag{40}$$

The detuning and saturation of the plasma wave can be estimated as follows. The growth of the plasma wave will stop when the phase difference between the laser beat wave and the plasma wave is $\pi/2$, i.e., $\int d\zeta(k_p-k_{Np})\simeq\pi/2$. Using the linear result for the plasma wave amplitude, $\phi_s=a_1a_2k_p|\zeta|/4$, yields a detuning distance $L_t=(2\pi/a_1^2a_2^2)^{1/3}4/k_p$. Hence, the plasma wave amplitude will saturate after a distance L_t behind the front of the laser pulse, which gives a plasma wave amplitude of $\phi_{\rm sat}=(2\pi a_1a_2)^{1/3}=E_{\rm sat}/E_0$. A more careful derivation (Rosenbluth and Liu, 1972) of resonant detuning yields a maximum value of the electric field at saturation of

$$E_{\rm sat}/E_0=(16a_1a_2/3)^{1/3}, \tag{41}$$

which assumes that the laser beat frequency is exactly equal to the ambient plasma frequency $\Delta\omega=\omega_p$. Saturation occurs because the plasma wave period increases as the wave grows. Hence, to partly compensate for the increasing nonlinear plasma period, the plasma wave can be driven to higher amplitudes by using a laser beat period that is slightly longer (Tang *et al.*, 1985). In other words, the beat frequency is slightly detuned such that $\Delta\omega<\omega_p$. Tang *et al.* (1985) showed that the optimum detuning, which maximizes the plasma wave amplitude at saturation, is

$$\Delta\omega_{\rm opt}/\omega_p=1-(9a_1a_2)^{2/3}/8. \tag{42}$$

This gives a maximum saturation amplitude of

$$E_{\rm sat}/E_0=4(a_1a_2/3)^{1/3}. \tag{43}$$

The above results are valid in the limit of weak pump amplitudes $a_1a_2\ll1$ for which the plasma wave is driven to saturation over a large number of beat periods. In the highly nonlinear regime, $a_1a_2\gtrsim1$, however, the same general concepts apply to beat wave generation, i.e., the beat wave amplitude is limited by the increasing nonlinear plasma wavelength and the beat wave amplitude can be optimized by increasing the beat wave period such that $\Delta\omega<\omega_p$. To illustrate this, Eq. (20) is solved numerically (Umstadter *et al.*, 1995) for a laser beat wave consisting of four beat periods, as shown in Fig. 10. The amplitudes of the lasers are $a_1=a_2=a_0$, with $a_0=1.2$, and linear polarization is assumed, such that $(a_1a_1)_s=a_0^2/2$, where the subscript s refers to an averaging over the fast laser period. The ambient plasma density is $n_0=10^{16}$ cm^{-3} ($\lambda_p=330$ μm). The case $\Delta\omega=\omega_p$ is shown in Fig. 10(a), and it is clear that the plasma wave amplitude saturates (reaches maximum amplitude) after just the second beat pulse. The effect of the third and fourth beat pulses is to drive the plasma wave down to a low amplitude. In Fig. 10(b) the beat period has been optimized numerically such that the plasma wave amplitude after the fourth beat pulse is maximized, i.e., the beat period is increased $\Delta\omega<\omega_p$ such that the length of the beat pulse is closer to the final nonlinear plasma wavelength λ_{Np}. This results in a dramatic increase in the final

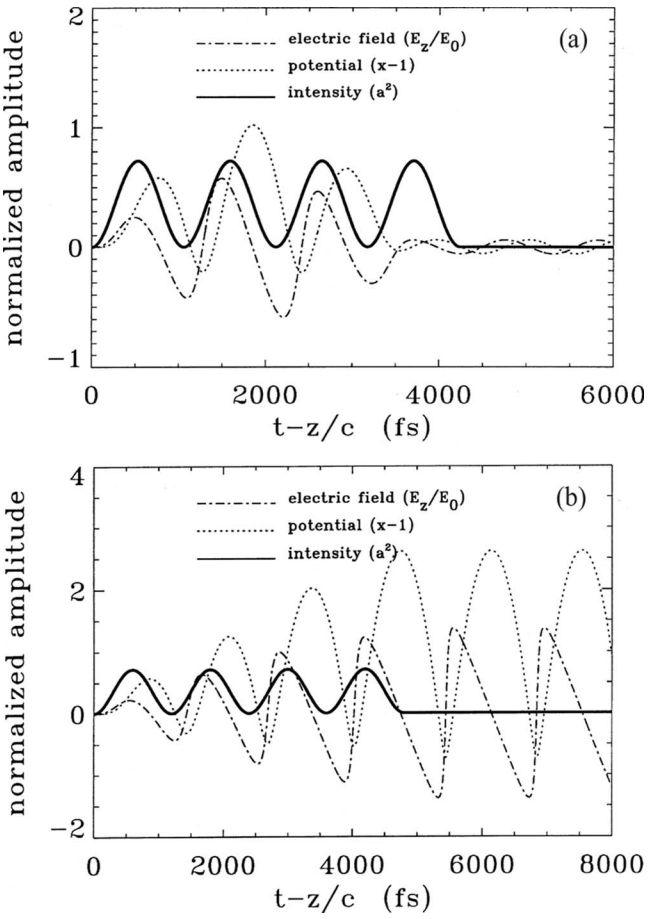

FIG. 10. Examples of PBWA consisting of four beat pulses with $a_0=1.2$ in a plasma of density $n_0=10^{16}$ cm^{-3} (Umstadter *et al.*, 1995): (a) without optimization $\Delta\omega=\omega_p$, showing the effects of detuning, and (b) with optimization $\Delta\omega<\omega_p$. Normalized intensity profile a^2 (solid curve), wake potential ϕ (dotted curve), and axial field E_z/E_0 (dashed curve) vs $t-z/c$. Pulses are linearly polarized (moving to the left).

amplitude of the plasma wave electric field, $E_{\max}\simeq 1.4$ $E_0=13$ GV/m, in comparison to the $\Delta\omega=\omega_p$ case.

The resonant detuning can be overcome by chirping the lasers to compensate for the change in nonlinear plasma wavelength (Deutsch *et al.*, 1991), resulting in a significant increase in the plasma wave amplitude. A modified version of the PBWA based on autoresonant phase locking of the plasma wave to the slowly chirped beat frequency of the driving lasers has also been proposed (Lindberg *et al.*, 2004, 2006). This autoresonant method allows plasma wave amplitudes beyond the detuning limit and is relatively insensitive to variations in plasma and laser parameters.

In addition to resonant detuning, the plasma wave amplitude in the PBWA can be limited by laser-plasma instabilities. Experiments at Ecole Polytechnique observed saturation of the beat-generated plasma wave by a parametric coupling to ion waves (Amiranoff *et al.*, 1992). In general, since the laser pulse lengths in the PBWA are long, $L>\lambda_p$, the pulses are subject to various laser-plasma instabilities, which are discussed in Sec. VI.

The observation of plasma wave generation in the PBWA via Thomson scattering was first demonstrated by Clayton *et al.* (1985) and later observed by several groups (Amiranoff *et al.*, 1992; Kitagawa *et al.*, 1992; Clayton *et al.*, 1993). Acceleration of background plasma electrons in the PBWA was first observed by Kitagawa *et al.* (1992) using two lines of a CO_2 laser in a plasma of density 10^{17} cm^{-3}. Plasma electrons were trapped and accelerated to an energy in excess of 10 MeV. A plasma wave amplitude of $\delta n/n_0=0.05$ was observed and an acceleration gradient of 1.5 GV/m was estimated. Clayton *et al.* (1993) observed electron acceleration in a series of PBWA experiments preformed at the University of California at Los Angeles (UCLA) using two lines of a CO_2 laser in a plasma of density 9×10^{15} cm^{-3}. A 28 MeV energy gain was observed using a 2 MeV injected electron bunch, corresponding to a gradient of 2.8 MV/m and a plasma wave amplitude of $\delta n/n_0=0.28$. The UCLA experiments were particularly well diagnosed and various laser-plasma interaction phenomena and instabilities have been observed (Leemans *et al.*, 1991, 1992b; Everett, Lal, Clayton, *et al.*, 1995a). In experiments at Ecole Polytechnique, Amiranoff *et al.* (1995) observed acceleration in a PBWA experiment using two Nd laser lines in a plasma of density 10^{17} cm^{-3}. The energy of a 3.4 MeV injected electron bunch was observed to increase by 1.4 MeV. A plasma wave amplitude of 2% and a gradient of 0.6 GV/m were observed. Plasma wave saturation and parametric coupling to ion waves were also observed in these experiments (Amiranoff *et al.*, 1995). Nonresonant beat wave excitation has also been explored as a method for operating at higher plasma densities (Filip *et al.*, 2004). Extended laser-plasma interaction lengths have been achieved in PBWA experiments through plasma-channel generation (Tochitsky *et al.*, 2004), resulting in enhanced energy gain of injected electrons.

Parametric excitation of plasma waves by counterpropagating lasers has also been explored analytically (Shvets *et al.*, 2002). For example, plasma wave generation via four-wave mixing is possible: two copropagating laser pulses detuned by ω_p interact with a counterpropagating laser, driving two slow phase velocity waves, and the beating of these slow waves (a superbeat wave) drives a fast plasma wave for acceleration. A variation in this scheme is to replace the two detuned copropagating lasers with a single frequency ultrashort resonant laser pulse (Shvets *et al.*, 1999). The laser intensities required for a given accelerating gradient can be smaller for the counterpropagating geometry compared to those required for the PBWA.

C. Multiple laser pulses

In the previous section discussing the PBWA, it was pointed out that (i) the laser beat wave acted in effect as a series of short laser pulses, (ii) as the plasma wave grew the plasma period increased, which led to a loss of resonance with respect to the laser beat pulses, and (iii)

the beat period, i.e., the width of the beat pulses, could be adjusted and optimized to maximize the plasma wave amplitude. These general principles can be extended to describe plasma wave generation by a series of short laser pulses (Berezhiani and Murusidze, 1992; Nakajima, 1992; Bonnaud *et al.*, 1994; Dalla and Lontano, 1994; Umstadter *et al.*, 1994). For example, the resonant laser-plasma accelerator (Umstadter *et al.*, 1994) uses an optimized train of short laser pulses to drive a plasma wave, in which the width of each pulse and the spacing between pulses are independently controlled. By optimizing the pulse widths and interpulse spacings, resonance with the plasma wave can be maintained and saturation of the plasma wave by resonant detuning can be eliminated. A sequence of m pulses is optimized when the pulse widths and spacings are chosen to maximize the plasma wave amplitude.

For square pulses in the linear regime ($a^2 \ll 1$ and $E_{\max}/E_0 \ll 1$), the optimum pulse train consists of m identical pulses, each of width $L=\lambda_p/2$ and separated by a distance $(2\ell+1)\lambda_p/2$, where ℓ is an integer. The plasma wave amplitude will be m times the single pulse value, $E_{\max}/E_0 = ma_0^2$. This result neglects nonlinear effects. In particular, as the nonlinear plasma wavelength increases, resonant detuning will eventually saturate the plasma wave amplitude.

In the nonlinear regime, however, resonance can only be maintained by optimizing both the pulse widths and spacings of each individual pulse. In the 1D limit with $\omega_p^2/\omega^2 \ll 1$, this can be examined by solving Eq. (20). For square pulse profiles, analytic solutions can be obtained. It can be shown (Umstadter *et al.*, 1994, 1995) that the optimal width of the mth pulse L_m, the nonlinear wavelength λ_{Nm} of the wake behind the mth pulse, and the electric field amplitude E_{zm} of the wake behind the m pulse are

$$L_m = (2/k_p)x_m^{1/2}E_2(y_m), \tag{44}$$

$$\lambda_{Nm} = (4/k_p)x_m^{1/2}E_2(\hat{y}_m), \tag{45}$$

$$E_{zm}/E_0 = x_m^{1/2} - x_m^{-1/2}, \tag{46}$$

where $x_m = \gamma_{\perp 1}^2\gamma_{\perp 2}^2\cdots\gamma_{\perp m}^2$, $\gamma_{\perp m}^2 = 1+a_m^2$, a_m is the amplitude of the mth pulse, E_2 is the complete elliptic integral of the second kind, $y_m^2 = 1-\gamma_{\perp m}^2 x_m^{-2}$, and $\hat{y}_m^2 = 1-x_m^{-2}$. The optimal spacing between the end of the mth pulse and the beginning of the $(m+1)$th pulse is given by $(2\ell+1)\lambda_{Nm}/2$ (ℓ an integer). The maximum normalized electric field of the wake $E_{\max}/E_0$, for an optimized train of m square pulses of equal amplitudes $a_m = a_0$, is plotted in Fig. 11 versus the quantity $a_T^2 = ma_0^2$ (Umstadter *et al.*, 1994, 1995). The curves show the results for 1, 3, 4, 10, and 100 pulses. In the linear regime, $E_{zm} = mE_{z1} = ma_0^2E_0$, i.e., these curves are just straight lines. Figure 11, however, shows that in the nonlinear regime m pulses are more efficient than the linear result, i.e., $E_{zm} > mE_{z1}$. In the highly nonlinear regime, this enhancement can be quite dramatic. Furthermore, Fig. 11 indicates that just a few optimized square pulses are far more efficient than a single pulse.

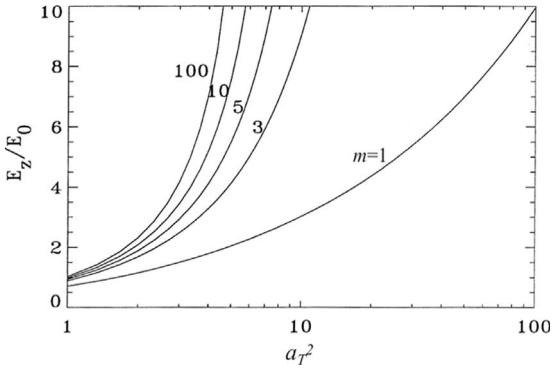

FIG. 11. Maximum electric field amplitude E_z/E_0 vs $a_T^2 = ma_0^2$ for $m=1$, 3, 5, 10, and 100 optimized square laser pulses with $a_0=1$.

For square pulse profiles, both the width of the pulse and the spacing between pulses increase for subsequent pulses in the train since the nonlinear wavelength of the plasma wave is increasing. For more realistic pulse profiles, this is not necessarily the case. Consider the electric field envelope of each pulse modeled by a half period of a sine function, e.g., $a = a_1 \sin(\pi\zeta/L_1)$, with $0 < \zeta < L_1$, for the first pulse. The result from a numerical optimization (Umstadter *et al.*, 1994, 1995) of Eq. (20) for a train of four sine pulses is shown in Fig. 12. Here the plasma density is $n_0 = 10^{16}$ cm^{-3} and the pulses are linearly polarized with equal amplitudes $a_m = a_0 = 1.2$. Notice that the pulse width is decreasing, i.e., the width of the first pulse is 940 fs, whereas the width of the fourth laser pulse is 200 fs. From Fig. 12, it can be seen that the pulses are optimized when they reside in the region of the plasma wave for which $\phi < 0$ and $d\phi/d\zeta < 0$, where $\zeta = z-ct$. This is the phase region of the plasma wave for

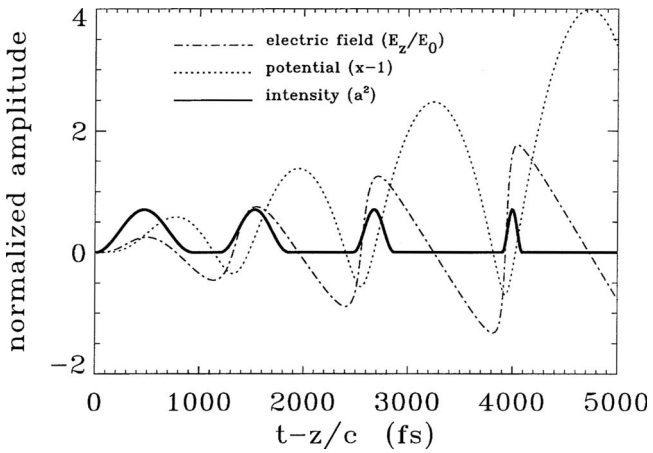

FIG. 12. Laser pulse train consisting of four optimized sine-shaped laser pulses with $a_0=1.2$ and $n_0=10^{16}$ cm^{-3}. Normalized intensity profile a^2 (solid curve), wake potential ϕ (dotted curve), and axial field E_z/E_0 (dashed curve) are plotted vs the comoving variable $t-z/c$ (Umstadter *et al.*, 1995). Pulses are linearly polarized (moving to the left).

which the laser pulse drives the plasma wave most efficiently. As in the square wave case, λ_{Nm}, and thus the spacing between pulses, increases with each succeeding pulse. For this example, the total laser fluence for the pulse train is $I\tau_{\rm tot}=2.2$ MJ/cm^2 and the final accelerating field is $E_{\max}\simeq 1.9\ E_0=18$ GV/m.

D. Self-modulated laser wakefield accelerator

In the previous section it was described how a train of laser pulses can be used to generate a large amplitude wakefield. Under appropriate conditions, however, it is possible for a single long laser pulse to break up into a train of short pulses, each of these short pulses having a width on the order of λ_p. Associated with the break up of the long pulse and the formation of the pulse train is a large amplitude plasma wave. This process is referred to as self-modulation (Joshi *et al.*, 1981; Andreev *et al.*, 1992; Antonsen and Mora, 1992; Sprangle *et al.*, 1992; Esarey, Sprangle, *et al.*, 1993; Coverdale *et al.*, 1995; Modena *et al.*, 1995; Nakajima *et al.*, 1995; Moore *et al.*, 1997; Wagner *et al.*, 1997; Gordon *et al.*, 1998; Leemans *et al.*, 2001, 2002; Malka *et al.*, 2001; Chen *et al.*, 2004). Physically, self-modulation occurs from the plasma wave producing periodic regions of enhanced focusing and diffraction (Esarey *et al.*, 1994). The self-modulation instability resembles a 2D version of a near-forward Raman instability. Forward Raman scattering occurs simultaneously, adding to the modulation, and in the 1D limit, pulse modulation can occur via Raman forward scattering alone (Mori *et al.*, 1994).

The process by which a plasma wave can modulate a laser pulse by producing periodic regions of enhanced focusing and diffraction was first described by Esarey and Ting (1990). The self-modulation of relativistically guided laser pulses was first observed in the fluid simulations of Andreev *et al.* (1992), Antonsen and Mora (1992, 1993), and Sprangle *et al.* (1992). Krall *et al.* (1993) simulated a self-modulated LWFA, including the acceleration of an injected electron bunch, and showed that this configuration can have certain advantages over the standard LWFA. The self-modulation instability was subsequently analyzed by Andreev *et al.* (1994, 1995) and Esarey *et al.* (1994) and, in the 1D limit, Raman forward scattering was analyzed by Mori *et al.* (1994). Extensive PIC simulations of short intense pulses propagating in the high-density regime have been carried out by Decker *et al.* (1994) and Bulanov *et al.* (1995).

To operate in the self-modulated regime (Antonsen and Mora, 1992, 1993; Sprangle *et al.*, 1992; Esarey, Sprangle, *et al.*, 1993; Krall *et al.*, 1993; Andreev *et al.*, 1994, 1995; Esarey *et al.*, 1994) it is desirable that (i) the pulse length be long compared to the plasma wavelength, $L>\lambda_p$, and (ii) the pulse power to be larger than the power required to guide a long laser pulse, $P>P_c(1-\Delta n/\Delta n_c)$. Here $P_c=17(\omega/\omega_p)^2$ GW is the critical power required for relativistic optical guiding, Δn is the depth of a preformed parabolic density channel (if present), $\Delta n_c=1/\pi r_e r_0^2$ is the critical channel depth, and r_e is the classical electron radius. The optical guiding of laser pulses by relativistic effects and density channels will be discussed in the Sec. V. In the remainder of this section, it will be assumed that the laser pulse is propagating in an initially uniform plasma ($\Delta n=0$). Since $\lambda_p \propto n_0^{-1/2}$ and $P_c\propto n_0^{-1}$, for fixed laser parameters, the conditions $L>\lambda_p$ and $P>P_c$ can usually be satisfied by operating at a sufficiently high plasma density.

Consider the generation of plasma wakefields with a 300 fs ($L=90\ \mu$m) laser pulse of wavelength $\lambda=1\ \mu$m and power $P=10$ TW. To operate in the standard LWFA configuration, $L\simeq\lambda_p$ implies a density of $n_0\simeq 1.4\times 10^{17}$ cm^{-3}. At this density $P\ll P_c\simeq 140$ TW and the effects of relativistic guiding are unimportant. To operate in the self-modulated regime, it is desirable that $L>\lambda_p$ and $P>P_c$. Choosing a plasma density such that $P=1.5P_c$ implies $n_0\simeq 2.8\times 10^{18}$ cm^{-3} and $L\simeq 4.5\lambda_p$. Hence, for this laser pulse, the self-modulated regime can be reached by increasing the plasma density by a factor of 20 compared to the standard LWFA configuration. Furthermore, the corresponding energy gain, for fixed interaction length, can be enhanced by nearly a factor of 10 compared to the standard LWFA configuration, as is indicated by simulations discussed below.

The advantages of the self-modulated LWFA over the standard LWFA are simplicity and enhanced acceleration. Simplicity in that a matching condition of $L\simeq\lambda_p$, a preformed density channel, or special pulse tailoring are not required. Enhanced acceleration is achieved for several reasons. (i) The self-modulated LWFA operates at higher density, hence a larger wakefield will be generated since $E_z\propto\sqrt{n_0}$, as indicated by Eq. (11). (ii) Since $P>P_c$, the laser pulse will tend to focus to a higher intensity, thus increasing a_0 and E_z. (iii) The wakefield is resonantly excited, i.e., excited by a series of beamlets as opposed to a single pulse as in the standard LWFA. (iv) Relativistic optical guiding allows the modulated pulse structure to propagate for several Rayleigh lengths, thus extending the acceleration distance. The disadvantages of the self-modulated LWFA are (i) at higher densities the laser pulse group velocity (approximately equal to the plasma wakefield phase velocity) decreases and, hence, electron dephasing from the plasma wakefield can limit the acceleration distance, (ii) broad energy spread electron bunches are typically produced due to continual trapping and short dephasing lengths compared to the laser propagation distances (see Sec. IV.B), and (iii) the modulated pulse structure eventually diffracts.

The properties of the self-modulated LWFA are illustrated by the following fluid simulations (Krall *et al.*, 1993). For fixed laser pulse parameters, two cases will be considered: (1) a standard LWFA in which $L\simeq\lambda_p$ and $P<P_c$ and (2) a self-modulated LWFA, in which $L>\lambda_p$ and $P>P_c$. The laser parameters for both these cases are identical: a Gaussian axial intensity profile with a pulse length $L=90\ \mu$m (300 fs), $\lambda=1\ \mu$m, $a_0=0.7$, $r_0=31\ \mu$m (in vacuum, which corresponds to $Z_R=3$ mm), $P=10$ TW, and a pulse energy of 1.5 J. The simulation

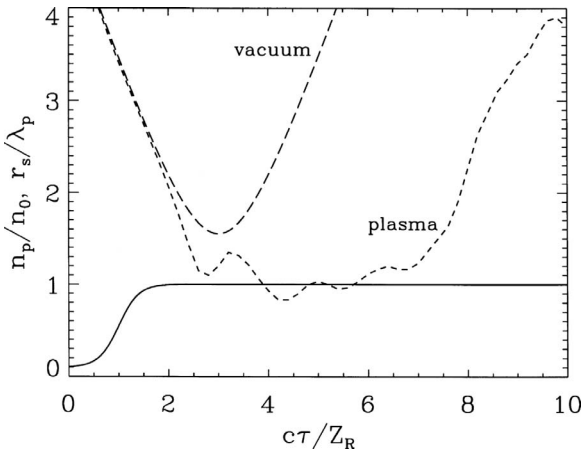

FIG. 13. Ambient plasma density n_p/n_0 (solid curve) and spot size r_s/λ_p (dashed curve) vs normalized propagation distance $c\tau/Z_R$ for a self-modulated LWFA with $n_0=2.8\times10^{18}$ cm^{-3}. Laser is initially converging such that the minimum spot size in vacuum is reached at $c\tau=3Z_R$. From Krall *et al.*, 1993

begins at $t=0$ as the laser pulse enters the plasma, initially converging such that in vacuum it would focus to a minimum spot size of $r_0=31$ μm at $ct=3Z_R$. The plasma density is initially increasing, reaching full density at $ct=2Z_R$. The simulation continues until $ct=10Z_R=3$ cm. In both cases, the acceleration and trapping of a continuous electron beam with initial energy of 3 MeV and normalized emittance $\varepsilon_n=130$ mm mrad are considered.

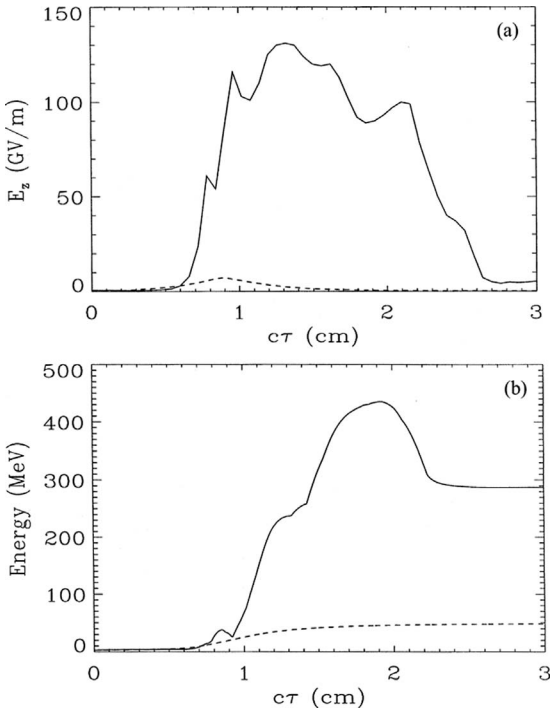

FIG. 14. Standard LWFA (dashed curve) with $n_0=1.4\times10^{17}$ cm^{-3} and the self-modulated LWFA (solid curve) with $n_0=2.8\times10^{18}$ cm^{-3}: (a) Peak accelerating field and (b) peak energy of the injected particles vs propagation distance $c\tau$. From Krall *et al.*, 1993.

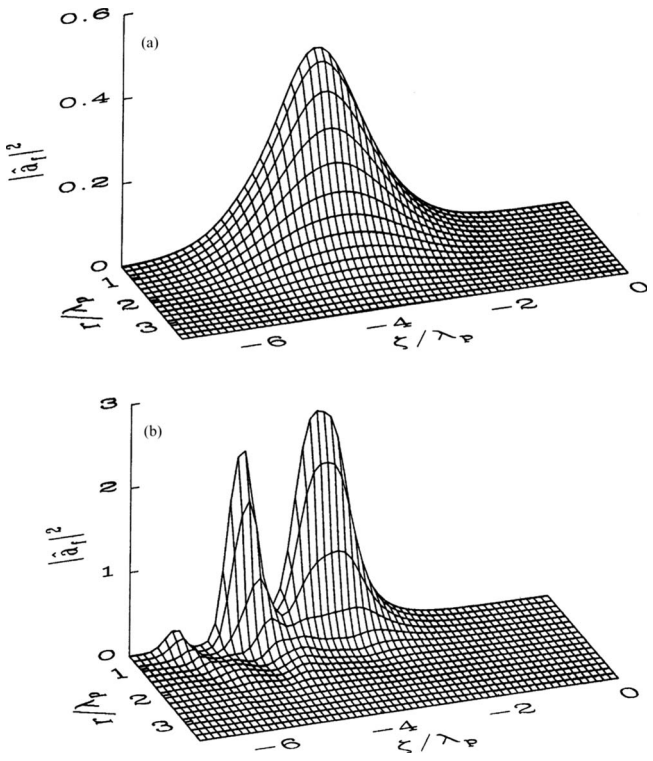

FIG. 15. Normalized laser intensity $|a|^2$ for the self-modulated LWFA case at (a) $c\tau=2Z_R$ and (b) $c\tau=3.2Z_R$. Laser pulse is moving to the right. From Krall *et al.*, 1993

The electron beam is initially converging such that in vacuum it would focus to a minimum rms radius $r_b=200$ μm at $ct=3Z_R$. With such a large initial emittance, only a small fraction ($\sim1\%$) of the particles will be trapped and accelerated.

For the standard LWFA, case (1), the requirement $L=\lambda_p=90$ μm implies a density of $n_0=1.4\times10^{17}$ cm^{-3}. At this density, $P\ll P_c=140$ TW, such that relativistic guiding effects are unimportant. The presence of the plasma has little effect on the evolution of the laser pulse, which reaches a peak intensity of $|a|^2=0.56$ at $ct=3Z_R$. The evolution of the spot size (Fig. 13) is very close to vacuum diffraction. This is also evident in Fig. 14(a) (dashed line), where the peak accelerating field, plotted versus time, is symmetric about the focus, $ct=3Z_R$. After $ct=10Z_R=3$ cm, a small fraction ($\sim0.1\%$) of the test electron beam particles have been trapped and accelerated. At $ct=2$ cm, the peak particle energy is 48 MeV, which implies an average acceleration of 2.4 GeV/m, as shown in Fig. 14(b) (dashed line).

For the self-modulated LWFA, case (2), the density is increased such that $P=1.5P_c=10$ TW, which implies $n_0=2.8\times10^{18}$ cm^{-3}, which is 20 times higher than in case (1). At this density $L>\lambda_p=20$ μm, i.e., the laser pulse now extends over $\simeq4.5\lambda_p$. Figure 15 shows the laser intensity at (a) $ct=2Z_R$ and (b) $ct=3.2Z_R$. The axial electric field and the plasma density response on axis at $ct=3.2Z_R$ are shown in Figs. 16(a) and 16(b), respectively. The laser pulse has become modulated (three peaks are observable, separated by λ_p) and the plasma wave is

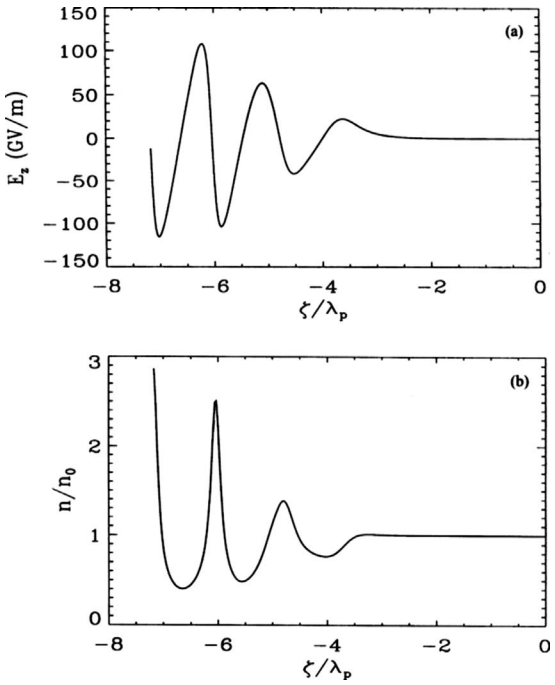

FIG. 16. Self-modulated LWFA case. (a) Axial electric field E_z and (b) normalized plasma electron density n/n_0 vs ζ at $c\tau = 3.2Z_R$. From Krall *et al.*, 1993.

highly nonlinear. In addition, relativistic optical guiding effects have focused the laser to a much higher intensity than was observed in case (1). The evolution of the laser spot size is shown in Fig. 13 indicating that the pulse has focused to a smaller spot size and remains guided over $\simeq 5.5Z_R$. A plot of the peak accelerating field versus time [Fig. 14(a) (solid line)] shows that the highly nonlinear fields persist as the laser pulse is optically guided. A maximum accelerating field of $\simeq 130$ GV/m was obtained. Because of the larger fields, a greater fraction (2%) of the test electron beam particles were trapped and accelerated. The peak particle energy of 430 MeV is observed at $ct = 6Z_R = 1.8$ cm. At $ct = 10Z_R = 3$ cm, however, the peak particle energy has dropped to 290 MeV due to the reduced group velocity of the laser pulse, which causes the electrons to slip out of phase with the wakefield and become decelerated. Figure 14(b) (solid line) shows acceleration to 430 MeV over 1.8 cm that gives an average gradient of 24 GeV/m. This is an order of magnitude increase compared to the standard LWFA of case (1). In the above fluid simulations, the excited plasma wave was below wave breaking $E < E_{WB}$, and an externally injected electron bunch was used. However, in the experiments discussed below, it is possible to drive the plasma wave in the self-modulated regime to the wave breaking field, resulting in copious amounts of self-trapped electrons, albeit with large energy spread.

Evidence for plasma wave generation in the high-density self-modulated regime was first detected by Coverdale *et al.* (1995). The presence of a plasma wave leads to the generation of Stokes and anti-Stokes lines in the frequency spectrum of the pump laser pulse. The first two anti-Stokes lines were observed by Coverdale *et al.* (1995), the appearance of which were correlated with production of fast electrons, as discussed below. Subsequently, multiple anti-Stokes lines in the forward spectrum of the pump laser have been observed by several others (Modena *et al.*, 1995; Ting *et al.*, 1996; Wagner *et al.*, 1997). The plasma wave generation in the self-modulated regime has been measured via coherent Thomson scattering with a frequency-doubled probe pulse (Le Blanc *et al.*, 1996; Ting *et al.*, 1996). The evolution of the plasma wave was observed by varying the time delay between the pump and probe pulses. Evidence for self-channeling and plasma wave excitation over the length of the channel (4 mm or $\approx 12Z_R$) has also been measured via 90° Thomson scattering (Clayton *et al.*, 1998).

Joshi *et al.* (1981) detected fast electrons in an early experiment via forward Raman scattering. A single, long (700 ps), CO_2 laser pulse of modest intensity (10^{15} W/cm^2) interacting with a thin carbon foil was observed to produce 1.4 MeV electrons. Electron acceleration in the high-density self-modulated regime has been observed using ultrashort pulses ($\lesssim 1$ ps). Nakajima *et al.* (1995) observed electron acceleration to energies $\geqslant 18$ MeV using a 3 TW, 1 ps, 10^{17} W/cm^2 laser pulse in a plasma of density near 10^{19} cm^{-3}. A laser-solid interaction was used to produce a source of injected electrons with energies near 1 MeV. Particle simulations suggested acceleration gradients on the order of 30 GV/m. Coverdale *et al.* (1995) observed 2 MeV electrons, which were trapped and accelerated from the background plasma, when a 600 fs, 5 TW, 8×10^{17} W/cm^2 laser pulse propagated in a plasma of density 2×10^{19} cm^{-3}. The generation of electrons was also correlated with the occurrence of anti-Stokes lines in the laser pulse spectrum, which indicates the presence of a plasma wave. Modena *et al.* (1995) demonstrated the acceleration of self-trapped electrons to energies $\geqslant 44$ MeV (limit of the detector) using a 1 ps, 20 TW, 5×10^{18} W/cm^2 laser pulse in a plasma of density 1.5×10^{19} cm^{-3}. A large flux of electrons was observed (10^6 electrons/MeV at 44 MeV) and the electron signal was correlated to the broadening of the anti-Stokes lines in the laser spectrum. Estimates based on the electron dephasing length imply an acceleration gradient >100 GV/m. Acceleration of self-trapped electrons has also been observed by Wagner *et al.* (1997). The electrons were emitted in a well-collimated bunch in the forward direction (a divergence angle $\simeq 8°$) and the cross section of the bunch resembled the shape of the cross section of the laser at focus. By varying the laser pulse energy, a threshold for electron acceleration was observed near $P \simeq P_c$. Subsequently, others have measured energetic electron production in the self-modulated regime (Moore *et al.*, 1997; Gordon *et al.*, 1998; Leemans *et al.*, 2001; Malka *et al.* 2001). The plasma density dependence on the electron spectra has been studied, and it was confirmed that the maximum energy increased with decreasing plasma density (Malka *et al.*, 2001), providing further evidence of electron acceleration via plasma waves.

Experiments have shown the importance of pulse shape on self-modulation and electron production (Leemans *et al.*, 2002). These experiments compared electron production for laser pulses with slow and fast rise times. For fast rise times the ponderomotive force is larger, resulting in a larger initial plasma wave, which acts as the seed for the self-modulation instability (Schroeder, Esarey, Geddes, *et al.*, 2003). Seeding of self-modulation by ionization-induced wakefields (Mori and Katsouleas, 1992; Fisher and Tajima, 1996) has been studied by Gordon *et al.* (2001), and controlled seeding via ionization-induced wakefields has been demonstrated experimentally (Chen *et al.*, 2004). Experiments and simulations by Malka *et al.* (2002) have explored an intermediate regime between the standard and self-modulated LWFA, in which the laser pulse is only somewhat longer than the plasma wavelength. In this regime, the pulse undergoes significant self-steepening, resulting in enhanced plasma wave generation.

Another process that can contribute to acceleration in the self-modulated regime ($\lambda_p < L$ and $P > P_c$) is "direct laser acceleration" (Pukhov *et al.*, 1999). In this mechanism, it is necessary that the accelerated electrons undergo transverse betatron oscillations. When the betatron frequency ω_β is near the laser frequency in the frame of the accelerated electrons, $\omega \sim 2\omega_\beta \gamma^2/\gamma_\perp^2$, energy can efficiently exchange between the electrons and the transverse laser field. This is the inverse process of the electromagnetic instability responsible for the ion channel laser (Whittum *et al.*, 1990). The transverse betatron oscillations are produced by transverse forces generated by the plasma wake excitation. For example, transverse forces can be generated from the radial structure of the plasma wave ($\phi = \phi_0 \exp(-2r^2/r_0^2)\cos[k_p(z - ct)]$ for a Gaussian laser in the linear regime), from induced quasistatic magnetic fields, or, in the blow-out regime, from the formation of an ion cavity through the expulsion of background plasma electrons by the radial ponderomotive force of the laser. In the blow-out regime the electrons oscillate with the betatron frequency $\omega_\beta \simeq \omega_p/(2\gamma)^{1/2}$ (Esarey *et al.*, 2002). Gahn *et al.* (1999) reported multi-MeV electrons accelerated by a 1.2 TW, 200 fs laser pulse channeling in a high-density (10^{20} cm^{-3}) plasma and attributed the dominant acceleration process to direct laser acceleration.

E. Blow-out regime

In the mildly relativistic wakefield regime ($a^2 < 1$), the wakefield can be described analytically in three dimensions using plasma fluid theory, as in Sec. II.B, which is valid provided that the perturbed fluid quantities remain small (e.g., the perturbed density $|\delta n| < n_0$). In the high-intensity limit ($a^2 \gtrsim 1$), the wakefield can be modeled analytically in the 1D limit (broad pulse $k_p r_0 \gg 1$), as in Sec. II.C. However, for a radially bounded pulse in three dimensions ($k_p r_0 \lesssim 1$) in the high-intensity limit, the wakefield must typically be modeled numerically. For a bounded pulse in three dimensions, as the intensity increases, the wakefield structure can depart significantly from the sinusoidal form described by linear theory. In addition to wave steepening and period lengthening, which occur in the 1D limit, the radial structure of the wake can exhibit nonlinearities. One such effect is that the wave front of the plasma wave can be curved, as described in Sec. II.C. The greater the distance behind the driver, the more severe the curvature becomes, as a result of the nonlinear plasma wavelength being greater on axis (where the wake amplitude is high) than off axis. Another effect is that the laser intensity can be sufficiently high so as to completely expel all plasma electrons from the vicinity of the axis (Mora and Antonsen, 1996; Pukhov and Meyer-ter-Vehn, 2002; Lu, Huang, Zhou, Tzoufras, *et al.*, 2006). This high-intensity 3D regime has been referred to as the blow-out, bubble, or cavitation regime. In addition to electron cavitation, a fraction of the plasma electrons can become self-trapped in the ion cavity and can be accelerated to high energies (Faure *et al.*, 2004; Geddes *et al.*, 2004; Mangles *et al.*, 2004).

This regime of complete expulsion of the plasma electrons from some region about the axis has been studied for both laser (Pukhov and Meyer-ter-Vehn, 2002) and electron beam drivers (Rosenzweig *et al.*, 1991) [referred to as a nonlinear plasma wakefield accelerator (PWFA)]. For electron beam drivers, the blow-out regime was first analyzed by Rosenzweig *et al.* (1991), and, more recently, nonlinear PWFA experiments have been performed at the Stanford Linear Accelerator Center (SLAC) using the 30–40 GeV electron beam to drive plasma waves (Hogan *et al.*, 2000, 2005). In the blow-out regime of the PWFA ($n_b/n_0 > 1$, $k_p\sigma_z < 1$, and $k_p\sigma_r < 1$, where σ_z and σ_r are the axial and radial bunch lengths, respectively), all plasma electrons can be expelled from the vicinity of and immediately behind the driver. The blow-out region of the wake is characterized by an accelerating field that is constant as a function of radius and varies linearly as a function of distance behind the driver and a focusing field that is linear as a function of radius. This regime can have beneficial accelerating properties, e.g., because the focusing forces are linear; the normalized emittance of an accelerated electron bunch will be preserved. In the experiments at SLAC, the blow-out wake has led to an energy gain of more than 40 GeV for a fraction of the electrons in the tail of the bunch (Blumenfeld *et al.*, 2007). The majority of electrons in the body of the bunch lost energy, which represents the energy needed to generate the plasma wave.

The focusing force of the cavitated or blow-out region can be very large. For example, the radial space charge field of a long ion channel is $E_r = E_0(k_p r/2)$ (Rosenzweig *et al.*, 1991). At the edge of an electron beam with radius σ_r, this can be written in convenient units as

$$E_r(\mathrm{MV/m}) \simeq 9.06 \times 10^{-15} n(\mathrm{cm}^{-3}) \sigma_r(\mu\mathrm{m}). \tag{47}$$

This radial force will cause a relativistic electron with $\gamma \gg 1$ to perform betatron oscillations about the axis with a betatron wavelength $\lambda_\beta = (2\gamma)^{1/2}\lambda_p$ (Esarey *et al.*, 2002). The rms radius of a highly relativistic electron bunch will

evolve via $d^2\sigma_r/dz^2+k_\beta^2\sigma_r-\epsilon_n^2/\gamma^2\sigma_r^3=0$, where ϵ_n is the normalized beam emittance, assuming linear focusing forces and neglecting beam space charge, energy spread, and acceleration. Here $k_\beta^2=eE_r/\gamma m_e c^2 r$, e.g., $k_\beta=2\pi/\lambda_\beta=k_p/\sqrt{2\gamma}$ in the blow-out regime. The condition for the bunch to be matched (propagates at constant bunch radius σ_{rm}) in such a focusing channel is $\sigma_{rm}=(\epsilon_n/\gamma k_\beta)^{1/2}$. For example, $n_0=10^{17}$ cm^{-3} ($\lambda_p=100$ μm), $\gamma=1000$, and $\epsilon_n=1$ mm mrad give $\lambda_\beta=4.7$ mm, $\sigma_{rm}=0.86$ μm, and $E_r(\sigma_{rm})=780$ MV/m.

One consequence of betatron motion of a relativistic electron in the plasma focusing fields is the emission of betatron (i.e., synchrotron) radiation (Wang *et al.*, 2002; Esarey *et al.*, 2002; Kostyukov *et al.*, 2003; Rousse *et al.*, 2004). This radiation is characterized by the betatron strength parameter $a_\beta=\gamma k_\beta r_\beta$, which is analogous to the undulator strength parameter in conventional synchrotrons, where r_β is the betatron orbit amplitude. The radiation frequency on axis is $\omega=2\gamma^2 N_h c k_\beta/(1+a_\beta^2/2)$, assuming $\gamma^2\gg 1+a_\beta^2/2$, where N_h is the harmonic number (Esarey *et al.*, 2002). For $a_\beta^2\ll 1$, emissions occur primarily at $N_h=1$. For $a_\beta^2\gg 1$, emission occurs in a multitude of harmonics with the maximum intensity occurring near the critical harmonic $N_c\simeq 3a_\beta^3/4$. Note that a_β varies throughout an electron beam, e.g., an electron propagating along the axis has $r_\beta=0$ and an electron at the beam edge has the maximum r_β. As the beam radiates, the mean energy decreases and the normalized energy spread can increase (Michel, Schroeder, *et al.*, 2006). For plasma accelerators, a_β can be large and the radiation can extend into the hard x-ray regime. Betatron radiation has been observed in the blow-out regime for both electron beam-driven (Wang *et al.*, 2002; Johnson *et al.*, 2006) and laser-driven (Rousse *et al.*, 2004; Ta Phuoc *et al.*, 2006) wakes.

Assuming a spherical ion cavity of radius r_B (centered at $r=0$ and $\xi=0$), moving at relativistic velocities, the axial electric field E_z, radial electric field E_r, and azimuthal magnetic field B_θ within the cavity are (Kostyukov *et al.*, 2004; Lu, Huang, Zhou, Tzoufras, *et al.*, 2006)

$$E_z \simeq (k_p\zeta/2)E_0, \tag{48}$$

$$E_r \simeq (k_p r/4)E_0, \tag{49}$$

$$B_\theta \simeq -(k_p r/4)E_0. \tag{50}$$

The axial electric field is maximum when $\zeta\simeq r_B$. The transverse wakefields are electromagnetic such that the radial focusing force on a highly relativistic electron moving along the axis is $F_r=E_r-B_\theta=(k_p r/2)E_0$, i.e., an effective focusing field given by Eq. (47).

An example of an electron beam driven wake in the blow-out regime is shown in Fig. 17, which shows the spatial plasma density response to an electron beam with energy 0.5 GeV, density $n_b=5n_0$, and rms longitudinal and transverse beam sizes $k_p\sigma_z=k_p\sigma_x=k_p\sigma_y=1/\sqrt{2}$ (Gaussian profiles), propagating in an initially uniform plasma of density $n_0=5\times 10^{17}$ cm^{-3} (the electron beam is moving toward the right). These electron beam parameters are similar to those produced by LPA experiments at Lawrence Berkeley National Laboratory (LBNL) (Leemans, Nagler, *et al.*, 2006). Figure 17 was obtained using a modified version of the PIC code PSC (Ruhl, 2000) in three dimensions using four particles per cell and transverse and longitudinal cell sizes of 0.7 μm. In Fig. 17, the beam has pinched to $n_b\simeq 10n_0$ with $n_b\sigma_r^2$ approximately equal to the initial value. Behind the electron beam, the cavitated region extends out to a radius $k_p r_B\simeq 3$, which is much larger than the electron beam radius and somewhat smaller than that predicted by theory (Lu *et al.*, 2005), $k_b r_B\simeq 2\sqrt{\Lambda_b}\simeq 4.5$, where $\Lambda_b=(n_b/n_0)k_p^2\sigma_r^2=5$.

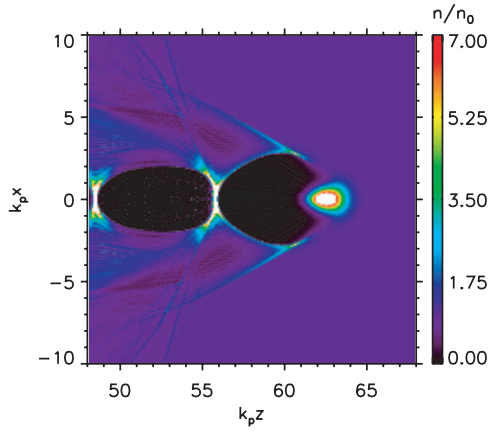

FIG. 17. (Color) Electron density wake from an electron beam with energy 0.5 GeV, peak density $n_b=5n_0$, and rms beam sizes $k_p\sigma_x=k_p\sigma_y=k_p\sigma_z=1/\sqrt{2}$ (Gaussian profiles). The electron beam is moving toward the right with its center located at $k_p z=62.5$ in a plasma of density $n_0=5\times 10^{17}$ cm^{-3}. Numerical parameters: four particles per cell and cell size (in all directions) of 0.7 μm.

For laser drivers, plasma blowout can occur in many regimes, including the long pulse self-modulated regime (Sun *et al.*, 1987; Kurki-Suonio *et al.*, 1989; Sprangle *et al.*, 1992; Mora and Antonsen, 1996) and the short-pulse LWFA regime (Pukhov and Meyer-ter-Vehn, 2002; Kostyukov *et al.*, 2004; Gordienko and Pukhov 2005; Lu, Huang, Zhou, Mori, *et al.*, 2006, 2007; Lu, Huang, Zhou, Tzoufras, *et al.*, 2006). For example, for a long laser pulse with a slowly varying axial profile (Sun *et al.*, 1987), the plasma density profile is determined by balancing the radial ponderomotive force with the space charge force. The plasma density in the long pulse adiabatic limit is then given by

$$n/n_0 = 1 + k_p^{-2}\nabla_\perp^2(1+a^2)^{1/2}, \tag{51}$$

assuming circular polarization. For a Gaussian pulse profile, $a^2=a_0^2\exp(-2r^2/r_0^2)$, the on-axis ($r=0$) density is $n(0)/n_0=1-(4/k_p^2 r_0^2)a_0^2/(1+a_0^2)^{1/2}$. This indicates that complete blowout of the plasma electrons, $n(0)=0$, occurs for a laser intensity satisfying

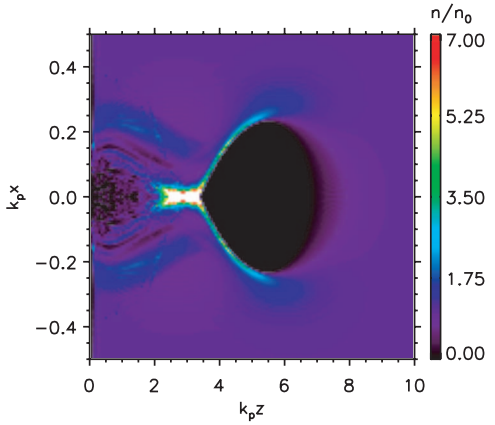

FIG. 18. (Color) Electron density wake driven by a laser pulse with $a_0=0.3$, rms length 68 μm (Gaussian longitudinal profile), and spot size $r_0=10$ μm (Gaussian transverse profile). The laser is moving toward the right (peak located at $k_pz=7$) in a plasma density $n_0=1.2\times10^{16}$ cm^{-3} ($\lambda_p=300$ μm). Numerical parameters: four particles per cell, transverse resolution $dx=dy=0.33$ μm, and longitudinal resolution $dz=3.125$ μm.

$$a_0^2/(1+a_0^2)^{1/2} \geqslant k_p^2 r_0^2/4. \tag{52}$$

In the high-intensity limit $a_0^2 \gg 1$, blowout requires $a_0 \geqslant k_p^2 r_0^2/4$ or, alternatively, a spot size $r_0 \leqslant (2/k_p)\sqrt{a_0}$. To cavitate the electrons out to a larger radius requires larger intensity. For example, a blow-out region of $r=r_0/\sqrt{2}$ requires $a_0=0.82k_p^2r_0^2$, assuming $a_0^2 \gg 5.4$.

For a short ($L \lesssim \lambda_p$) intense ($a^2 \gtrsim 1$) pulse, i.e., an LWFA in the highly nonlinear regime, the generation of a large amplitude wake can occur simultaneously with plasma cavitation in a manner analogous to that of an electron beam driver in the PWFA. Laser cavitation was studied by Mora and Antonsen (1996) for laser intensities in the range $a_0=0.25$–3, spot sizes $k_pr_0=4$–16, and pulses lengths $k_pL \sim 10$ using a quasistatic time-averaged particle code. Mora and Antonsen (1996) observed self-steepening, pulse compression (to $k_pL \sim 2$), self-focused propagation up to $30Z_R$ through an initially uniform plasma, and complete cavitation (blowout) of electrons from the region of the laser pulse with the formation of a highly nonlinear wake. Self-trapping of relativistic particles in the wake was also observed.

An example of a cavitated wake driven by a short laser pulse in the mildly relativistic regime ($a_0^2<1$) is shown in Fig. 18. Figure 18 shows the spatial plasma density response to a linearly polarized laser pulse with $a_0=0.3$, rms length 68 μm, and spot size $r_0=10$ μm (Gaussian spatial profiles), propagating in an initially uniform plasma of density $n_0=1.2\times10^{16}$ cm^{-3} (plasma wavelength $\lambda_p=300$ μm). The laser is moving toward the right (peak laser field located at $k_pz=7$). Figure 18 was obtained using a time-averaged version of the PIC code PSC in three dimensions using four particles per cell, with transverse resolution $dx=dy=0.33$ μm and longitudinal resolution $dz=3.125$ μm. The above laser-plasma parameters satisfy $a_0>k_pr_0/2$, Eq. (52) with $a_0<1$. The radius of the cavitated region behind the laser is $k_pr_B \simeq 0.23$ and is near that of the laser spot size $k_pr_0=0.21$.

Laser blowout with short ($L<\lambda_p$), ultraintense ($a^2 \gg 1$) pulses was studied using PIC simulations and theoretical modeling by Pukhov and Meyer-ter-Vehn (2002) and Lu, Huang, Zhou, Tzoufras, *et al.* (2006). Gordienko and Pukhov (2005) presented a similarity theory in which the wake is characterized by the similarity parameter $S=k_p^2/a_0k^2$. They find that optimal wake generation occurs for a laser spot radius of $k_pr_0 \approx \sqrt{a_0}$, a pulse length $L=c\tau \leqslant r_0$, and a power $P(\mathrm{GW}) > 30[\tau(\mathrm{fs})/\lambda(\mu\mathrm{m})]^2$. Furthermore, they predicted an acceleration length $L_{\mathrm{acc}} \approx 0.7(L/\lambda)Z_R$ and the formation of a quasimonoenergetic electron bunch with energy $W \approx 0.22(L/\lambda)[P(\mathrm{GW})]^{1/2}m_ec^2$. Gordienko and Pukhov (2005) gave simulation examples with $a_0=10$–80. For the $a_0=80$ case (1.5 kJ pulse energy), a quasimonoenergetic electron peak was observed at 12 GeV after a propagation length of 7200λ.

An analytic theory of wake generation in the blow-out regime was also developed by Lu, Hung, Zhou, Tzoufras, *et al.* (2006). In the high-intensity limit ($a_0 \geqslant 4$), they find that wake generation is optimal when the laser spot size satisfies $k_pr_0 \approx 2\sqrt{a_0}$. In this case, they predicted that the dimension of the blow-out region or bubble is approximately a sphere with a radius $r_B \simeq (2/k_p)\sqrt{a_0}$, which is similar to the result obtained from balancing the radial ponderomotive force with the space charge force. The diameter of the bubble is approximately equal to the 1D nonlinear plasma wavelength [Eq. (25)], $\lambda_{Np} \simeq (2/\pi)(E_{\max}/E_0)\lambda_p \simeq (2\sqrt{a_0}/\pi)\lambda_p$, where $E_{\max}$ is the maximum electric field amplitude of the wake. The axial electric field is maximum when $\zeta \simeq r_B$, i.e., from Eq. (48), $E_{\max} \simeq \sqrt{a_0}E_0$. To be in this spherical blow-out regime requires (Lu, Huang, Zhou, Mori, *et al.*, 2006; Lu, Huang, Zhou, Tzoufras, *et al.*, 2006) a laser power $P(\mathrm{GW}) \simeq 21.5(a_0r_B/\lambda)^2$ or $P \simeq (a_0^3/8)P_c$ with $a_0 \gtrsim 4$, where P_c is the critical power for relativistic self-focusing. For laser powers in the range $15 \lesssim P \lesssim 100$ TW, reaching the blow-out regime requires plasma densities in the range $2\times10^{19} \gtrsim n \gtrsim 2\times10^{18}$ cm^{-3} (Lu, Huang, Zhou, Mori, *et al.*, 2006; Lu, Huang, Zhou, Tzoufras, *et al.*, 2006). PIC simulations also indicated that electrons can be self-trapped in the trailing edge of the blow-out region and accelerated up to relativistic energies.

An example of a blow-out wake driven by a short laser pulse in the highly relativistic regime ($a_0^2 \gg 1$) is shown in Figs. 19–21, which shows the spatial plasma density response (Fig. 19) and the spatial profiles of the longitudinal [Fig. 20(a)] and transverse [Fig. 20(b)] electric fields after propagating $\omega_pt=27.7$ (the center of the laser pulse is at $k_pz=17.6$). Also shown are line outs of the longitudinal electric field on axis as a function z [Fig. 21(a)] and the transverse electric field at $k_pz=13$ as a function of x [Fig. 21(b)] at $\omega_pt=27.7$. The initial laser pulse envelope is $a=a_0\exp(-z^2/2L^2)\exp(-r^2/r_0^2)$, with $a_0=5$, $L=4.2$ μm, $r_0=9$ μm, and $\lambda=0.8$ μm. The laser enters the plasma of density $n_0=7\times10^{18}$ cm^{-3} (λ_p

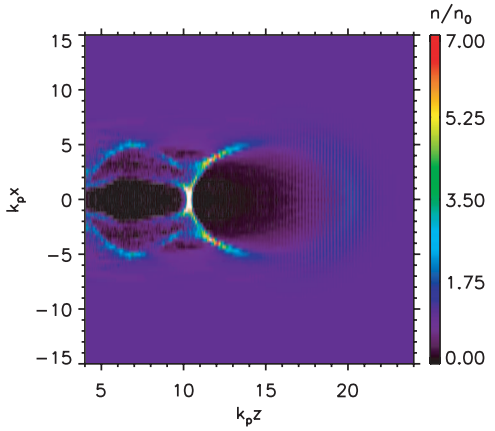

FIG. 19. (Color) Electron density wake at $\omega_p t=27.7$ driven by a laser pulse with an initial envelope given by $a=a_0\exp(-z^2/2L^2)\exp(-x^2/r_0^2)$ with $a_0=5$, $L=4.2$ μm, $r_0=9$ μm, and $\lambda=0.8$ μm. The laser is propagating to the right in a plasma of density $n_0=7\times10^{18}$ cm^{-3}. Numerical parameters: longitudinal cell size $dz=0.03$ μm, transverse cell size $dx=dy=0.7$ μm, and four particles per cell.

$=12$ μm) and propagates to the right. These results were obtained using a modified version of the PIC code PSC in three dimensions with longitudinal cell size $dz=0.03$ μm, transverse cell size $dx=dy=0.7$ μm, and four particles per cell. For these laser-plasma parameters, $k_p r_0\approx 2\sqrt{a_0}$. As can be seen in Fig. 21, near the center of the cavity E_z is approximately a linear function of z and E_x is approximately a linear function of x. Furthermore, the amplitudes of E_z and E_x are comparable, excluding the spike in E_z that occurs near the back of the cavity.

According to the theoretical descriptions of the blow-out regime (Kostyukov *et al.*, 2004; Lu, Huang, Zhou,

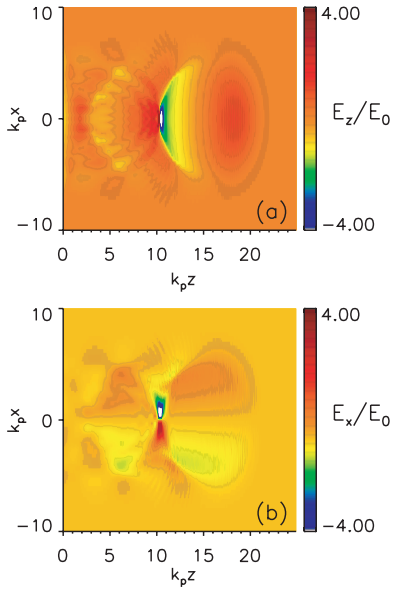

FIG. 20. (Color) Wakefields driven by a laser pulse with $a=0.5$ in the blow-out regime. (a) Longitudinal electric field and (b) transverse electric field, normalized to E_0, as a function of $k_p z$ and $k_p x$, for the parameters of Fig. 19 at $\omega_p t=27.7$.

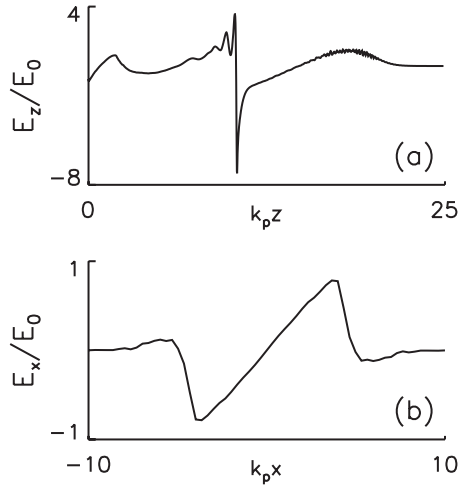

FIG. 21. Lineouts of (a) longitudinal electric field on axis (b) and transverse electric field at $k_p z=13$ for the parameters of Fig. 19 at $\omega_p t=27.7$.

Mori, *et al.*, 2006) the example presented in Figs. 19–21 should produce a near spherical bubble (with radius $k_p r_B\approx 2\sqrt{a_0}=4.5$). From Fig. 19, the cavitated region is elliptical with a blow-out radius of $k_p r_B\simeq 3$ (the peak density $n/n_0\simeq 8$ is at $k_p r\simeq 3.7$) for $k_p z=12$, $k_p r_B\simeq 4$ (the peak density $n/n_0\simeq 2.5$ is at $k_p r\simeq 4.5$) for $k_p z=13$, and a peak density $n/n_0\simeq 1.5$ at $k_p r\simeq 5.5$ (here the blow-out radius is not well defined since the cavity "walls" are becoming broad) for $k_p z=15$. For later times, the laser pulse evolves and distorts leading to a cavitated region with significantly larger dimensions, even though the peak laser intensity is only slightly different than earlier times. One reason that the cavity has expanded is that the laser has steepened and shortened, and even though the peak laser field is approximately the same in Fig. 19, the ponderomotive force is larger due to the larger gradients in the steepened intensity profile. Since the ponderomotive force depends on both the laser intensity amplitude and gradient scale length, so should the properties of the wake, and this behavior is not captured by the simple scaling law $k_p r_B\approx 2\sqrt{a_0}$, which does not include the effect of the laser intensity gradient scale length or the laser pulse length.

Simulations (Kostyukov *et al.*, 2004; Lu, Huang, Zhou, Mori, *et al.*, 2006) also indicate that at later times a trapped and accelerated electron bunch is evident within the blow-out region. These electrons are self-injected near the back of the cavity. The wakefield associated with the trapped bunch can lead to beam loading, which can distort and elongate the blow-out region. Examples of this cavity distortion are presented in Sec. VII.A.

F. Other laser wakefield acceleration regimes

Excitation of large plasma wakefields by laser pulses can be divided roughly in two categories. A "standard" regime in which the laser intensity is sufficiently high ($a_0\gtrsim 1$) and the laser pulse is sufficiently short (or the gradients in the axial intensity profile are sufficiently

short), $L \lesssim \lambda_p$, such that the initial laser pulse profile immediately drives a large plasma wave. In the standard regime, pulse evolution is not required to excite a large wakefield. The other general category is the "self-modulated" regime, typically denoted from the standard regime by longer pulses of lower intensities. In the self-modulated regime, the initial laser profile does not immediately drive a sufficiently large wakefield, and evolution of the laser pulse is necessary to excite a large plasma wave. Pulse evolution is the result of the initial plasma density perturbation acting back on the laser pulse, such as in the case of the forward Raman or self-modulation instabilities. Although, for some intensity ranges, the standard and self-modulated regimes may correspond to short and long pulse regimes, respectively, there are many intermediate regimes in which self-modulation of the laser pulse by the plasma wave is the dominant mechanism, and some of these regimes have been referred to as "pseudo-resonance" (Kimura *et al.*, 2005) or "forced" laser wakefield regimes (Malka *et al.*, 2002). It should be noted that the experimental evidence for the forced laser wakefield regime based on optical spectra is controversial as it was reported that the spectrum blueshifts (Malka *et al.*, 2002) counter to energy conservation (pump depletion) expectations.

The precise evolution of both the laser pulse and the plasma wave, however, depends on the precise laser and plasma parameters. Pulse evolution, via the feedback of the plasma wave on the pulse, will eventually play a significant role in the wakefield evolution in all regimes. Nonlinear effects such as pump depletion and pulse self-steepening will always occur if the laser pulse is allowed to propagate a sufficiently long distance, which affects both the laser profile and the wakefield amplitude.

G. Acceleration limits and scaling laws

Several mechanisms can limit the energy gain in an LPA: laser diffraction, electron dephasing, pump depletion, and laser-plasma instabilities. In vacuum a laser pulse undergoes Rayleigh diffraction, i.e., the laser spot size evolves according to $r_s = r_0(1+z^2/Z_R^2)^{1/2}$, where r_0 is the minimum spot size at the focal point $z=0$ and $Z_R = kr_0^2/2$ is the Rayleigh length. Without some form of optical guiding, the laser-plasma interaction distance will be limited to a few Z_R. Various methods for optical guiding, such as using a plasma density channel, are discussed in Sec. V. Electron dephasing, i.e., a highly relativistic electron outrunning the plasma wave, can limit the energy gain to a dephasing length L_d, as discussed in Sec. II.E. As the laser driver excites a plasma wave, it loses energy, i.e., its pump depletes (Horton and Tajima, 1986; Ting *et al.*, 1990; Bulanov *et al.*, 1992; Teychenné *et al.*, 1994a). The pump depletion length L_{pd} can be estimated by equating the laser pulse energy to the energy left behind in the wakefield, $E_z^2 L_{pd} \simeq E_L^2 L$, where E_L is the laser field.

As an illustration, consider a standard LWFA driven by a linearly polarized square profile laser pulse with $L \simeq \lambda_{Np}/2$ in the 1D limit. The dephasing and pump depletion lengths are given by (Esarey *et al.*, 2004; Shadwick *et al.*, 2009)

$$L_d \simeq \frac{\lambda_p^3}{2\lambda^2} \times \begin{cases} 1 & \text{for } a_0^2 \ll 1 \\ (\sqrt{2}/\pi) a_0/N_p & \text{for } a_0^2 \gg 1, \end{cases} \tag{53}$$

$$L_{pd} \simeq \frac{\lambda_p^3}{\lambda^2} \times \begin{cases} 2/a_0^2 & \text{for } a_0^2 \ll 1 \\ (\sqrt{2}/\pi) a_0 & \text{for } a_0^2 \gg 1, \end{cases} \tag{54}$$

where N_p is the number of plasma periods behind the drive laser pulse. In Eq. (53), the factor of $\lambda_p^3/(2\lambda^2)$ is from requiring a highly relativistic electron (traveling at c) to phase slip by $\lambda_p/4$ (since only $1/4$ of a plasma wave period is both accelerating and focusing). In the $a_0^2 \gg 1$ limit of Eq. (53), the factor $1/N_p$ is from the plasma wave period increasing as the laser pulse steepens, which is the dominant effect in determining the plasma wave phase velocity in the nonlinear limit. Furthermore, it can be shown (Esarey *et al.*, 2004) that, initially, the spatial rate at which the laser pulse energy changes scales as $-1/L_{pd}$ (pump depletion), the rate at which the mean frequency changes scales as $-1/L_{pd}$ (redshifts) and rate at which the mean laser intensity changes scales as $1/L_{pd}$ (pulse steepens).

As an example, consider the linear regime with the parameters $a_0 = 0.3$, $\lambda = 0.8\ \mu$m, and $r_0 = \lambda_p = 33\ \mu$m ($P = 3.3$ TW and $n_0 = 10^{18}$ cm^{-3}). The relevant propagation lengths are $Z_R = 0.43$ cm, $L_d \simeq 2.8$ cm, and $L_{pd} \simeq 1.2$ m, i.e., $Z_R \ll L_d \ll L_{pd}$. Furthermore, since $L_d \propto n_0^{-3/2}$ and $L_{pd} \propto n_0^{-3/2}$, the dephasing length and pump depletion lengths can be increased by operating at lower densities. Since $L \sim \lambda_p$ in the standard LWFA, lower densities correspond to longer laser pulse durations $L \propto n_0^{-1/2}$. In principle, a static magnetic field can be introduced to reduce dephasing (Katsouleas and Dawson, 1983). Use of an active medium has also been proposed as a method for reducing pump depletion (Fisher *et al.*, 1995).

In the linear regime ($a_0^2 \ll 1$), $L_d \ll L_{pd}$ and the electron energy gain is limited by dephasing, not pump depletion, assuming an axially uniform plasma. However, by appropriately tapering the axial plasma density profile, dephasing limitations can be overcome, resulting in a larger single-stage energy gain (Katsouleas, 1986; Sprangle *et al.*, 2001). By slowly increasing the plasma density as a function of propagation distance, the phase velocity of the wakefield can be increased, as is described in Sec. IV.D. In principle, an axial density taper can be found for which $v_p = c$ at some point behind the drive laser pulse. However, slippage between the bunch ($v_e \simeq c$) and the drive laser [$v_g \simeq 1 - \omega_p^2(z)/2\omega^2 < c$] limits the length over which tapering is possible, and infinite densities are eventually required. Injecting a bunch several plasma periods behind the laser will extend the distance over which one can taper. Appropriate tapering may mitigate dephasing such that acceleration will be limited by pump depletion, $L_{pd} \sim (\lambda_p^3/\lambda^2) a_0^{-2}$.

In the nonlinear regime ($a_0^2 > 1$), $L_d \sim L_{pd}$ and no density tapering is needed since the electron energy gain is

limited by pump depletion, not dephasing. In particular, the regime $a_0^2 \sim 1$, such that $L_d \sim L_{pd}$, has advantages over the linear regime. In addition to not requiring density tapering, a single channel-guided stage with $a_0^2 \sim 1$ results in higher accelerating gradients, shorter channel lengths, and efficient depletion of the laser pulse energy while yielding comparable energy gains.

The ideal energy gain in a standard LWFA can be estimated by $\Delta W = eE_z L_{\rm acc}$, where $L_{\rm acc}$ is the acceleration length and $E_z = E_0(a_0^2/2)(1+a_0^2/2)^{-1/2}$ is the maximum electric field amplitude driven by an optimized flat-top, linearly polarized laser pulse in the 1D limit (Esarey *et al.*, 2004; Leemans, Esarey, *et al.*, 2006). If the acceleration distance is limited by diffraction, $L_{\rm acc} \simeq \pi Z_R < L_d, L_{pd}$, the energy gain in practical units is

$$\Delta W_R({\rm MeV}) \simeq 740(\lambda/\lambda_p)(1+a_0^2/2)^{-1/2} P({\rm TW}). \quad (55)$$

If the acceleration distance is limited by dephasing, $L_{\rm acc} \simeq L_d$, the energy gain is

$$\Delta W_d({\rm MeV}) \simeq \frac{630 I({\rm W/cm^2})}{n({\rm cm^{-3}})} \times \begin{cases} 1, & a_0^2 \ll 1 \\ (2/\pi)/N_p, & a_0^2 \gg 1. \end{cases} \quad (56)$$

If the acceleration distance is limited by depletion, $L_{\rm acc} \simeq L_{pd}/2$, the energy gain is

$$\Delta W_{pd}({\rm MeV}) \simeq \begin{cases} 3.4 \times 10^{21}/[\lambda^2(\mu{\rm m}) n({\rm cm^{-3}})], & a_0^2 \ll 1 \\ 400 I({\rm W/cm^2})/n({\rm cm^{-3}}), & a_0^2 \gg 1. \end{cases} \quad (57)$$

These estimates are based on the idealized assumptions stated above and neglect various nonideal effects, such as self-focusing and laser-plasma instabilities. Self-focusing, guiding, and various instabilities are discussed later in this article.

Fluid simulations have been carried out in one and two dimensions for a channel-guided LWFA ($k_p r_0 > 1$) in the standard regime, including the nonlinear evolution of the laser pulse and wake, and the effects of dephasing and depletion (Esarey *et al.*, 2004; Shadwick *et al.*, 2009). It is found that for a Gaussian laser pulse with $k_p L_{\rm rms} = 1$ and $a_0 \simeq 1-2$, the energy gain is $\Delta W_f({\rm MeV}) \simeq 350 I({\rm W/cm^2})/\gamma_\perp n({\rm cm^{-3}})$, where $\gamma_\perp = (1+a_0^2/2)^{1/2}$. The dephasing length is found to be $k_p L_d \simeq C_d(\lambda_p/\lambda)^2$, with $C_d \approx 4$ for $a_0 = 1$ and $C_d \approx 3$ for $a_0 = 2$. As an example, a 40 J laser pulse with $P = 380$ TW, $a_0 = 2$, $\lambda = 0.8$ μm, $r_0 = 53$ μm, and $L_{\rm rms} = 12.5$ μm, propagating in a plasma with $\lambda_p = 80$ μm ($n_0 = 2 \times 10^{17}$ cm^{-3}), produces an energy gain of $\Delta W_f = 10$ GeV over a dephasing length of $L_d = 40$ cm.

The above scaling laws for ΔW_d and ΔW_{pd} apply to an LWFA in the standard configuration ($L \sim \lambda_p$) with a broad laser pulse ($k_p^2 r_0^2 \gg 1$) propagating in a density channel that provides guiding. For sufficiently high powers $P \gg P_c$, it may be possible to guide the laser pulse over multiple Z_R without the use of a density channel due to a combination of relativistic self-focusing and ponderomotive self-channeling. This is the case in the blow-out or bubble regime (Pukhov and Meyer-ter-Vehn, 2002). Assuming that the energy gain is limited by dephasing with $a_0 > 1$ again implies $\Delta W_d({\rm MeV}) \simeq 0.9(k_p r_0)^{-2} P({\rm GW})$, using Eq. (56), only now with the additional constraint $P \gg P_c$.

Scaling laws for the energy gain in the highly nonlinear blowout regime have been obtained through analytical and numerical studies (see also Sec. III.E). For example, Gordienko and Pukhov (2005) obtained $\Delta W_{\rm GP}({\rm MeV}) \simeq 0.1(c\tau_L/\lambda)[P({\rm GW})]^{1/2}$. Alternatively, Lu *et al.* (2007) found $\Delta W_{\rm L}({\rm MeV}) \simeq 0.25(\lambda_p/\lambda)^{4/3}[P({\rm GW})]^{1/3}$. To be in these regimes, however, require pulse lengths $c\tau_L \sim \lambda_p$ and laser powers greater than the critical power for relativistic self-focusing, $P > P_c$. It is interesting to note (Leemans, Esarey, *et al.*, 2006) that by letting $c\tau_L = R_p \lambda_p$ and $P = R_{cr} P_c$, then $\Delta W_{\rm GP}({\rm MeV}) \simeq 0.03 R_p R_{cr}^{-1/2} P({\rm GW})$ and $\Delta W_{\rm L}({\rm MeV}) \simeq 0.04 R_{cr}^{-2/3} P({\rm GW})$. For many regimes of interest, e.g., $R_p \sim 1$ and $R_{cr} \sim 1-10$, $\Delta W_{\rm GP}$ and $\Delta W_{\rm L}$ yield similar results.

Although ΔW is limited by depletion and dephasing for both a channel-guided LWFA or a self-guided LWFA with $P \gg P_c$, there may be additional advantages to using a channel over relying on self-guiding. One obvious difference is that the additional constraint $P \gg P_c$ needs not be satisfied when using a channel. This implies that the channel-guided LWFA may be operated at lower intensities (lower a_0), which may be a more stable regime. The channel may also provide some resistance to instabilities, such as the laser-hose instability. Without a channel, the laser pulse will be subject to some amount of diffractive erosion since the head of the pulse will not be self-guided, which can limit the propagation distance. For example, if the pulse is self-guided for a distance of $L = R_R Z_R$, where $R_R \gg 1$ is the number of Rayleigh lengths, then pulse erosion will limit the energy gain and not dephasing when $R_R Z_R < L_d$ or $R_R(k_p r_0)^3 < 3.8[P({\rm GW})]^{1/2}$ for $q > 1$. Last, it is hoped that by operating a channel-guided LWFA in the "dark-current-free" mode (no self-trapping), a high-quality electron bunch can be obtained by injecting a low energy spread, low emittance bunch into the LWFA, allowing staging of multiple LWFA modules. If the LWFA is to be operated in a highly nonlinear self-guided mode (i.e., the blow-out or bubble regime), it may not be possible to operate in this regime without self-trapping, which may limit the energy spread and emittance of the accelerated bunch.

H. Beam loading

A relativistic charged particle bunch moving through a plasma can excite wakefields in a manner similar to that of an intense laser pulse. For a laser driver, the ponderomotive force expels plasma electrons and initiates a plasma wave (or wake). For a relativistic electron bunch, the space charge force of the bunch (with a relativistically large mass) displaces plasma electrons (with a relativistically lighter mass) and initiates a wake. For a narrow beam ($\sigma_r < \lambda_p$, where σ_r is the transverse

beam size), the larger the charge in the bunch, the larger the wake is. In a plasma-based accelerator, the wake from the accelerated bunch will be out of phase with, and thus reduce, the wake generated by the drive beam. The process by which the wake produced by the accelerated bunch significantly modifies the fields of the accelerating plasma wave is referred to as beam loading. Beam loading can place severe limitations on the beam current that can be accelerated, the quality of the accelerated particle bunch, and the efficiency of the plasma-based accelerator.

The wakefield generated by a relativistic electron bunch moving through a plasma can be calculated using linear perturbation theory of the cold plasma fluid and Maxwell equations (Katsouleas *et al.*, 1987; Keinigs and Jones, 1987; Lu *et al.*, 2005). The normalized density perturbation $\delta n/n_0 < 1$ and normalized axial electric field $E_z/E_0 < 1$ driven in an initially uniform plasma by a short electron bunch (with number density n_b) are given by

$$\left(\frac{\partial^2}{\partial\zeta^2} + k_p^2\right)\frac{\delta n}{n_0} = -k_p^2\frac{n_b}{n_0}, \tag{58}$$

$$(\nabla_\perp^2 - k_p^2)\frac{E_z}{E_0} = -k_p\frac{\partial}{\partial\zeta}\frac{\delta n}{n_0}, \tag{59}$$

assuming the quasistatic approximation and a highly relativistic beam, $\beta_e \simeq 1$, where $c\beta_e$ is the electron bunch velocity. Solving Eqs. (58) and (59) for a cylindrically symmetric beam yields

$$E_z/E_0 = -k_p^3\int_\infty^\zeta d\zeta'\int_0^\infty dr' r'\cos[k_p(\zeta-\zeta')] \times I_0(k_p r_<)K_0(k_p r_>)n_b(r',\zeta')/n_0, \tag{60}$$

where I_0 and K_0 are the zeroth-order modified Bessel functions of the second kind and $r_<$ ($r_>$) denotes the smaller (larger) of r and r', respectively. An electron bunch will excite a plasma wave provided that the length scale of the axial gradients in the bunch profile (e.g., the bunch length) is comparable to or shorter than the plasma period, e.g., $k_p\sigma_z \lesssim 1$, where σ_z is the bunch length. Furthermore, the wakefields from a narrow bunch with radius $\ll k_p^{-1}$ will extend out to a radius $\sim k_p^{-1}$.

For a drive electron bunch with Gaussian axial profile of the form $\rho(\zeta) = n_b\exp(-\zeta^2/2\sigma_z^2)$, the amplitude of the axial electric field is given by

$$E_z/E_0 = (2\pi)^{1/2}(n_b/n_0)k_p\sigma_z\exp(-k_p^2\sigma_z^2/2)H_R. \tag{61}$$

Note that the wakefield amplitude is maximum when $k_p\sigma_z = 1$. Here H_R depends on the radial bunch profile. For a flattop radial profile, $\rho(r) = n_b$ for $r \leqslant r_b$ and zero otherwise,

$$H_R(r) = \begin{cases} 1 - k_p r_b K_1(k_p r_b)I_0(k_p r) & \text{for } r < r_b \\ k_p r_b I_1(k_p r_b)K_0(k_p r) & \text{for } r > r_b \end{cases} \tag{62}$$

with I_1 and K_1 the first-order modified Bessel functions. For a wide beam $k_p r_b \gg 1$, $H_R(0) \simeq 1$ and for a narrow beam $k_p r_b \ll 1$, $H_R(0) \simeq (k_p^2 r_b^2/2)[0.62 - \ln(k_p r_b)]$. Note that for a Gaussian radial profile, $\rho(r) = n_b\exp(-r^2/2\sigma_r^2)$,

$$H_R(0) = (k_p^2\sigma_r^2/2)\exp(k_p^2\sigma_r^2/2)\Gamma(0, k_p^2\sigma_r^2/2) \tag{63}$$

on axis with Γ the incomplete gamma function. Equation (63) reduces to $H_R(0) \simeq (k_p^2\sigma_r^2)[0.058 - \ln(k_p\sigma_r)]$ assuming $k_p\sigma_r \ll 1$.

Particle-in-cell simulations (Lu *et al.*, 2005) indicate that a pseudolinear expression for the wakefield holds as the linear wake transitions into the blow-out regime. Specifically, in the regime $k_p\sigma_z \simeq \sqrt{2}$, $k_p\sigma_r \ll 1$, and $\Lambda_b < 1$, the wakefield is given by the above linear expressions if $n_b/n_0 \leqslant 10$ and by $E_z/E_0 \simeq 1.3\Lambda_b\ln(\Lambda_b/10)^{-1/2}$ if $n_b/n_0 > 10$, with a blow-out radius of $k_p r_B \simeq 2\sqrt{\Lambda_b}$, where $\Lambda_b = (n_b/n_0)k_p^2\sigma_r^2$.

The maximum number of bunch electrons that can be loaded into a small ($\ll \lambda_p$) axial segment of a linear wakefield for acceleration (i.e., the number of electrons required to produce a wakefield that will cancel the accelerating field, which defines the beam loading limit) is (Katsouleas *et al.*, 1987)

$$N_{\max} = \frac{n_0 A_b}{k_p}\frac{E_z}{E_0} \simeq 5\times 10^5\frac{E_z}{E_0}A_b(\mathrm{cm}^2)\sqrt{n_0(\mathrm{cm}^{-3})}, \tag{64}$$

assuming $k_p\sigma_z < 1$ and $E_z/E_0 < 1$, where $A_b \gg \pi/k_p^2$ is the cross-sectional area of the bunch (for $k_p\sigma_r \ll 1$, A_b becomes of order k_p^{-2}). For an unshaped symmetric bunch (e.g., a Gaussian axial profile) containing N electrons, the wake-induced energy spread scales as $N/N_{\max}$ and the efficiency of converting wake energy to electron energy scales as $(N/N_{\max})(2 - N/N_{\max})$. As N approaches $N_{\max}$ the efficiency approaches 100%, but the energy spread becomes large, also approaching 100%.

The energy spread induced on the loaded bunch can be reduced by shaping the bunch profile (Katsouleas *et al.*, 1987). Linear theory predicts that for a bunch with triangular axial profile (high charge in front), the wakefield inside the bunch can be made constant, thus eliminating energy spread. For $N_{\max}(2\cos k_p\zeta_b)^{-1}\sin^2 k_p\zeta_b$ particles in the shaped bunch (of length $k_p^{-1}\tan k_p\zeta_b$), the axial field inside the bunch is $E_z\cos k_p\zeta_b$, and the efficiency is $\sin^2 k_p\zeta_b$, where ζ_b is the phase location of the front of the bunch. For example, if a triangular bunch is loaded at $k_p\zeta_b = \pi/3$ with length $\sqrt{3}/k_p$, then $0.75N_{\max}$ particles can be accelerated by a field of $0.5E_z$ with an efficiency of 75%, and no wake-induced energy spreads. This neglects slippage effects between the bunch and the wakefield and transverse variations in the wakefield, which can lead to finite energy spreads.

Estimates for the beam loading limit have been given for laser-driven wakefields in the blow-out regime (Gordienko and Pukhov, 2005; Lu *et al.*, 2007). For example, Lu *et al.* (2007) found $N_{\max} \simeq (k_p r_B)^3/30k_p r_e$, which gives $N_{\max} \simeq 3.1\times 10^9\lambda_0(\mu\mathrm{m})[P(\mathrm{TW})]^{1/2}$, assuming a blow-out radius of $k_p r_B \simeq 2\sqrt{a_0}$ and a laser spot size $r_0 \simeq r_B$. Notice that a similar result can be obtained from the linear expression for $N_{\max}$ [Eq. (64)] by assuming $A_b \simeq r_B^2$ and

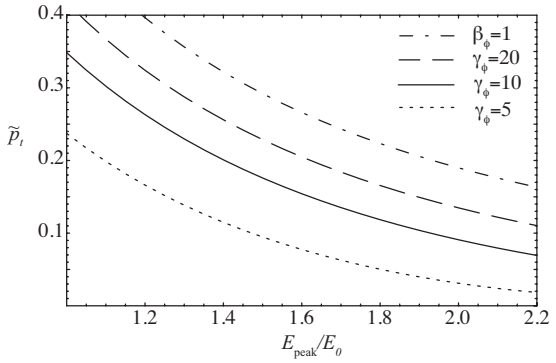

FIG. 22. Initial electron momentum $\tilde{p}_t$ required to be trapped by a plasma wave with field amplitude $E_{\rm peak}/E_0$ and phase velocity $\gamma_p=5$ (dotted curve), $\gamma_p=10$ (solid curve), $\gamma_p=20$ (dashed curve), and $\beta_p=1$ (dash-dotted curve), assuming an initial plasma temperature $\beta_{\rm th}=10^{-2}$.

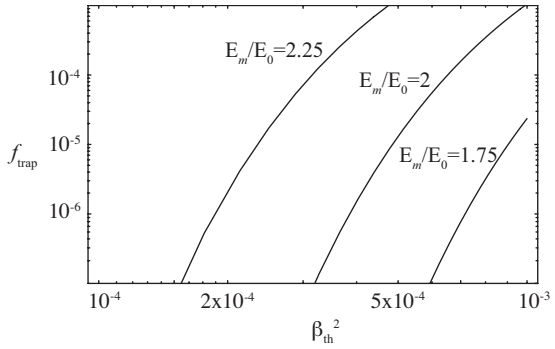

FIG. 23. Fraction of trapped electrons $f_{\rm trap}$ [Eq. (67)] vs the initial temperature of a Gaussian plasma electron distribution $\beta_{\rm th}^2=k_BT_0/mc^2$ for three different nonlinear plasma wave amplitudes driven by a laser with $k_pL_{\rm rms}=1$ and $a_0=3.65$ ($\hat{E}_m\simeq1.75$), $a_0=4.15$ ($\hat{E}_m\simeq2$), and $a_0=4.75$ ($\hat{E}_m\simeq2.25$), with $\gamma_p=10$.

$E_z/E_0\simeq k_pr_B/4$, which gives $N_{\rm max}\simeq(k_pr_B)^3/16\pi k_pr_e$. Gordienko and Pukhov (2005) found $N_{\rm max}\simeq1.1\times10^9\lambda_0(\mu{\rm m})[P({\rm TW})]^{1/2}$. The efficiency was estimated to be in the range of ten to a few tens of percent (Gordienko and Pukhov, 2005; Lu *et al.*, 2007).

IV. ELECTRON TRAPPING AND INJECTION

A. Trapping and dark current

The dynamics of an electron in the presence of a plasma wave and a laser pulse is determined by the Hamiltonian in the comoving frame $H=(\gamma_\perp^2+\tilde{p}^2)^{1/2}-\beta_p\tilde{p}-\phi$, as discussed in Sec. II.E. The orbit of an electron with initial normalized momentum $\tilde{p}_t$ will be defined by $H=(1+\tilde{p}_t^2)^{1/2}-\beta_p\tilde{p}_t=H_t$. Trapping of the electron will occur when the orbit defined by H_t coincides with a trapped orbit, defined as lying with the separatrix orbit (defined by H_s), i.e., when $H_t\leqslant H_s$. Solving $H_t=H_s$ yields in the minimum initial electron momentum for trapping in the plasma wave (Schroeder *et al.*, 2006),

$$\tilde{p}_t=\gamma_p\beta_p(\gamma_\perp-\gamma_p\phi_{\rm min})-\gamma_p[(\gamma_\perp-\gamma_p\phi_{\rm min})^2-1]^{1/2}, \tag{65}$$

where $\phi_{\rm min}$ is the minima of the plasma wave potential. Figure 22 shows the initial momentum $\tilde{p}_t$ required for the electron to be trapped by a plasma wave with amplitude $\hat{E}_m=E_{\rm max}/E_0$, with $\gamma_\perp=1$ for a warm plasma [i.e., solving Eq. (27) for the plasma wave potential] with $\beta_{\rm th}^2=k_BT_0/mc^2=10^{-4}$. The threshold momentum required for trapping decreases for larger plasma wave amplitude and for lower plasma wave phase velocity. Curvature of the plasma wave fronts in two dimensions can enhance trapping into the focusing and accelerating regions (Kalmykov *et al.*, 2006).

If the electric field of the plasma wave can be well approximated by the cold result (i.e., $E<E_{\rm WB}$ and $\beta_p\gg\beta_{\rm th}$), then the peak field E_t required for the onset of particle trapping as a function of the initial electron momentum $\tilde{p}_t$ is (Schroeder *et al.*, 2006)

$$(E_t/E_0)^2\simeq2\gamma_\perp(\gamma_p-1)+2\gamma_p^2\beta_p\{\tilde{p}_t-[(\beta_p\tilde{p}_t)^2+2\beta_p\tilde{p}_t\gamma_\perp/\gamma_p]^{1/2}\}, \tag{66}$$

assuming $\tilde{p}_t\ll1$ (nonrelativistic initial momentum). Note that trapping can always occur even for plasma waves with ultrarelativistic phase velocities ($\beta_p=1$), as shown in Fig. 22. For $\gamma_\perp=1$, $\beta_p=1$, and $\tilde{p}_t\ll1$, $\phi_{\rm min}\simeq-1+\tilde{p}_t$ and the peak field of an ultrarelativistic plasma wave required for trapping an electron with initial momentum $\tilde{p}_t$ is $E_t/E_0\simeq\tilde{p}_t^{-1/2}$.

For a thermal plasma electron distribution, electrons on the tail of the distribution may have sufficiently high momentum so as to reside on trapped orbits. For example, assuming an initial Gaussian momentum distribution with initial rms momentum spread $\beta_{\rm th}^2=k_BT_0/mc^2$, i.e., a momentum distribution $F(\tilde{p})\propto\exp(-\tilde{p}^2/2\beta_{\rm th}^2)$, the fraction of trapped electrons is

$$f_{\rm trap}=\tfrac{1}{2}\,{\rm erfc}(\tilde{p}_t/\sqrt{2}\beta_{\rm th}), \tag{67}$$

where $\tilde{p}_t$ is given by Eq. (65). Figure 23 shows the fraction of trapped electrons versus the initial temperature of a Gaussian plasma electron momentum distribution for three different nonlinear plasma wave amplitudes driven by a laser in a warm plasma [i.e., $\hat{E}_m$ determined via Eq. (27)] with $k_pL_{\rm rms}=1$ and $a_0=3.65$ ($\hat{E}_m\simeq1.75$), $a_0=4.15$ ($\hat{E}_m\simeq2$), and $a_0=4.75$ ($\hat{E}_m\simeq2.25$), with $\gamma_p=10$.

The particle trapping model can also be used to calculate the fraction trapped at the wave breaking field (Esarey *et al.*, 2007). For example, when $\gamma_\perp=1$, Eq. (65) can be solved for the plasma wave potential required for trapping an electron, i.e., $\phi_{\rm min}\simeq\gamma_p^{-1}-1+\beta_p\tilde{p}_t$, for $\tilde{p}_t\ll1$, whereas using warm fluid theory (Schroeder *et al.*, 2005) the minimum potential at the wave breaking amplitude is $\phi_{\rm min}\simeq\gamma_p^{-1}-1+\beta_p\sqrt{3}\beta_{\rm th}$. Hence, a significant fraction of the plasma electrons (satisfying $\tilde{p}_t>\sqrt{3}\beta_{\rm th}$) can be trapped as the field approaches the wave breaking amplitude: $f_{\rm trap}={\rm erfc}(\sqrt{3/2})/2\simeq0.04$ for an initial Gaussian momentum distribution.

The total number of trapped electrons (i.e., dark current in the plasma accelerator) can be estimated from Eq. (67). For example, for a plasma density of $n_0 = 10^{19}$ cm^{-3}, driver transverse size of $r_\perp = 10$ μm, and accelerator length of 1 mm, a trapping fraction of $f_{\rm trap} = 10^{-3}$ indicates $\sim$0.1 nC of trapped charge. This trapping calculation neglects beam loading, which implies the wakefield induced by trapped electrons is much smaller than the primary plasma wave.

As the driver propagates into the plasma, more charge will be trapped until the amplitude of the plasma wave is substantially reduced due to beam loading. The beam loading limit is defined as the number of accelerated electrons required to produce a wakefield that cancels the accelerating field of the plasma wave (Katsouleas *et al.*, 1987). The trapped bunch density is $n_b \simeq f_{\rm trap} n_0 z/L_b$, where z is the propagation distance and L_b is the bunch length. Assuming $k_p L_b \lesssim 1$, the wakefield generated by the bunch is given by $E_b/E_0 \simeq k_p L_b n_b/n_0$ in the 1D limit, assuming $E_b/E_0 < 1$. The beam loading limit at which $E_b \simeq E_{\rm max}$ is then reached after a propagation distance of $z_{\rm BL} \simeq k_p^{-1} f_{\rm trap}^{-1} \hat{E}_m$. For $\hat{E}_m \sim 1$ and $f_{\rm trap} \ll 1$, $k_p z_{\rm BL} \gg 1$ and beam loading will be significant after many plasma periods of propagation.

B. Trapping in the self-modulated LWFA

Perhaps the most basic and simplest form of a laser-plasma injector is the self-modulated LWFA, in which a single laser pulse results in self-trapping and generation of a subpicosecond electron bunch, however, with a large energy spread. Typically the self-trapped bunch is of high charge (up to 10 nC), with an energy distribution characterized by a Boltzmann distribution with a few MeV temperature. One possible mechanism for self-trapping is via generation of large amplitude plasma wakefields, approaching the wave breaking field (Modena *et al.*, 1995; Tzeng *et al.*, 1997; Gordon *et al.*, 1998). Since the phase velocity of the wakefield is very near the speed of light, it is difficult to trap background plasma electrons, which are undergoing the fluid oscillation that sustains the wake field. As discussed in Sec. IV.A, the wake will trap background electrons when the separatrix of the wake overlaps the plasma electron orbits. Electron trapping in a cold plasma wave in one dimension occurs at $E_{\rm WB} = [2(\gamma_p - 1)]^{1/2} E_0 \gg E_0$. Thermal and 2D effects can lower this value, but typically self-trapping requires nonlinear plasma waves with $E_z > E_0$. The observed wakefield amplitude, however, as measured in several experiments (Ting *et al.*, 1996), appears to be in the range $E_z/E_0 \sim 10$–30 %, well below the cold wave breaking limit. This suggests that additional laser-plasma instabilities may play a role in lowering the effective amplitude for electron self-trapping.

Alternatively, self-trapping and acceleration can result from the coupling of Raman backscatter (RBS) and Raman sidescatter (RSS) to the wakefield (Esarey *et al.*, 1998). As the pump laser self-modulates, it also undergoes RBS, which is the fastest growing laser-plasma instability (cf. Sec. VI.A). RBS is observed in intense short pulse experiments, with reflectivities as high as 10 -30 % (Rousseaux *et al.*, 1995; Ting *et al.*, 1996). RBS generates redshifted backward light of frequency $\omega_0 - \omega_p$ and wave number $-k_0$, which beats with the pump laser (ω_0, k_0) to drive a ponderomotive wave $(\omega_p, 2k_0)$. As the instability grows, the Raman backscatter beat wave, which has a slow phase velocity $v_p \simeq \omega_p/2k_0 \ll c$, can trap and heat background plasma electrons (Joshi *et al.*, 1981; Bertrand *et al.*, 1995). These electrons can gain sufficient energy and be displaced in phase by the beat wave such that they are trapped and accelerated to high energies in the wakefield. Simulations (Esarey *et al.*, 1998) indicate that coupling to RBS can lead to self-trapping at modest wakefield amplitudes, $E_z/E_0 \simeq 0.25$, much lower than the 1D threshold for self-trapping.

In two dimensions, this process can be enhanced by coupling to RSS. As the scattering angle decreases from 180° (backscatter), the Raman growth rate decreases and the phase velocity of the Raman plasma wave increases. The electrons that are initially trapped and heated by RBS can be subsequently trapped by RSS modes propagating at smaller angles, which will accelerate the electrons to higher energies (owing to the higher phase velocity of the RSS modes) (Joshi *et al.*, 1981; Esarey *et al.*, 1998). Eventually, these background electrons can be trapped and accelerated to very high energies by the plasma wave associated with the forward Raman instability or the self-modulation instability, which has $v_p \simeq c$.

When electrons become trapped in the fast wakefield, they become accelerated to high energies as they circulate inside the separatrix of the wake. A large energy spread for the trapped electrons results because (i) some fraction of the background electrons are continually being swept up and trapped in the wakefield as the laser pulse propagates into fresh plasma and (ii) typically the self-guided propagation distance of the laser pulse is much greater than the dephasing length for trapped electrons (cf. Sec. II.E). In the self-modulated regime the dephasing length can be very short, e.g., $L_d < 50$ μm. This implies that deeply trapped electrons will circulate many revolutions within the separatrix, again resulting in a large energy spread. The maximum energy of the trapped electrons is given by the maximum of the separatrix, which corresponds to an energy (Esarey and Pilloff, 1995) $W_{\rm max} \simeq 4\gamma_p^2 m_e c^2 E_z/E_0$, for $E_z/E_0 \ll 1$, where γ_p is the phase velocity of the plasma wave.

For many applications, a small energy spread is desired. One method for improving the self-modulated bunch quality is by postacceleration. For example, the self-modulated bunch could be immediately injected into a second-stage composed of a standard LWFA with $L \sim \lambda_p$ in which the wakefield is produced in a controlled manner at an amplitude below the self-trapping threshold. This could be achieved using a plasma that transitions from a high plasma density ($\lambda_p \ll L$, self-modulated LWFA) to a low plasma density ($\lambda_p \sim L$, standard LWFA). Simulations (Reitsma *et al.*, 2002) show that in

this two-stage acceleration scheme, about 40% of the injected bunch charge can be trapped and accelerated in the LWFA with a reduced energy spread.

C. Optical injection techniques

In principle, if a small energy spread electron bunch of length small compared to λ_p is injected into the wakefield at the proper phase, then the bunch can be accelerated while maintaining a small energy spread. This becomes problematic in the LWFA since the wavelength of the accelerating field is small, e.g., $\lambda_p \simeq 30\ \mu$m for $n_0 \simeq 10^{18}$ cm^{-3}. Hence, a low energy spread requires an ultrashort bunch duration $\tau_b < \lambda_p/c$ that is injected at the optimal plasma wave phase with femtosecond timing accuracy. These requirements are very challenging for conventional electron beam injector technology (e.g., rf photoinjectors), although novel experimental designs are being explored (Irman *et al.*, 2007). On the other hand, the production of ultrashort laser pulses and the femtosecond timing of multiple pulses is routine with compact CPA technology. As discussed below, ultrashort high-intensity laser pulses can be used to optically trigger the injection of electrons into a single bucket (plasma wave period) of a standard LWFA (Umstadter, Kim, *et al.*, 1996; Esarey, Hubbard, *et al.*, 1997; Hemker *et al.*, 1998; Schroeder, Lee, *et al.*, 1999; Fubiani *et al.*, 2004; Kotaki *et al.*, 2004). Optical injection via colliding counterpropagating laser pulses has also been demonstrated experimentally by Faure, Rechatin, *et al.* (2006) and Kotaki *et al.* (2008).

1. Ponderomotive injection

Umstadter, Kim, *et al.* (1996) first proposed using an additional laser pulse to inject background plasma electrons into the wake for acceleration to high energies. To generate ultrashort electron bunches with low energy spreads, the original laser injection method of Umstadter, Kim, *et al.* (1996) used two laser pulses that propagate perpendicular to one another. The first pulse (pump pulse) generates a plasma wakefield via the standard LWFA mechanism, and the second pulse (injection pulse) intersects the wakefield some distance behind the pump pulse. The ponderomotive force $\boldsymbol{F}_p \simeq -(m_e c^2/\tilde{\gamma})\nabla a^2/2$ associated with the intensity gradients of the injection pulse can accelerate a fraction of the plasma electrons such that they become trapped in the wakefield. Specifically, the axial (direction of propagation of the pump pulse along the z axis) ponderomotive force of the injection pulse (propagating along the x axis) scales as

$$F_z = -(m_e c^2/\tilde{\gamma})(\partial/\partial z)a_1^2/2 \sim (m_e c^2/\tilde{\gamma})a_1^2/r_1, \tag{68}$$

where a_1^2 and r_1 are the normalized intensity and spot size of the injection pulse, respectively. A simple estimate for the change in momentum that an electron will experience owing to the ponderomotive force of the injection pulse is $\Delta\tilde{p}_z \simeq F_z\tau_1 \sim (m_e c^2/\tilde{\gamma})a_1^2\tau_1/r_1$, where τ_1 is the injection pulse duration. It is possible for $\Delta\tilde{p}_z$ to be sufficiently large that electrons are injected into the separatrix of the wakefield such that they become trapped and accelerated to high energies. To inject into a single plasma wave bucket, it is necessary for both the injection pulse spot size and pulse length to be small compared to the plasma wavelength, i.e., $r_1^2 \ll \lambda_p^2$ and $c^2\tau_1^2 \ll \lambda_p^2$. Numerical simulations (Umstadter, Kim, *et al.*, 1996), which were performed for ultrashort pulses at high densities ($\lambda_p/\lambda = 10$ and $E_z/E_0 = 0.7$), indicated the production of a 10 fs, 21 MeV electron bunch with a 6% energy spread. However, high intensities ($I > 10^{18}$ W/cm^2) are required in both the pump and injection pulses ($a_0 \simeq a_1 \simeq 2$). In the work of Umstadter, Kim, *et al.* (1996), the pump and injection pulses do not overlap in space and time, and a laser beat wave is not generated, as discussed below. Similarly, the axial ponderomotive force of a cross-polarized counterpropagating laser pulse could be used to trigger electron injection.

Simulations by Hemker *et al.* (1998) point out that additional electron injection into one or more wake buckets can result through the influence of the wake associated with the injection pulse, which can be significant because of the high intensity of the injection pulse ($a_1 \gtrsim 1$). Umstadter, Kim, *et al.* (1996) also discussed the possibility of using an injection pulse that propagates parallel, but some distance behind, the pump pulse. The injection pulse would have a tighter focus (and hence smaller Rayleigh length) than the pump pulse and would be phased appropriately such that it locally drives the wakefield to an amplitude that exceeds the self-trapping threshold, thus resulting in local trapping and acceleration of electrons. In addition, Umstadter, Kim, *et al.* (1996) discussed the possibility of the injection pulse being focused to sufficiently high intensity such that it produces, locally, additional ionization. The ionized electrons, which are born dephased from the background plasma electron in the wake, could become trapped and accelerated by the wake.

Injection by laser-induced ionization and ponderomotive acceleration (LIPA) has also been discussed by Moore *et al.* (1999) in a low-density regime. Here an intense laser pulse (3×10^{18} W/cm^2) interacts with a high-Z gas (Kr) at low pressure (1 Torr). The ionized electrons from high-charge states are directly accelerated by the laser ponderomotive force. Electrons with energies up to a few 100 keV were ejected from the laser focal region at large angles. A high-density LIPA regime has also been investigated (Ting *et al.*, 2005), where additional acceleration can result from the laser excited wakefield.

2. Colliding pulse injection

Beat wave injection using colliding laser pulses (Esarey, Hubbard, *et al.*, 1997, 1999; Leemans *et al.*, 1998; Schroeder, Lee, *et al.*, 1999; Fubiani *et al.*, 2004; Kotaki *et al.*, 2004) differs intrinsically from the method of ponderomotive injection discussed above in that the source and form of the ponderomotive force differ in these two methods. In ponderomotive injection, injection is the re-

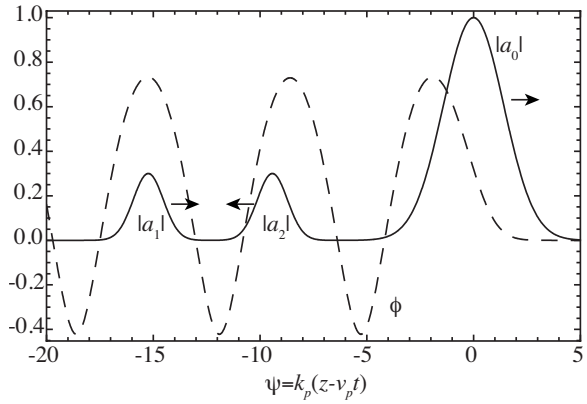

FIG. 24. Profiles of the pump laser pulse a_0, the wake ϕ (dashed curve), and the forward a_1 injection pulse, all of which are stationary in the $\psi=k_p(z-v_pt)$ frame and the backward injection pulse a_2, which moves to the left at $\simeq 2c$.

sult of the ponderomotive force associated with the *envelope* (time-averaged intensity profile) of a single pulse. In beat wave injection, injection is the result of the ponderomotive force associated with the *slow beat wave* of two intersecting pulses. Beat wave injection was first proposed by Esarey *et al.* (1997) in a concept referred to as colliding pulse injection.

Colliding pulse injection in its original configuration (Esarey *et al.*, 1997a, 1999; Leemans *et al.*, 1998; Schroeder, Lee, *et al.*, 1999) uses three short laser pulses: an intense ($a_0^2 \simeq 1$) pump pulse (denoted by subscript 0) for plasma wave generation, a forward going injection pulse (subscript 1), and a backward going injection pulse (subscript 2), as shown in Fig. 24. The frequency, wave number, and normalized intensity are denoted by ω_i, k_i, and a_i ($i=0,1,2$), respectively. Furthermore, it is assumed that $k_1 \simeq k_0$, $k_2 \simeq -k_0$, and $\omega_1 - \omega_2 = \Delta\omega \gg \omega_p$. The pump pulse generates a plasma wave with phase velocity near the speed of light ($v_{p0} \simeq c$). The forward injection pulse travels at a fixed distance behind the pump pulse, which determines the position (i.e., phase) of the injected electrons. The injection pulses are orthogonally polarized to the pump laser pulse, such that the pump pulse and backward going injection pulse do not beat.

When the injection pulses collide some distance behind the pump, they generate a slow ponderomotive beat wave of the form $a_1 a_2 \cos(\Delta k z - \Delta\omega t)$ (here $\Delta k = k_1 - k_2 \simeq 2k_0$) with a phase velocity $v_{pb} \simeq |\Delta\omega|/2k_0 \ll c$. The axial force associated with this beat wave scales as

$$F_z = -(m_e c^2/\tilde{\gamma})(\partial/\partial z) a_1 a_2 \cos(2k_0 z - \Delta\omega t) \sim (m_e c^2/\tilde{\gamma}) 2k_0 a_1 a_2. \quad (69)$$

During the time in which the two injection pulses overlap, a two-stage acceleration process can occur, i.e., the slow beat wave traps and heats background plasma electrons that, as a result of shifts in their momentum and phase, can be injected into the fast wakefield for acceleration to high energies.

The ratio of the axial force of the beat wave to that of a single pulse in the ponderomotive injection scheme (owing to the gradient in the envelope of the laser intensity) scales as

$$F_{z,\mathrm{beat}}/F_{z,\mathrm{env}} \sim 2k_0 a_1 a_2/(a_p^2/r_p), \quad (70)$$

where the subscript p refers to the single ponderomotive injection pulse and the contribution of the relativistic Lorentz factor $\tilde{\gamma}$ (which is different for the two cases) is neglected. For comparable injection pulse intensities ($a_1 \simeq a_2 \simeq a_p$), the ratio scales as $4\pi r_p/\lambda_0 \gg 1$, i.e., the axial force of the beat wave is much greater than the ponderomotive force from the intensity envelope of a single pulse. Consequently, colliding pulses can result in electron injection at relatively low intensities ($a_1 \sim a_2 \sim 0.2$), as well as at relatively low densities ($\lambda_p/\lambda \sim 100$), thus allowing for high single-stage energy gains. Furthermore, the colliding pulse concept offers detailed control of the injection process: the injection phase can be controlled via the position of the forward injection pulse, the beat phase velocity via $\Delta\omega$, the injection energy via the pulse amplitudes, and the injection time (number of trapped electrons) via the backward pulse duration.

To further understand the colliding pulse injection mechanism, it is insightful to consider the electron motion in the wakefield and in the colliding laser fields individually. Here we consider colliding laser pulses in a plasma wave behind a drive laser pulse. In the absence of the injection pulses, electron motion in a 1D wakefield is described by the Hamiltonian $H_w = \tilde{\gamma} - \beta_p(\tilde{\gamma}^2 - 1)^{1/2} - \phi(\psi)$ (cf. Sec. II.E), where $\phi = \phi_0 \cos\psi$, $v_p = c\beta_p$ is the phase velocity of the plasma wave, $\gamma_p = (1-\beta_p^2)^{-1/2}$, and $\psi = k_p(z - v_p t)$. The electron orbits in phase space $(\tilde{p}_z, \psi)$ are given by $H_w(\tilde{p}_z, \psi) = H_0$, where H_0 is a constant, $\tilde{\gamma}^2 = 1 + \tilde{p}_z^2$, and $\tilde{p}_z$ is the normalized (to $m_e c$) axial momentum of an electron, which is given by

$$\tilde{p}_z = \beta_p \gamma_p^2 [H_0 + \phi(\psi)] \pm \gamma_p \{\gamma_p^2 [H_0 + \phi(\psi)]^2 - 1\}^{1/2}. \quad (71)$$

The 1D separatrix (the boundary between trapped and untrapped orbits) is given by $H_w(\tilde{p}_z, \psi) = H_w(\gamma_p\beta_p, \pi)$, i.e., $H_0 = H_{1\mathrm{D}} = 1/\gamma_p - \phi(\pi)$. The maximum and minimum electron momenta on the 1D separatrix occur at $\psi = 0$ and are (in the limits $2\phi_0\gamma_p \gg 1$ and $\gamma_p \gg 1$) $\tilde{p}_{w,\max} \simeq 4\gamma_p^2\phi_0$ and $\tilde{p}_{w,\min} \simeq (4\phi_0)^{-1} - \phi_0$.

The 1D theory neglects the effects of transverse focusing. Associated with a 3D wake is a periodic radial field that is $\pi/2$ out of phase with the accelerating field, i.e., there exists a phase region of $\lambda_p/4$ for which the wake is both accelerating and focusing (as opposed to the $\lambda_p/2$ accelerating region in one dimension). If an electron is to remain in this phase region, it must lie within the "3D separatrix" defined by $H_w(\tilde{p}_z, \psi) = H_w(\gamma_p\beta_p, \pi/2)$, i.e., Eq. (71) with $H_0 = H_{3\mathrm{D}} = 1/\gamma_p - \phi(\pi/2)$. The extrema on the 3D separatrix are given by $\tilde{p}_{w,\max} \simeq 2\gamma_p^2\phi_0$ and $\tilde{p}_{w,\min} \simeq (\phi_0^{-1} - \phi_0)/2$. This value of $\tilde{p}_{w,\max} \simeq 2\gamma_p^2\phi_0$ gives the usual maximum energy gain due to linear dephasing in a 3D wake.

The background plasma electrons (assumed initially cold) lie on an untrapped orbit (below the separatrix) $\tilde{p}_{zf}$

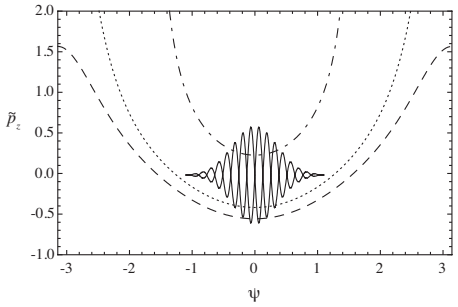

FIG. 25. Longitudinal phase space showing beat wave separatrices (solid curve), an untrapped plasma wave orbit (dashed, lower curve), a trapped plasma wave orbit (dotted curve), and a trapped and focused plasma wave orbit (dash-dotted, upper curve).

given by $H_w(\tilde{p}_{zf},\psi)=1$, i.e., Eq. (71) with $H_0=1$. The separatrix $\tilde{p}_{w,\min}$ coalesces with the plasma fluid orbit, $\tilde{p}_{zf}=\tilde{p}_{w,\min}$, at the well-known cold wave breaking field of $E_{\mathrm{WB}}/E_0=[2(\gamma_p-1)]^{1/2}$.

Consider the motion of electrons in the colliding laser fields in the absence of the wakefield. The beat wave leads to formation of phase space buckets (separatrices) of width $2\pi/\Delta k \simeq \lambda_0/2$, which are much shorter than those of the wakefield (λ_p). In the colliding laser fields, the electron motion is described by the Hamiltonian (Esarey *et al.*, 1997a) $H_b=\tilde{\gamma}-\beta_b[\tilde{\gamma}^2-\gamma_\perp^2(\psi_b)]^{1/2}$, where the space charge potential is neglected. Circular polarization is assumed such that $\gamma_\perp^2=1+a_0^2+a_1^2+2a_0a_1\cos\psi_b$, where $\psi_b=(k_1-k_2)(z-v_bt)$ and $v_b=c\beta_b=\Delta\omega/(k_1-k_2)\simeq\Delta\omega/2k_0$ is the beat phase velocity, assuming $\omega_p^2/\omega_0^2\ll 1$. The beat separatrix is given by $H_b(\tilde{p}_z,\psi_b)=H_b(\gamma_b\beta_b,0)$ with maximum and minimum axial momenta of

$$\tilde{p}_{b,m}=\gamma_b\beta_b[1+(a_0+a_1)^2]^{1/2}\pm 2\gamma_b(a_0a_1)^{1/2}. \tag{72}$$

An estimate for the threshold for injection into the wakefield can be obtained by a simple phase-space island overlap criteria. This is done by considering the effects of the wakefield and the beat wave individually, as done above, and by requiring that the beat wave separatrix overlaps both the wakefield separatrix and the plasma fluid oscillation (illustrated in Fig. 25): (i) the maximum momentum of the beat wave separatrix $\tilde{p}_{b,\max}$ exceeds the minimum momentum of the wakefield separatrix $\tilde{p}_{w,\min}$, i.e., $\tilde{p}_{b,\max}\geqslant\tilde{p}_{w,\min}$ and (ii) the minimum momentum of the beat wave separatrix $\tilde{p}_{b,\min}$ be less than the plasma electron fluid momentum $\tilde{p}_{zf}$, i.e., $\tilde{p}_{b,\min}\leqslant\tilde{p}_{zf}$. Conditions (i) and (ii) imply a beat wave threshold (Esarey *et al.*, 1997a; Schroeder, Lee, *et al.*, 1999)

$$(a_1a_2)_{\mathrm{th}}^{1/2}=(1-H_0)/4\gamma_b(\beta_p-\beta_b), \tag{73}$$

and an optimal wake phase for injection (location of the forward injection pulse)

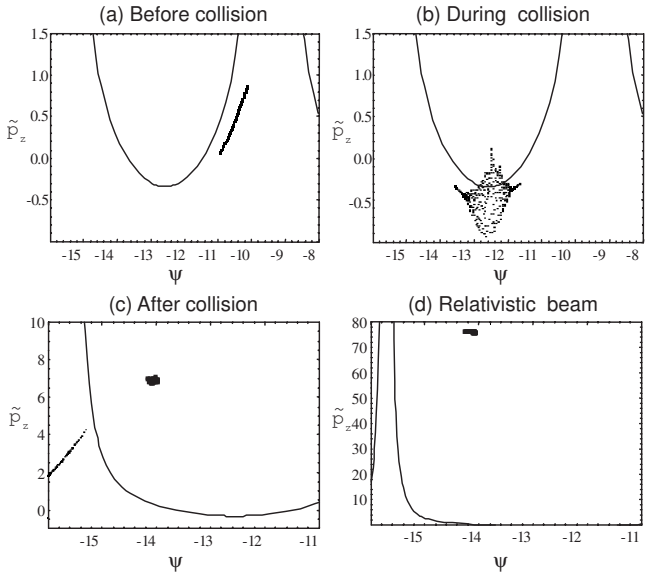

FIG. 26. Electron distribution in longitudinal (u_z,ψ) phase space (a) before injection pulse collision ($\omega_p\Delta t=0$), (b) during collision ($\omega_p\Delta t=3$), (c) just after collision ($\omega_p\Delta t=14$), and (d) at $\omega_p\Delta t=114$ (38 MeV electron bunch with 1 fs duration, 0.2% energy spread, and 0.9 mm mrad normalized transverse emittance). The separatrix between trapped and untrapped wake orbits (solid line) is shown. From Schroeder, Lee, *et al.*, 1999.

$$\cos\psi_{\mathrm{opt}}=\phi_0^{-1}[(1-\beta_b\beta_p)\gamma_b\gamma_\perp(0)-(1+H_0)/2], \tag{74}$$

where $H_0=H_{1\mathrm{D}}=1/\gamma_p+\phi_0$ for the 1D wake separatrix and $H_0=H_{3\mathrm{D}}=1/\gamma_p$ for the 3D wake separatrix (trapped and focused). In the limits $\gamma_p^2\gg 1$, $\beta_b^2\ll 1$, and $a_i^2\ll 1$, Eqs. (73) and (74) become $4(a_1a_2)_{\mathrm{th}}^{1/2}\simeq(1-H_0)(1+\beta_b)$ and $2\phi_0\cos\psi_{\mathrm{opt}}\simeq 1-H_0-2\beta_b$ with $H_{1\mathrm{D}}\simeq\phi_0$ and $H_{3\mathrm{D}}\simeq 0$. As an example, $\phi_0=0.7$, $\beta_b=-0.02$, and $\gamma_p=50$ imply a threshold of $(a_1a_2)_{\mathrm{th}}^{1/2}\simeq 0.25$ and an optimal injection phase of $\psi_{\mathrm{opt}}\simeq 0$ for injection onto a trapped and focused orbit.

The above expressions are valid for $\omega_p<|\Delta\omega|\ll\omega_0$, such that the separation in time scales is valid and beat wave excitation of plasma waves is negligible. For equal laser frequencies ($\beta_b=0$) a standing laser beat wave exists that will produce a large amplitude space-charge response, which is neglected in the above analysis. Electron acceleration and heating with intense standing beat waves were studied by Sheng *et al.* (2004).

The colliding laser injection method has been modeled by numerically solving the motion of test particles in the combined wake and laser fields for the three-pulse (Schroeder, Lee, *et al.*, 1999) configuration. An example of the injection process for colliding pulses behind a drive laser is given in Fig. 26, which shows the evolution in longitudinal phase space of the test electron distribution (a) before the collision of the injection laser pulses (in the untrapped fluid orbit of the wake) at $\omega_p\Delta t=0$, (b) during the collision (crossing the wake separatrix) at $\omega_p\Delta t=3$, (c) after the collision at $\omega_p\Delta t=14$, and (d) the resulting energetic electron bunch at $\omega_p\Delta t=114$. Figure 26 also shows the 1D wake separatrix.

In the numerical studies, the laser pulse axial profiles were half-period sine waves (linearly polarized with Gaussian radial profiles) with peak amplitude a_i and length L_i. The parameters of Fig. 26 are $a_1=a_2=0.32$, $L_0=4L_1=4L_2=\lambda_p=40$ μm, $\phi_0=0.7$, $\lambda_0=\lambda_2=0.8$ μm, $\lambda_1=0.83$ μm, and $r_0=r_1=r_2=15$ μm, with the position of the forward injection pulse centered at $\psi_{\rm inj}=-12.6$. After $z\simeq 0.7$ mm of propagation following the collision [Fig. 26(d)], the bunch length is 1 fs with a mean energy of 38 MeV, a fractional energy spread of 0.2%, and a normalized transverse emittance of 0.9 mm mrad. The example contains a bunch charge of 2.6×10^6 electrons. Note that the bunch number can be increased by increasing the laser spot sizes (i.e., laser powers). For example, when the laser spot sizes are doubled to $r_i=30$ μm with all other parameters as in Fig. 26, the number of trapped electrons increases to 1.5×10^7 and the normalized transverse emittance increases to 3.9 mm mrad.

Colliding pulse injection can also be achieved using two laser pulses, with the same polarization, such that the tail of the pump laser pulse beats with the counterpropagating pulse, trapping electrons in the plasma wave (Fubiani *et al.*, 2004; Kotaki *et al.*, 2004). Colliding the laser pulses at an angle has also been investigated (Fubiani *et al.*, 2004). These configurations have the advantage of simplicity and experimental ease (at the cost of some detailed control of the trapping process).

The two-pulse configuration has been studied with 1D PIC simulations for colliding pulses of equal frequency ($\beta_b=0$) (Rechatin *et al.*, 2007). Plasma wake disruption, due to the strong wave-particle resonance between the beat wave and the cold plasma for equal frequencies, and the resulting degradation of the beam were observed (Rechatin *et al.*, 2007). Beam quality improvement can be obtained by properly choosing the beat phase velocity (Fubiani *et al.*, 2004). Further improvement can be achieved using higher-order laser modes for plasma wave excitation to reverse the focusing and defocusing phase regions (Michel, Esarey, *et al.*, 2006). The laser-injected electron beam quality can also be improved using negative plasma density gradients (Fubiani *et al.*, 2006). Negative plasma density gradients can be used to shift the injection phase and lower the trapping threshold by lowering the wakefield phase velocity (as described in Sec. IV.D).

The initial set of optical trapping experiments used the experimentally simpler two-pulse colliding pulse injection geometry (Kotaki *et al.*, 2004; Nakamura *et al.*, 2004; Faure, Rechatin, *et al.*, 2006). Details of high-quality bunch production using this technique (Faure, Rechatin, *et al.*, 2006; Kotaki *et al.*, 2008) are discussed in Sec. VII.C.

D. Density transitions

Bulanov *et al.* (1998) described how a downward transition in the plasma density with a scale length $L_{\rm tr}$ long compared to λ_p could be used to induce local self-trapping in the plasma wave. Consider the position of a phase peak on a plasma wave of the form $\phi=\phi_0\cos k_p\zeta$ (where $-\zeta=ct-z$ is the distance behind the drive beam) located N_p periods behind the drive beam. Before the density transition, the phase peak is located at $|\zeta_1|=N_p\lambda_{p1}$, and after the transition, the phase peak is located at $|\zeta_2|=N_p\lambda_{p2}$, where λ_{p1} (n_1) and λ_{p2} (n_2) are the plasma wavelengths (densities) before and after the transition with $\lambda_{p1}<\lambda_{p2}$ ($n_1>n_2$). The density transition changes the location of the phase peak by the relative amount $\Delta|\zeta_p|=N_p(\lambda_{p1}-\lambda_{p2})$. If this transition occurs over a length $L_{\rm tr}$, then the change in the phase velocity is $\Delta v_p/c\simeq N_p(\lambda_{p1}-\lambda_{p2})/L_{\rm tr}$. This effect increases proportional to the distance behind the driver (increasing N_p), as well as the magnitude of the density gradient, $(\lambda_{p1}-\lambda_{p2})/L_{\rm tr}\simeq d\lambda_p/dz=-(\lambda_p/2n)dn/dz$.

More rigorously, the phase velocity of the wake during a density transition can be calculated by considering the local phase of the wake, which is given to leading order by $\psi=k_p(z)(z-ct)$, where $v_g\simeq c$ has been assumed since changes to the group velocity due to a slow variation in density are small in an underdense plasma $\omega_p^2/\omega^2\ll 1$. Using the definitions of the effective frequency $\omega_{p,\rm eff}=-\partial\psi/\partial t$and wave number $k_{p,\rm eff}=\partial\psi/\partial z$ of the plasma wave, the local phase velocity of the wake is given by $v_p=\omega_{p,\rm eff}/k_{p,\rm eff}$, i.e.,

$$v_p/c=[1+(\zeta/k_p)dk_p/dz]^{-1}. \tag{75}$$

For a small variation, $v_p/c-1\simeq-(\zeta/k_p)dk_p/dz=-(\zeta/2n)dn/dz$. Since $\zeta<0$ behind the drive pulse, the wake phase velocity will decrease for decreasing density $dn/dz<0$.

Local trapping of electrons in the wake will occur at the point at which the local phase velocity equals the fluid velocity of the plasma electrons $v_p=v_e$. To leading order, the size of the fluid oscillation depends on the intensity of the drive pulse, the pulse length, and the local plasma density. Since the resonance for exciting a large amplitude wake is rather broad, $L\sim\lambda_p$ (weakly dependent on density), a large wake can be excited on the density ramp with a fluid velocity given by $v_e/c\simeq E_z/E_0$, where $E_z/E_0\ll 1$ is the normalized electric field amplitude of the wake. Equation (75) indicates that the wake phase velocity will continue to decrease as a function of time for a fixed point on the density down ramp, and, hence, the phase velocity of the plasma wave will always decrease to the fluid velocity on a density down ramp at a sufficiently large distance behind the drive pulse (assuming the wake is not damped by some other mechanism). Using Eq. (75), $v_p=v_e$ will occur at a distance behind the drive pulse given by $\zeta=2(c/v_e-1)n/(dn/dz)$. For example, if $v_e/c=1/3$ and $L_{\rm tr}=n|dn/dz|^{-1}=3\lambda_p$, then $v_p=v_e$ occurs at $|\zeta|=12\lambda_p$.

Bulanov *et al.* (1998) performed 1D PIC simulations of a laser pulse with $a_0=2$ and $L=12\lambda$ propagating in a plasma with $\lambda_{p1}=23.4\lambda$, $\lambda_{p2}=25\lambda$, and $L_{\rm tr}=24\lambda$. These simulations found that the plasma wave breaks on the ramp and injects a significant number of electrons into the second wake bucket behind the laser pulse, which

are accelerated to high energy but with a large energy spread. Simulations in two and three dimensions have shown generation of well-collimated, narrow energy spread, short electron beams via a decreasing plasma density gradient (Tomassini *et al.*, 2003; Brantov *et al.*, 2008).

Suk *et al.* (2001) considered the limit of a step function downward plasma density transition ($n_1=5\times10^{13}$ cm^{-3} and $n_2=3.5\times10^{13}$ cm^{-3}) and a wake generated by an electron beam driver of energy 16 MeV, bunch length $0.16\lambda_{p2}$, bunch radius $0.089\lambda_{p2}$, and peak density $n_b=2.4n_1=3.4n_2$. Using 2D PIC simulations, the trapped electron bunch, after propagating a few plasma wavelengths pass the transition, had a total charge near 0.5 nC, a bunch length near $0.09\lambda_{p2}$, and electron energies in the range of 5–15 MeV. Trapping across a parabolic density profile, which has the advantage of ease of experimental production and control, has also been considered (Kim *et al.*, 2004). Electron injection via a sharp laser-induced plasma density ramp (scale length of ramp less than the plasma wavelength) has been demonstrated in the self-modulated LWFA regime (Chien *et al.*, 2005). Stable production of electron bunches ($\sim$1 MeV) has been experimentally demonstrated by focusing a laser on the downstream edge of a gas jet producing a negative plasma density gradient (Geddes *et al.*, 2008) and is discussed in Sec. VII.D.

V. PULSE PROPAGATION AND GUIDING

To describe laser pulse propagation in a fully ionized plasma, it is convenient to represent the electric $\boldsymbol{E}$ and magnetic fields $\boldsymbol{B}$ by the scaler Φ and vector $\boldsymbol{A}$ potentials, $\boldsymbol{E}=-\nabla\Phi-\partial\boldsymbol{A}/\partial ct$ and $\boldsymbol{B}=\nabla\times\boldsymbol{A}$, and to use Coulomb gauge, $\nabla\cdot\boldsymbol{A}=0$. In terms of the normalized potentials $\phi=e\Phi/m_ec^2$ and $\boldsymbol{a}=e\boldsymbol{A}/m_ec^2$, the wave equation and the Poisson equation are given by, respectively,

$$\left(\nabla^2-\frac{1}{c^2}\frac{\partial^2}{\partial t^2}\right)\boldsymbol{a}=k_p^2\frac{n}{n_0}\frac{\boldsymbol{u}}{\gamma}+\frac{1}{c}\frac{\partial}{\partial t}\nabla\phi, \tag{76}$$

$$\nabla^2\phi=k_p^2(n-n_i)/n_0, \tag{77}$$

where $\boldsymbol{u}=\gamma\boldsymbol{v}/c=\boldsymbol{p}/m_ec$ is the normalized electron plasma fluid momentum, $\gamma=(1-\beta^2)^{1/2}=(1+u^2)^{1/2}$ is the relativistic Lorentz factor, n is the plasma electron density, n_i is the initial density profile (prior to the passage of the laser pulse), $n_0=n_i(r=0)$ with $r=0$ corresponding to the direction of propagation (the z axis), and $\omega_{p0}=ck_p=(4\pi n_0e^2/m_e)^{1/2}$. Here and in the following, it is assumed that the ions remain stationary, which is typical for short pulse lasers ($\lesssim$1 ps) propagating in underdense plasma ($\omega_{p0}^2/\omega^2\ll1$). Furthermore, collisions and thermal effects are neglected since the collision time is typically much greater than the laser pulse length and the thermal velocity is typically much less than the quiver velocity of an electron in the laser field.

The first term on the right-hand side of Eq. (76) is the contribution due to the plasma current $\boldsymbol{J}$. In the cold fluid limit, $\boldsymbol{J}=-en\boldsymbol{c}\boldsymbol{u}/\gamma$, where the plasma density n and momentum $\boldsymbol{u}$ satisfy the continuity and momentum equations, which are given by, respectively,

$$\partial n/\partial ct+\nabla\cdot(n\boldsymbol{u}/\gamma)=0, \tag{78}$$

$$[\partial/\partial ct+(\boldsymbol{u}/\gamma)\cdot\nabla]\boldsymbol{u}=\nabla\phi+\partial\boldsymbol{a}/\partial ct-(\boldsymbol{u}/\gamma)\times(\nabla\times\boldsymbol{a}). \tag{79}$$

It is also convenient to introduce the independent variables $\zeta=z-ct$ and $\tau=t$, where ζ is an approximate measure of the distance back from the head of the pulse (which is moving with a group velocity $v_g\simeq c$). Initially, the front of the laser pulse is assumed to be at $\zeta=0$ and the pulse body extends into the region $\zeta\leqslant0$ (the plasma is unperturbed in the region $\zeta>0$). In terms of the ζ,τ coordinates, the wave equation is given by (Esarey, Sprangle, *et al.*, 1993)

$$\left(\nabla_\perp^2+\frac{2}{c}\frac{\partial^2}{\partial\zeta\partial\tau}-\frac{1}{c^2}\frac{\partial^2}{\partial\tau^2}\right)\boldsymbol{a}\simeq k_p^2\frac{n}{n_0\gamma}\boldsymbol{u}. \tag{80}$$

On the right-hand side of Eq. (80), the term $\nabla\partial\phi/\partial ct$ has been neglected since the fast part of the electrostatic potential, $\phi\sim\exp(ik\zeta)$, is typically small compared to relevant terms contributing to the fast part of the plasma current. Typically, the third term on the left-hand side of Eq. (80) can be neglected for forward going light waves. As discussed in Sec. II, the leading-order transverse motion is the quiver motion. Hence, for a wide variety of phenomena it is sufficient to approximate $\boldsymbol{u}=\boldsymbol{a}$ on the right-hand side of Eq. (80).

The wave equation can be further simplified by the slowly varying envelope approximation. Assuming a linearly polarized laser field with a transverse component of the form $\boldsymbol{a}_f=\hat{\boldsymbol{a}}_s(r,\zeta,\tau)\exp(ik\zeta)/2+$c.c., where $|\partial_\zeta\hat{\boldsymbol{a}}_s|\ll|k\hat{\boldsymbol{a}}_s|$, the wave equation describing the evolution of the slowly varying amplitude $\hat{\boldsymbol{a}}_s$ is given by

$$\left(\nabla_\perp^2+2i\omega\frac{\partial}{\partial\tau}+\frac{2}{c}\frac{\partial^2}{\partial\zeta\partial\tau}\right)\hat{\boldsymbol{a}}_s=k_p^2\rho_s\hat{\boldsymbol{a}}_s, \tag{81}$$

where $\rho_s=(n/n_0)/\gamma$, $\boldsymbol{u}_{\perp f}\simeq\boldsymbol{a}_f$, $\omega=ck$ is the laser frequency, and the subscripts f and s denote the fast and slow components, respectively. The term $\partial^2/\partial\tau^2$, which is small for forward going waves but important for backward going waves (e.g., Raman backscatter), has been neglected in the wave operator. However, the $\partial^2/\partial\zeta\partial\tau$ term is retained so as to correctly describe variations in the laser pulse group velocity. Typically the operators in the reduced wave equation scale as $\nabla_\perp\sim1/r_0$, $\partial_\zeta\sim1/L$, and $\partial_{c\tau}\sim1/Z_R$. Throughout the following, the subscripts s and f will be dropped for convenience.

The paraxial approximation is the result of neglecting the term $\partial^2/\partial\zeta\partial\tau$ in Eq. (81). In the paraxial approximation, each ζ slice of the laser pulse propagates at the same velocity ($=c$), and the power in each ζ slice is conserved. Solutions to the paraxial wave equation in vacuum describe laser pulse diffraction, e.g., the fundamental Gaussian laser mode diffracts via $\hat{a}_\perp=(a_0r_0/r_s)\exp[-(1-iz/Z_R)r^2/r_s^2-i\tan^{-1}(z/Z_R)]$, where $r_s=r_0(1+z^2/Z_R^2)^{1/2}$, $Z_R=kr_0^2/2$, and $z=c\tau$.

A useful approximation in the study of short pulse interactions with plasmas is the quasistatic approximation (QSA), which was first applied to nonlinear laser-plasma interactions by Sprangle *et al.* (1990a, 1990b). In the QSA, the plasma fluid equations are written in terms of the independent variables ζ and τ, as above. The QSA assumes that in the time it takes the laser pulse to transit a plasma electron (i.e., the slippage time for an electron through the laser pulse), the laser pulse does not significantly evolve. In other words, $\tau_L \ll \tau_E$, where $\tau_L = L/c$ is the laser pulse duration and τ_E is the laser pulse evolution time (typically $c\tau_E \sim Z_R$). Thus the plasma electrons experience a static (independent of τ) laser field. In the QSA, the $\partial/\partial\tau$ derivatives are neglected in the plasma fluid equations that determine the plasma response to the laser pulse. The $\partial/\partial\tau$ derivatives, however, are retained in the wave equation that describes the evolution of the laser pulse. The QSA allows the laser-plasma interaction to be calculated in an iterative fashion. For a fixed τ, the plasma response to the laser field is determined as a function of ζ by solving the QSA fluid equations [e.g., Eq. (16) in the 1D limit]. Using this QSA fluid response, the wave equation is then solved to update the laser pulse in τ.

The fluid quantity $\rho = n/\gamma n_0$ in Eq. (81) can be determined from the quasistatic fluid equations. For example, in the 1D limit, it can be shown (Esarey, Ting, *et al.*, 1993) that $\rho \simeq (1+\phi)^{-1}(1+k_p^{-2}\gamma_g^{-2}\partial_\xi^2\phi)$, where ϕ satisfies Eq. (16). In two dimensions and assuming $v_g \simeq c$, it can be shown (Krall *et al.*, 1994) that

$$\rho \simeq (1+\Psi)^{-1}(\rho_0 + k_p^{-2}\nabla_\perp^2\Psi), \tag{82}$$

where ρ_0 is the initial value of ρ (prior to the laser pulse) and the quantity $\Psi = \phi - a_z$ satisfies

$$\frac{\partial^2\Psi}{\partial\zeta^2} = (k_p^2\rho - \nabla_\perp^2)u_z + \frac{\partial}{\partial\zeta}\nabla_\perp\cdot\boldsymbol{u}_\perp, \tag{83}$$

with $\boldsymbol{u}_\perp = (k_p^2\rho)^{-1}\partial_\zeta(\nabla_\perp\Psi)$ and $u_z = [u_\perp^2 + a^2 - \Psi(2+\Psi)]/[2(1+\Psi)]$. The wake potential Ψ is related to the axial electric field E_z induced in the plasma by $k_p\hat{E}_z = -\partial\Psi/\partial\zeta$, where $\hat{E}_z = E_z/E_0$ and $E_0 = m_e c\omega_{p0}/e$.

A useful quantity in discussing phenomena such as optical guiding is the index of refraction η_r. The effective index of refraction η_r is defined by setting the right-hand side of Eq. (81) equal to $k^2(1-\eta_r^2)\boldsymbol{a}$, which yields $\eta_r \simeq 1 - k_p^2\rho/2k^2$.

Although this section discusses laser propagation in fully ionized plasma, some laser-gas propagation effects can be important to LPAs. LPA experiments may use either neutral gas, photoionized by the laser, or a preformed plasma. For cases where the laser first interacts with neutral gas, pulse propagation can be affected during transport to focus. Nonlinear effects (Esarey, Sprangle, *et al.*, 1997; Wu and Antonsen, 2003) such as self-focusing, dispersion, and self-modulation can occur during the laser-gas propagation at laser powers near the critical power for nonlinear self-focusing in gas (Esarey, Sprangle, *et al.*, 1997), $P_N = \lambda^2/(2\pi\eta_0\eta_2)$ (for a Gaussian radial intensity profile, with the index of refraction given by $\eta = \eta_0 + \eta_2 I$). For example, $P_N \approx 1.8$ GW for a $\lambda = 0.8$ μm pulse propagating in air at 1 atm. Temporal pulse narrowing and splitting are found to occur due to phase modulation and group velocity dispersion (Wu and Antonsen, 2003). When the laser power exceeds the ionization threshold of the gas, a plasma is formed, resulting in ionization-induced refraction (Leemans *et al.*, 1992), which defocuses the pulse. Ionization can also result in modulational instabilities due to varying degrees of ionization throughout the laser pulse (Sprangle *et al.*, 1996b; Bian and Antonsen, 2001). For even higher powers, partial trapping of the laser pulse in the plasma and self-interference effects can occur (Wu and Antonsen, 2003). Such effects can result in unstable performance of the LPA.

In the case of hydrogen (helium) gas, laser prepulses or amplified spontaneous emission from the laser system that exceeds 10^{14} W/cm^2 (10^{15} W/cm^2) can result in a preplasma that can impact the performance of the LPA (Hosokai *et al.*, 2003). Controlling the preplasma has been done by, for example, a localized magnetic field (Hosokai, Kinoshita, *et al.*, 2006), by controlling the laser prepulse levels (Mangles *et al.*, 2006), or through laser preionization (Volfbeyn *et al.*, 1999).

A. Optical guiding in plasmas

The optical guiding mechanisms (Esarey, Sprangle, *et al.*, 1997) discussed below are based on the principle of refractive guiding. Refractive guiding becomes possible when the radial profile of the index of refraction $\eta_r(r)$ exhibits a maximum on axis, i.e., $\partial\eta_r/\partial r < 0$. Since $\eta_r \simeq ck_z/\omega$, $\partial\eta_r/\partial r < 0$ implies that the phase velocity along the propagation axis is less than off axis. This causes the laser phase fronts to curve such that the beam focuses toward the axis.

The index of refraction for a small amplitude electromagnetic wave propagating in a plasma of uniform density $n = n_0$, in the 1D limit, is given by $\eta_r = (1-\omega_p^2/\omega^2)^{1/2}$. For large amplitude waves, however, variations in the electron density and mass will occur, i.e., $\omega_p^2(r) = (\omega_{p0}^2/\gamma)n/n_0$. Hence, the general expression for the index of refraction for a large amplitude electromagnetic wave in a plasma is given by (Sprangle *et al.*, 1992, 1990)

$$\eta_r(r) \simeq 1 - \frac{\omega_{p0}^2}{2\omega^2}\frac{n(r)}{n_0\gamma(r)}, \tag{84}$$

assuming $\omega_{p0}^2/\omega^2 \ll 1$. The index of refraction profile $\eta_r(r)$ can be modified by the relativistic factor $\gamma(r)$ or the radial density profile $n(r)$. The leading-order motion of the electrons in the laser field is the quiver motion $\boldsymbol{p}_\perp = m_e c\boldsymbol{a}$ and, hence, $\gamma \simeq \gamma_\perp = (1+a^2)^{1/2}$. A laser intensity profile peaked on axis $\partial a^2/\partial r < 0$ leads to $\partial\eta_r/\partial r < 0$ and the possibility of guiding (i.e., relativistic self-focusing). The density profile can have contributions from a preformed density channel $\Delta n_p \sim \Delta n r^2/r_0^2$ or a plasma wave $\delta n \sim \delta\hat{n}(r)\cos k_p\zeta$, where $n = n_0 + \Delta n_p + \delta n$. A radial density profile that has a minimum on axis (i.e., a channel)

implies $\partial\eta_r/\partial r<0$ and the possibility of guiding. In the limits $a^2\ll 1$, $|\Delta n_p/n_0|\ll 1$, and $|\delta n/n_0|\ll 1$, the refractive index is (Esarey *et al.*, 1996)

$$\eta_r \simeq 1-\frac{\omega_{p0}^2}{2\omega^2}\left(1-\frac{a^2}{2}+\frac{\Delta n_p}{n_0}+\frac{\delta n}{n_0}\right). \tag{85}$$

In the above expression, the $a^2/2$ term is responsible for relativistic optical guiding (Litvak, 1969; Max *et al.*, 1974; Sprangle, Tang, *et al.*, 1987; Sun *et al.*, 1987), the $\Delta n_p/n_0$ term is responsible for preformed density channel guiding (Steinhauer and Ahlstrom, 1971; Johnson and Chu, 1974; Sprangle and Esarey, 1992; Sprangle *et al.*, 1992; Durfee and Milchberg, 1993; Durfee *et al.*, 1995; Volfbeyn *et al.*, 1999; Gaul *et al.*, 2000; Goddes *et al.*, 2004, 2005a), and the $\delta n/n_0$ term is responsible for self-channeling (Sun *et al.*, 1987; Kurki-Suonio *et al.*, 1989; Sprangle *et al.*, 1992; Esarey, Sprangle, *et al.*, 1993), plasma wave guiding (Esarey and Ting, 1990; Sprangle *et al.*, 1990a; Ting *et al.*, 1990), and self-modulation of long laser pulses (Andreev *et al.*, 1992; Antonsen and Mora, 1992; Sprangle *et al.*, 1992 Esarey *et al.*, 1994).

B. Relativistic optical guiding

The self-focusing of laser beams by relativistic effects was first considered by Litvak (1969) and Max *et al.*, (1974). In the standard theory of relativistic optical guiding (Sprangle *et al.*, 1987), only the effects of the transverse quiver motion of the electrons are included in the expression for η_r, i.e., $n=n_0$ and $\gamma=\gamma_\perp(r)$, where $\gamma_\perp^2=1+a^2(r)$ and circular polarization is assumed. Inclusion of the self-consistent density response, however, indicates that relativistic self-focusing is ineffective in preventing the diffraction of short ($L\lesssim\lambda_p$) laser pulses (Sprangle *et al.*, 1990, 1992).

In the weakly relativistic limit ($a^2\ll 1$), the refractive index is given by

$$\eta_r \simeq 1-(\omega_{p0}^2/2\omega^2)(1-a^2/2), \tag{86}$$

where the density response has been neglected ($n=n_0$). Refractive guiding requires $\partial\eta_r/\partial r<0$, which is satisfied for a laser intensity profile peaked on axis, $\partial a^2/\partial r<0$. The paraxial wave equation with a refractive index given by Eq. (86) has the form of a Schrödinger equation with a third-order nonlinearity, as in nonlinear optics where $\eta_r=\eta_0+\eta_2 I$. Hence, self-focusing will occur when the laser power P exceeds a critical power P_c (Sprangle, Tang, *et al.*, 1987).

An equation for the laser spot size $r_s(\zeta,z)$ can be derived by applying a method such as the source dependent expansion (SDE) method (Sprangle, Ting, *et al.*, 1987) to the paraxial wave equation [Eq. (81) neglecting the term $\partial^2/\partial\zeta\partial\tau$]. In effect, the SDE method assumes that the radial intensity profile is approximately Gaussian, $|\hat{a}|^2=(a_0r_0/r_s)^2\exp(-2r^2/r_s^2)$, and finds a best fit for the spot size $r_s(\zeta,z)$ locally in space and time. Using the index of refraction given by Eq. (86), the laser spot size evolves according to (Sprangle, Tang, *et al.*, 1987)

$$\frac{d^2R}{dz^2}=\frac{1}{Z_R^2R^3}\left(1-\frac{P}{P_c}\right), \tag{87}$$

where $R=r_s/r_0$ is the normalized spot size, r_0 is the minimum spot size in vacuum, and $Z_R=kr_0^2/2$ is the vacuum Rayleigh length. The first term on the right-hand side of Eq. (87) represents vacuum diffraction, whereas the second term represents relativistic self-focusing. Here $P/P_c=k_p^2a_0^2r_0^2/16$ for circular polarization (for linear polarization, $a_0^2\to a_0^2/2$). The critical power for relativistic self-focusing is $P_c=2c(e/r_e)^2(\omega/\omega_{p0})^2$, where $r_e=e^2/m_ec^2$ or, in practical units,

$$P_c(\mathrm{GW})\simeq 17.4\,(\omega/\omega_{p0})^2. \tag{88}$$

The solution to Eq. (87) with $dr_s/dz=0$ at $z=0$ is

$$r_s^2/r_0^2=1+(1-P/P_c)z^2/Z_R^2, \tag{89}$$

which indicates that the spot size diffracts for $P<P_c$, remains guided or "matched" ($r_s=r_0$) for $P=P_c$, and focuses for $P>P_c$. Equation (87) predicts "catastrophic" focusing for $P>P_c$. This results from the approximation $(1+a^2)^{-1/2}\simeq 1-a^2/2$ in the $a^2\ll 1$ limit. Higher-order nonlinearities will prevent the laser from focusing indefinitely (Sprangle, Tang, *et al.*, 1987; Hafizi *et al.*, 2000).

The above discussion of relativistic guiding neglected the electron density response δn in the expression for the index of refraction. The effectiveness of relativistic guiding can be strongly influenced by the plasma response. In particular, relativistic optical guiding is ineffective in preventing the diffraction of sufficiently short pulses, $L\lesssim\lambda_p/\gamma_\perp$ (Sprangle *et al.*, 1990, 1992) because the index of refraction becomes modified by the laser pulse on the plasma frequency time scale, not the laser frequency time scale. Typically, relativistic guiding only affects the body of long pulses, $L>\lambda_p$.

In the 1D ($r_s^2k_p^2\gg 1$) and weakly relativistic ($a^2\ll 1$) limits, nonlinear quasistatic theory (Sprangle *et al.*, 1990a) indicates that the self-consistent electron density response satisfies $\delta n/n_0-a^2/2\simeq-\delta\phi$, hence,

$$\eta_r \simeq 1-(\omega_{p0}^2/2\omega^2)(1-\delta\phi), \tag{90}$$

where $\delta\phi$ is the normalized electrostatic potential that satisfies

$$(\partial^2/\partial\zeta^2+k_p^2)\delta\phi=k_p^2a^2/2. \tag{91}$$

For long laser pulses with sufficiently smooth envelopes ($|\partial a^2/\partial\zeta|\ll|k_pa^2|$), $\partial^2\phi/\partial\zeta^2$ can be neglected in Eq. (91) (which neglects the generation of plasma waves) and $\delta\phi\simeq a^2/2$. Hence, in the long pulse limit $L\gg\lambda_p$, the index of refraction has the form given by Eq. (86) and the standard theory of relativistic focusing discussed above can be applied to the body of long pulses. Although long pulses can be guided by relativistic effects, they can also be unstable to self-modulation (Andreev *et al.*, 1992; Antonsen and Mora, 1992; Sprangle *et al.*, 1992) and laser-hose instabilities (Shvets and Wurtele, 1994; Sprangle *et al.*, 1994), which are discussed in Sec. VI.B.

Short pulse $L\lesssim\lambda_p$ diffraction, even in the regime $P\gtrsim P_c$, can be most easily shown as follows. For very short

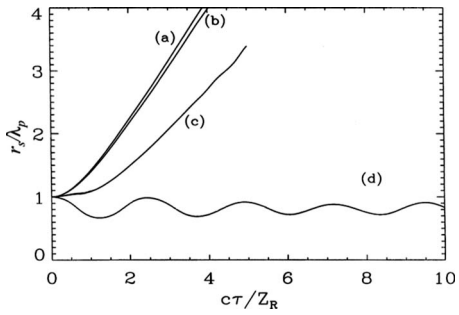

FIG. 27. Laser spot size r_s vs normalized propagation distance $c\tau/Z_R$ for (a) vacuum diffraction, (b) $L=\lambda_p/4$, and (c) $L=\lambda_p$, with parameters $P=P_c$, $a_0=0.9$, and $\lambda_p=0.03$ cm. (d) Guiding of $L=\lambda_p$ pulse in a preformed parabolic plasma density channel with $\Delta n=1/\pi r_e r_s^2$. From Sprangle *et al.*, 1992.

pulses $L<\lambda_p$, the k_p^2 term can be neglected on the left-hand side of Eq. (91). For example, a short pulse with a constant intensity profile ($a^2=a_0^2$) induces a space charge potential given by $\phi\simeq k_p^2 a_0^2\zeta^2/4$, and the refractive index becomes

$$\eta_r \simeq 1-(\omega_{p0}^2/2\omega^2)(1-k_p^2 a_0^2\zeta^2/4), \tag{92}$$

as opposed to Eq. (86). This indicates that the effective critical power for a short pulse (Sprangle *et al.*, 1990a) is $P_{c,\mathrm{sp}}\simeq 2P_c/k_p^2\zeta^2 \gg P_c$ since $k_p^2\zeta^2/2\ll 1$ for a short pulse. In particular, $P_{c,\mathrm{sp}}$ becomes infinite at the leading edge of the pulse $\zeta\to 0$. Hence, the leading portion $L<\lambda_p$ of a laser pulse will diffractively erode even when $P\simeq P_c$.

Simulations (Sprangle *et al.*, 1992), based on a 2D-axisymmetric quasistatic fluid model, confirm the inability of relativistic guiding to prevent the diffraction of short laser pulses. The results are shown in Fig. 27 for the parameters $\lambda_p=0.03$ cm ($n_0=1.2\times 10^{16}$ cm^{-3}), $r_0=\lambda_p$ (Gaussian radial profile), $\lambda=1$ μm ($Z_R=28$ cm), and $P=P_c$. The initial axial laser profile is given by $|\hat{a}(\zeta)|=a_0\sin(-\pi\zeta/L)$ for $0<-\zeta<L=c\tau_L$, where $a_0=0.9$ for the above parameters. Simulations are performed for two laser pulse lengths, $L=\lambda_p$ ($\tau_L=1$ ps) and $L=\lambda_p/4$ ($\tau_L=0.25$ ps). The spot size at the pulse center versus normalized propagation distance $c\tau/Z_R$ is shown in Fig. 27 for (a) the vacuum diffraction case, (b) the $L=\lambda_p/4$ pulse, and (c) the $L=\lambda_p$ pulse. The $L=\lambda_p/4$ pulse diffracts almost as if in vacuum. The $L=\lambda_p$ pulse experiences a small amount of initial guiding before diffracting. A preformed parabolic plasma density channel, however, is effective in guiding the $L=\lambda_p$ pulse, as shown in Fig. 27(d), where the channel depth is given by $\Delta n=1/\pi r_e r_0^2=1.3\times 10^{15}$ cm^{-3} and the density on axis is $n_0=1.2\times 10^{16}$ cm^{-3}.

Experiments on relativistic self-guiding have been performed for laser pulses propagating in gas-filled chambers, pulsed gas jets, or plasmas generated by exploding foils (Borisov *et al.*, 1992; Monot *et al.*, 1995; Young *et al.*, 1995; Chiron *et al.*, 1996; Borghesia *et al.*, 1997; Krushelnick *et al.*, 1997; Wagner *et al.*, 1997; Clayton *et al.*, 1998; Leemans *et al.*, 2002). For example, in experiments using gas jets (Krushelnick *et al.*, 1997; Wagner *et al.*, 1997; Clayton *et al.*, 1998; Santala, Najmudin, *et al.*, 2001; Leemans *et al.*, 2002), the laser pulse was typically observed to propagate through the entire width of the jet (approximately few millimeters, which correspond to a few tens of Z_R, depending on the focusing optics used) when $P>P_c$. Many of these experiment occurred in the self-modulated LWFA regime, and accelerated electrons were also observed (Krushelnick *et al.*, 1997; Wagner *et al.*, 1997; Clayton *et al.*, 1998; Santala, Najmudin, *et al.*, 2001a; Leemans *et al.*, 2002). In most of these experiments, ponderomotive self-channeling also occurs simultaneously with relativistic self-focusing, as discussed in Sec. V.D.

C. Preformed plasma density channels

The concept of using a plasma density channel to guide a laser beam dates back to early studies of laser fusion (Steinhauer and Ahlstrom, 1971; Johnson and Chu, 1974). Density channels in plasmas have been created by a number of methods. An intense laser pulse propagating in a plasma can create a channel through a combination of ponderomotive and thermal effects. The creation of a density channel through the hydrodynamic expansion of the radial plasma profile was observed in the early 1970s in long-pulse (150 ns) CO_2 laser experiments (Johnson and Chu, 1974). The length of such a channel, however, is limited to the propagation distance of the laser pulse that creates the channel, and the utility of using such a channel to guide a laser pulse, many Rayleigh lengths, is limited. High-power short laser pulses can be guided in plasma channels created by a variety of methods, including laser-induced hydrodynamic expansion (Durfee and Milchberg, 1993; Milchberg *et al.*, 1996; Volfbeyn *et al.*, 1999; Gaul *et al.*, 2000; Geddes *et al.*, 2004) and capillary discharges (Zigler *et al.*, 1996; Ehrlich *et al.*, 1998; Hooker *et al.*, 2000; Hosokai *et al.*, 2000; Butler *et al.*, 2002; Luther *et al.*, 2004; Leemans, Nagler, *et al.*, 2006; Gonsalves *et al.*, 2007; Nakamura *et al.*, 2007).

To understand the basic principles of channel guiding, consider a parabolic density channel of the form $n=n_0+\Delta n r^2/r_0^2$, where $\Delta n=n(r_0)-n(0)$ is the channel depth. For a low power $P\ll P_c$, low intensity $a^2\ll 1$ laser pulse, the index of refraction is given by

$$\eta_r = 1-\frac{\omega_{p0}^2}{2\omega^2}\left(1+\frac{\Delta n}{n_0}\frac{r^2}{r_0^2}\right). \tag{93}$$

Analysis of the paraxial wave equation with an index of refraction of this form indicates that the spot size r_s of a Gaussian laser beam with $|\hat{a}|^2=(a_0 r_0/r_s)^2\exp(-2r^2/r_s^2)$ evolves according to (Esarey *et al.*, 1994)

$$\frac{d^2R}{dz^2}=\frac{1}{Z_R^2R^3}\left(1-\frac{\Delta n}{\Delta n_c}R^4\right). \tag{94}$$

The first term on the right-hand side represents the effects of vacuum diffraction and the second term represents the focusing effects of the channel. Equation (94) indicates that a Gaussian beam will be guided at the

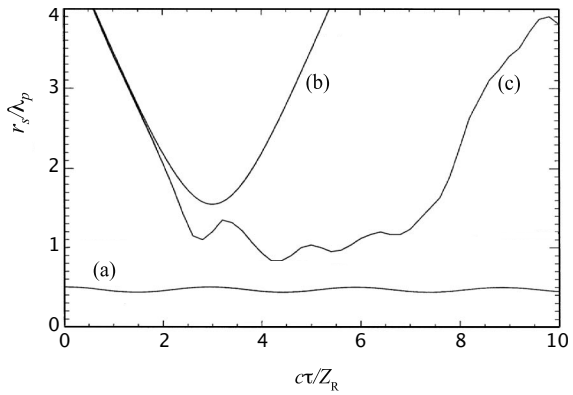

FIG. 28. Laser spot size r_s vs propagation distance $c\tau$ for (a) a channel-guided LWFA, (b) vacuum diffraction, and (c) the self-modulated LWFA shown in Figs. 14–16. From Esarey, Sprangle, *et al.*, 1993.

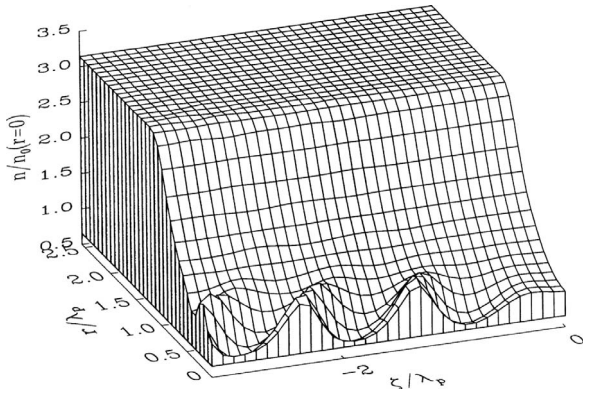

FIG. 29. Plasma electron density n/n_0 at $c\tau=20Z_R$ for a channel-guided LWFA. Initial density profile is parabolic with a depth $\Delta n=\Delta n_c=1/\pi r_e r_0^2$. From Esarey, Sprangle, *et al.*, 1993.

matched beam spot size $r_s=r_0$ provided that the channel depth Δn is equal to the critical channel depth given by (Sprangle and Esarey, 1992; Sprangle *et al.*, 1992)

$$\Delta n_c=(\pi r_e r_0^2)^{-1} \tag{95}$$

or $\Delta n_c(\mathrm{cm}^{-3})=1.13\times10^{20}/r_0^2(\mu\mathrm{m})$, where $r_e=e^2/m_ec^2$ is the classical electron radius.

The general solution to Eq. (94) for the initial ($z=0$) conditions $dr_s/dz=0$ and $r_s=r_i$ is (Esarey *et al.*, 1994)

$$2\frac{r_s^2}{r_i^2}=1+\frac{\Delta n_c r_0^4}{\Delta n r_i^4}+\left(1-\frac{\Delta n_c r_0^4}{\Delta n r_i^4}\right)\cos(k_{\mathrm{os}}z), \tag{96}$$

where $k_{\mathrm{os}}=(2/Z_R)(\Delta n/\Delta n_c)^{1/2}$ and r_i is the injected spot size. A matched beam requires $\Delta n r_i^4=\Delta n_c r_0^4$, e.g., $r_i=r_0$ and $\Delta n=\Delta n_c$. If the beam is not matched within the channel, the spot size oscillates between $r_s^2=r_i^2$ and $r_s^2=\Delta n_c r_0^4/\Delta n r_i^2$ with an average value $\langle r_s^2\rangle=(r_i^2/2)(1+\Delta n_c r_0^4/\Delta n r_i^4)$. The oscillation period within the channel is $\lambda_{\mathrm{os}}=2\pi/k_{\mathrm{os}}=\pi Z_R(\Delta n_c/\Delta n)^{1/2}$. The laser beam will remain confined within the channel provided that the maximum radius of the channel is sufficiently larger than r_s.

For a long ($L\gg\lambda_p$) laser pulse in a plasma channel, relativistic self-focusing will also contribute to guiding. In the $a^2\ll1$ limit, Eq. (94) is modified by including the term $-(Z_R^2R^3)^{-1}P/P_c$ on the right-hand side. The matched beam condition is then $\Delta n/\Delta n_c=1-P/P_c$. For a mismatched beam, Eq. (96) is modified by multiplying the $\Delta n_c r_0^4/\Delta n r_i^4$ terms by $1-P/P_c$. For a short pulse, the effects of P/P_c are diminished, as discussed in Sec. V.B.

To illustrate the effectiveness of optical guiding using preformed density channels, the results of two simulations are presented, based on the 2D-axisymmetric fluid model discussed in Sec. V. The first simulation (Esarey, Sprangle, *et al.*, 1993) is of a channel-guided LWFA with an ultrashort ($L\simeq\lambda_p$) high-intensity ($a_0\sim1$) laser pulse, the results of which are shown in Figs. 28(a), 29, and 30. In this example, the initial axial laser profile is given by $|\hat{a}(\zeta)|=a_0\sin(-\pi\zeta/L)$ for $0<-\zeta<L$, with $a_0=0.72$ and $L=120$ μm (400 fs). Also, $\lambda=1$ μm and $r_0=60$ μm (Gaussian radial profile), which implies $Z_R=1.1$ cm and $P=40$ TW. The density on axis is chosen such that $L=\lambda_p$ ($n_0=7.8\times10^{16}$ cm^{-3}) and a parabolic profile is assumed with $\Delta n=(\pi r_e r_0^2)^{-1}=3.2\times10^{16}$ cm^{-3}.

Figure 28(a) shows the evolution of the laser spot size versus normalized propagation distance $c\tau/Z_R$. The laser pulse remains guided by the density channel, the laser spot size exhibiting small oscillations about its initial value over the full $20Z_R=23$ cm simulation length. After $c\tau=20Z_R$, the pulse profile shows very little distortion from its initial profile. A surface plot of the electron density profile at $c\tau=20Z_R$ is shown in Fig. 29. The initial unperturbed parabolic profile can be seen at $\zeta=0$, and the distortion of the channel by the laser pulse, including the excitation of a large amplitude wakefield along the axis, is evident in the region $\zeta<0$. In this example nearly all electrons have been expelled from the vicinity of the laser pulse. The radial variation in the channel density causes a radial variation in the plasma wavelength and curvature of the plasma wave fronts. A slight axial damping of the plasma wave also occurs, as evident in Fig. 30, where the axial electric field E_z is plotted versus ζ along the axis at $c\tau=20Z_R$.

The second simulation is an example of mismatched laser propagation in a channel, which extends in the

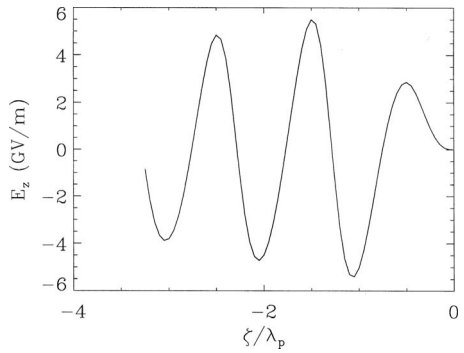

FIG. 30. Axial electric field E_z on axis at $c\tau=20Z_R$ for channel-guided LWFA shown in Fig. 29. From Esarey, Sprangle, *et al.*, 1993.

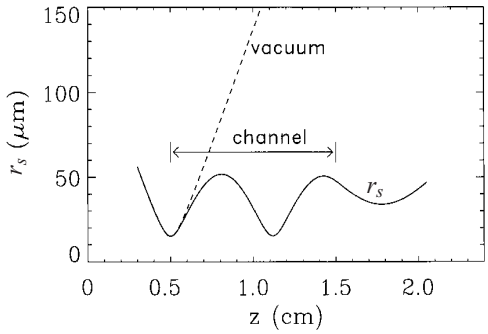

FIG. 31. Laser spot size vs propagation distance $z=c\tau$ in vacuum (dashed curve) and in a plasma channel (solid curve) located at $0.5<z<1.5$ cm for a low-power $P\ll P_c$ mismatched pulse. From Ehrlich *et al.*, 1996.

range $0.5<z<1.5$ cm with $n_0=5\times10^{18}$ cm^{-3} and $\Delta n_p(r=150\ \mu\text{m})=4n_0/5$ [parameters near those of the experiment of Ehrlich *et al.* (1996)]. Here a $\lambda=0.8$ μm, 100 fs, 30 GW (3 mJ), 1.6 times diffraction-limited laser pulse is focused on the channel entrance with spot size $r_i=15$ μm. Owing to the low laser power, the pulse does not become self-modulated. Figure 31 shows that the laser spot size oscillates about its matched value of $r_0=28$ μm, emerging from the 1 cm long channel with a radius of 45 μm and a divergence angle of 14 mrad, in approximate agreement with the experiment of Ehrlich *et al.* (1996).

The above discussion concerned parabolic channel profiles. Other channel profiles, however, may offer different advantages. Durfee *et al.* (1995) discussed the formation of "leaky" channels, in which the channel is approximately parabolic out to some radius, after which the density goes to zero. Such a profile occurs naturally in the creation of plasma channels by hydrodynamic expansion of a hot plasma core in a gas. Higher-order transverse modes may not be guided by such a channel, and Antonsen, and Mora (1995) described how leaky channels can stabilize certain instabilities, such as small angle forward Raman scattering (Antonsen and Mora 1993; Mori *et al.*, 1994) self-modulation (Andreev *et al.*, 1992; Sprangle *et al.*, 1992; Esarey *et al.*, 1994), and laser hosing (Shvets and Wurtele, 1994; Sprangle *et al.*, 1994). Hollow channels (e.g., a plasma channel with density zero on axis out to the channel radius r_{ch}) may have beneficial properties with regard to particle acceleration (Chiou *et al.*, 1995; Schroeder, Wurtele, *et al.*, 1999). Within the hollow channel, where the plasma density is essentially zero, the transverse profile of the axial wakefield is uniform and the focusing force linear. The excited wakefield is electromagnetic with fundamental mode frequency (Schroeder, Wurtele, *et al.*, 1999) $\omega_{hc}=\omega_p[1+k_p r_{\text{ch}}K_0(k_p r_{\text{ch}})/2K_1(k_p r_{\text{ch}})]^{-1/2}$, where $K_{0,1}$ are modified Bessel function. The wakefield in such a channel, however, may be damped through resonant absorption in the channel walls at $\omega_{hc}\simeq\omega_p(r)$ (Shvets *et al.*, 1996).

The ability to guide intense laser pulses over many Z_R is an essential element of a high-energy LWFA (Leemans *et al.*, 1996, 1998). Plasma channel guiding of short laser pulses was first demonstrated in hydrodynamically formed plasma channels produced by focusing a relatively intense laser beam with an axicon lens (Durfee and Milchberg, 1993; Milchberg *et al.*, 1996). In these pioneering experiments, high-Z gases were used to facilitate the ionization process. High-Z gases, however, are susceptible to further ionization when used with ultrahigh intensity lasers, and, therefore a method was needed to allow the use of low-Z gases. By separating out the ionization and heating phase of the channel formation, channels were produced in hydrogen gas with the ignitor-heater method (Volfbeyn *et al.*, 1999).

Another laser-induced channel guiding technique utilizes a pump-probe method (Krushelnick *et al.*, 1997; Wagner *et al.*, 1997). In these experiments, an intense pump pulse with $P>P_c$ was guided through a gas jet through a combination of relativistic self-focusing and ponderomotive self-channeling. The ponderomotive force of the pump pulse created a plasma channel after its passage. This channel was then used to guide a low power probe pulse propagating along the axis.

In addition to laser-induced channels, guiding has also been demonstrated in plasma channels produced by capillary discharges (Zigler *et al.*, 1996; Ehrlich *et al.*, 1998; Hooker *et al.*, 2000; Hosokai *et al.*, 2000; Butler *et al.*, 2002; Luther *et al.*, 2004; Leemans, Nagler, *et al.*, 2006; Nakamura, *et al.*, 2007). One advantage of capillary discharges over that of laser-induced plasma channels is length. Laser-induced channels have typically been limited to a few millimeters, whereas capillary discharges can be on the order a few centimeters. Possible disadvantages of capillary discharges include a limited lifetime and the introduction of higher Z impurities due to wall ablation. Guiding in curved capillaries has also been demonstrated (Ehrlich *et al.*, 1996).

Other channel techniques have also been considered, such as evacuated and gas-filled capillaries (Dorchies *et al.*, 1999) laser-ablated capillaries (Kitagawa *et al.*, 2004), discharge-initiated laser-induced channels (Gaul *et al.*, 2000), as well as laser-induced channels using a cluster jet (Kumarappan *et al.*, 2005), which has the possible advantage of producing lower density channels. Prior to 2004, however, all demonstrations of guiding in preformed plasma density channels were limited to the mildly relativistic regime, i.e., $a_0^2\ll1$.

Channeling at relativistic intensities (Geddes *et al.*, 2004, 2005a) was realized with preformed guiding channels created using a variation in the ignitor-heater method. In these experiments, a plasma was formed in a 2.4 mm long supersonic H_2 gas jet with an atomic density of 3×10^{19} cm^{-3} by an ignitor pulse (15 mJ,60 fs) that is co-axial with the drive pulse, then heated by a heater pulse (150 mJ,250 ps). Figure 32 shows the basic experimental setup. Hydrodynamic expansion of the plasma formed a channel that guided a relativistically intense drive pulse that was focused at the entrance to the channel. The drive pulse (500 mJ,55 fs) was focused with an off-axis parabola to a spot of 7 μm FWHM re-

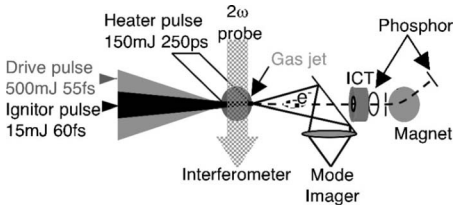

FIG. 32. Schematic of an channel-guided LPA experimental setup. Plasma channel formation uses the ignitor and heater laser pulses. The main drive pulse propagates down the plasma channel, driving a wakefield and self-trapping electrons. Density profiles are measured using a frequency-doubled probe beam. An integrating current transformer (ICT) is used to measure the charge per bunch of the electron beam. A dipole magnet permits electron beam energy distribution measurements. Additional detectors are used to monitor laser pulses, plasma, and secondary radiation (e.g., terahertz radiation, γ rays, and neutrons).

sulting in a laser intensity of 7×10^{18} W/cm^2.

The ignitor-heater method provides the ability to tailor the channel properties. By varying the time delay between the heater and drive pulses, energy of the heater pulse, and spatial overlap, channels can be created with different radial density profiles. Figure 33 shows an example of mode images of laser spots at 4 TW (7 μm input spot, 7×10^{18} W/cm^2). With the channel on, the output spot [Fig. 33(b)] matches the input spot [Fig. 33(a)]. The guided intensity within the channel is estimated to be 2.5×10^{18} W/cm^2. In the absence of any plasma, a large mode size consistent with vacuum diffraction is observed [Fig. 33(c)], and, with the gas jet on, but the channel off, Fig. 33(d) diffraction is increased by ionization effects (Rankin *et al.*, 1991; Leemans *et al.*, 1992b), showing that self-guiding alone is insufficient to efficiently guide the laser pulse.

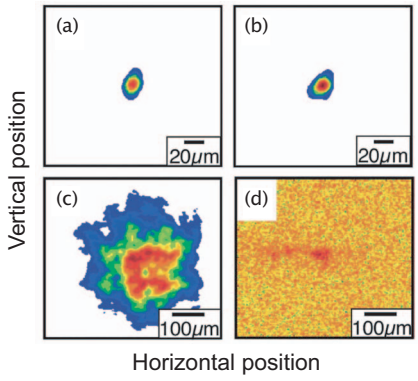

FIG. 33. (Color) Mode images of laser propagation with 4 TW ($P\simeq2P_c$) peak power. The guided output mode after 2.4 mm ($>10Z_R$) of propagation (b) is indistinguishable from the input mode (a). The effect of the channel can be seen by comparison to vacuum propagation over the same distance where the output mode is diffracted (c). The output mode with gas jet on but without the guide displays enhanced diffraction (d). Note enlarged scale in (c) and (d). From Geddes *et al.*, 2005a.

D. Ponderomotive self-channeling

The radial ponderomotive force of a long laser pulse ($L>\lambda_p$) propagating in an initially uniform plasma can expel electrons from the axis thus creating a density channel (i.e., self-channeling or electron cavitation) (Sun *et al.*, 1987; Kurki-Suonio *et al.*, 1989; Sprangle and Esarey, 1992; Sprangle *et al.*, 1992; Esarey, Sprangle, *et al.*, 1993; Hafizi *et al.*, 2000). This can enhance the effects of relativistic self-focusing. Consider a long ($L\gg\lambda_p$) axially uniform laser pulse propagating in an initially uniform plasma. The steady-state radial force balance indicates that the space charge force is equal to the ponderomotive force, i.e., $\nabla_\perp\phi=\nabla_\perp\gamma_\perp$, where $\gamma_\perp=(1+a^2)^{1/2}$ (with circular polarization). This implies a density perturbation via the Poisson equation $\nabla_\perp^2\phi=k_p^2\delta n/n_0$ given by (Sun *et al.*, 1987; Kurki-Suonio *et al.*, 1989; Sprangle *et al.*, 1992)

$$\delta n/n_0=k_p^{-2}\nabla_\perp^2(1+a^2)^{1/2}, \tag{97}$$

assuming $|\delta n/n_0|\leqslant1$. The corresponding index of refraction is given by

$$\eta_r\simeq1-\frac{\omega_{p0}^2}{2\omega^2}\left[\frac{1+k_p^{-2}\nabla_\perp^2(1+a^2)^{1/2}}{(1+a^2)^{1/2}}\right]. \tag{98}$$

This can also be derived from 2D nonlinear plasma theory via Eq. (82). In the long pulse limit $L\gg\lambda_p$, $|\partial\Psi/\partial\zeta|\ll|k_p\Psi|$ and $(1+\Psi)\simeq(1+a^2)^{1/2}$, which yield Eq. (98). Neglected in Eq. (98) is the generation of plasma waves, which can lead to the self-modulation of long pulses.

In the limit $a^2\ll1$, a Gaussian laser profile $a^2=a_0^2\exp(-2r^2/r_0^2)$ creates a density profile $\delta n=-\delta n(0)(1-2r^2/r_0^2)\exp(-2r^2/r_0^2)$. Along the axis, the depth of the ponderomotive channel is given by $\delta n(0)=a_0^2\Delta n_c$, where Δn_c is given by Eq. (95). Analysis of the paraxial wave equation with a density perturbation given by $\delta n/n_0=k_p^{-2}\nabla_\perp^2a^2/2$ indicates that the normalized spot size of a Gaussian laser pulse evolves according to (Sprangle *et al.*, 1991)

$$\frac{d^2R}{dz^2}=\frac{1}{Z_R^2R^3}\left(1-\frac{P}{P_c}-\frac{\delta n(0)}{2\Delta n_c}R^{-2}\right), \tag{99}$$

where $\delta n(0)=a_0^2\Delta n_c$ and $a^2\ll1$ is assumed. Hence, in the limit $P/P_c\ll1$, the ponderomotive channel depth required to guide a laser pulse is $\delta n(0)\geqslant2\Delta n_c$. When $a_0<1$, the ponderomotive self-channel alone will not guide the laser pulse. Furthermore, $|\delta n/n_0|<1$ implies $a_0^2<2(P/P_c)^{1/2}$ and $\delta n(0)<2(P/P_c)^{1/2}\Delta n_c$. Hence, $P/P_c\leqslant1$ implies $\delta n(0)<2\Delta n_c$, which again indicates that the ponderomotive channel alone will not guide the laser pulse. For laser powers approaching the critical power $P\to P_c$, guiding is achieved predominantly by relativistic self-focusing. Ponderomotive self-channeling can enhance this effect but does not dramatically alter the power threshold for guiding. More detailed studies (Sun *et al.*, 1987; Hafizi *et al.*, 2000), which include the effects of relativistic self-focusing and ponderomotive self-

channeling, concluded that the threshold power for guiding is $P(\mathrm{GW}) \geqslant 16.2(\omega^2/\omega_{p0}^2)$.

E. Plasma wave guiding

An ultrashort ($L < \lambda_p$) laser pulse can be guided by a plasma wave, provided that the laser pulse is properly phased within the wakefield and the wakefield amplitude is sufficiently large (Esarey and Ting, 1990; Sprangle *et al.*, 1990a; Ting *et al.*, 1990). The effective index of refraction for a low power ($P/P_c \ll 1$), low intensity ($a^2 \ll 1$) laser pulse propagating in a plasma wave is given by

$$\eta_r \simeq 1 - (\omega_{p0}^2/2\omega^2)(1 + \delta n/n_0), \tag{100}$$

where δn is the density oscillation of the plasma wave, which is assumed to be unaffected by the low intensity laser pulse. Consider a plasma wave of the form $\delta n = \delta\hat{n}(r)\sin(k_p\zeta)$, where $\delta\hat{n} > 0$ and $d\delta\hat{n}/dr < 0$. In regions where $\sin(k_p\zeta) < 0$, the plasma wave acts as a local density channel and enhances focusing, and in regions where $\sin(k_p\zeta) > 0$, the plasma wave enhances diffraction. Notice that a test laser pulse experiences maximum focusing at the minimum of δn (i.e., $\zeta = -\pi/2$). For a Gaussian laser mode, in the limit $a^2 \ll 1$, the wake amplitude required to guide a test laser pulse is $\delta\hat{n}(0) = 2\Delta n_c$ (Esarey, Sprangle, *et al.*, 1997). As discussed in Sec. II.G, it can be shown that a short laser pulse can be frequency upshifted by a plasma wave wakefield provided that it resides in the phase region where $\partial\delta n/\partial\zeta < 0$. In particular, maximum frequency upshifting occurs at the maximum of $-\partial\delta n/\partial\zeta$ (i.e., $\zeta = -\pi$ for the above example). In general, for a sinusoidal plasma wave, a test laser pulse will experience both enhanced focusing and frequency upshifting over a $|k_p\Delta\zeta| = \pi/4$ phase region of the plasma wave. Furthermore, Eq. (100) describes how a plasma wave can lead to the modulation of a long ($L > \lambda_p$) laser pulse (Esarey and Ting, 1990), as illustrated in Fig. 34.

In addition to a plasma wave acting as a local density channel and providing periodic regions of enhanced focusing and diffraction as described above, a plasma wave can enhance the self-focusing of long ($L \gg \lambda_p$) laser pulses by several other methods. For example, the electric field profile E_{pw} of the plasma wave can provide an additional radial ponderomotive force via ∇E_{pw}^2 (Joshi *et al.*, 1982). In addition, the oscillatory motion of the plasma electrons in the plasma wave can contribute to the relativistic Lorentz factor (Mori *et al.*, 1988). Furthermore, the plasma wave can lead to the generation of higher-order Stokes and anti-Stokes light waves (i.e., energy cascading) that can affect self-focusing (Gibbon and Bell, 1988). These effects have been observed in experiments (Joshi *et al.*, 1982) and simulations (Gibbon and Bell, 1988; Mori *et al.*, 1988) of two-frequency laser-plasma interactions, in which the plasma wave is resonantly driven by the laser beat wave.

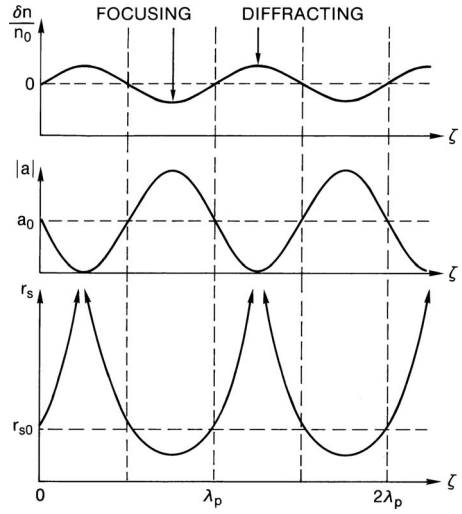

FIG. 34. Schematic of focusing effects of an externally generated plasma wave on an initially uniform low-intensity laser pulse.

VI. LASER-PLASMA INSTABILITIES

Laser-plasma instabilities can limit the laser propagation distance and degrade the performance of an LPA. This section will provide a brief overview of a few instabilities that are relevant to short-pulse LPAs: stimulated forward and backward Raman scatterings (Kruer, 1988; Esarey and Sprangle, 1992; McKinstrie and Bingham, 1992; Sakharov and Kirsanov, 1994; Decker, Mori, Katsouleas, *et al.*, 1996; Schroeder, Esarey, Shadwick, and Leemans, 2003), self-modulation (Andreev *et al.*, 1992; Antonsen and Mora, 1992, 1993; Sprangle *et al.*, 1992; Esarey *et al.*, 1994, 2000), and laser-hose instabilities (Shvets and Wurtele 1994; Sprangle *et al.*, 1994). In particular, this section will consider instabilities relevant to laser pulses short compared to the ion response time. Other instabilities present in long-pulse laser-plasma interactions, such as parametric coupling to ion modes, which have been observed in PBWA experiments (Amiranoff *et al.*, 1992), will not be discussed.

A. Stimulated Raman scattering

Stimulated Raman scattering involves the interaction of a light wave with an electron plasma wave (Kruer, 1988). In its most basic form, it consists of the decay of the pump laser field, with frequency and wave number $(\omega_0, \boldsymbol{k}_0)$, into an electron plasma wave $(\omega_e, \boldsymbol{k}_e)$ and two scattered light waves, namely, a Stokes wave $(\omega_0 - \omega_e, \boldsymbol{k}_0 - \boldsymbol{k}_e)$ and an anti-Stokes wave $(\omega_0 + \omega_e, \boldsymbol{k}_0 + \boldsymbol{k}_e)$. Typically, $\omega_e \simeq \omega_p + i\Gamma$, where the growth rate Γ is obtained through a standard linear instability analysis. In such an analysis, the pump laser field is assumed to be a 1D plane wave of the form $a \sim a_0 \exp(i\boldsymbol{k}_0 \cdot \boldsymbol{r} - i\omega_0 t)$. Perturbations are introduced, $\delta a \sim \exp[i(\boldsymbol{k}_0 \pm \boldsymbol{k}_e)\cdot \boldsymbol{r} - i(\omega_0 \pm \omega_e)t]$, and the linearized equations are then solved to determine the behavior of the instability. Since the pump laser is assumed to be a 1D plane wave, the

3D evolution of the pump laser is not taken into consideration. In particular, the effects of diffraction and self-focusing are neglected. Strictly speaking, the resulting analysis is only valid for times short compared to the characteristic evolution time τ_E of the pump laser, e.g., $t<\tau_E\sim Z_R/c$. In practice, however, the growth rates obtained from such an analysis can be adequate estimates provided that the mode frequency and growth rate are large compared to τ_E^{-1}.

For an infinite 1D plane wave pump field, the purely temporal Raman growth rates, i.e., $\delta a\sim\exp(\Gamma t)$ with growth rate Γ independent of t, can be obtained in a straightforward manner. The basic treatment of forward and backward Raman scattering is presented in the monograph by Kruer (1988). The coupled linearized equations for the scattered waves and the plasma wave, in the long pulse limit, yield the dispersion relation (Sakharov and Kirsanov, 1994; Schroeder, Esarey, Shadwick, and Leemans, 2003)

$$\frac{\omega_p^2 a_0^2}{4\gamma_\perp^3}\left(\frac{k^2c^2}{D_p}-1\right)=\left(\frac{1}{D_+}+\frac{1}{D_-}\right)^{-1}, \tag{101}$$

where $D_p=\omega_e^2-\omega_p^2/\gamma_\perp$ is the plasma wave dispersion relation and $D_\pm=(\omega_0\pm\omega_e)^2-(\boldsymbol{k}_0\pm\boldsymbol{k}_e)^2c^2-\omega_p^2/\gamma_\perp$ are the dispersion relations for the scattered light waves. Temporal growth rates for the Raman modes in various regimes can be derived from Eq. (101) [see, for example, Antonsen and Mora (1993)]. For short laser pulses, however, the growth and propagation of the instability with respect to the laser pulse front must be correctly taken into consideration. Antonsen and Mora (1992, 1993) first applied convective instability analysis, or a spatiotemporal analysis, to Raman instabilities in order to account for the short-pulse character of the instability.

1. Raman backward scattering

In Raman backscattering (RBS), the pump wave (ω_0,k_0) decays into a plasma wave (ω_e,k_e) and a backward going scattered wave $(\omega_0-\omega_e,k_0-k_e)$, where $\omega_e\simeq\omega_p$ and $k_e\simeq 2k_0$. The standard temporal growth rate (Kruer, 1988), in the limits $a_0^2\ll\omega_p/\omega_0\ll 1$, i.e., the weakly coupled regime, is $\Gamma=(a_0/2)(\omega_p\omega_0)^{1/2}$. In general, the scattered mode can propagate at some angle θ with respect to the pump wave, i.e., sidescatter, and the growth rate is given by $\sin(\theta/2)$ times the RBS result [when $2\sin(\theta/2)\gg\omega_p/\omega_0$]. The spatiotemporal analysis indicates that the number of e-folds N_e of the instability, $\delta a\sim\exp(N_e)$, is given by (Antonsen and Mora, 1993)

$$N_e\simeq(a_0^2k_pk_0/8)^{1/2}|\zeta|. \tag{102}$$

In effect, owing to the convective nature of the instability, the temporal growth is modified by $ct\to|\zeta|/\sqrt{2}$, where $\zeta=z-ct$ is a measure of the distance back from the front of the laser pulse.

Typically, RBS is the fastest growing of the Raman scattering instabilities. In LPAs, RBS is significant for a number of reasons. At low pump laser intensities, the spectrum of the backscattered radiation can be used to determine $\omega_0-\omega_p$, and hence the plasma density can be determined experimentally. For high pump intensities, however, it has been observed that the backscattered spectrum broadens (Darrow *et al.*, 1992; Krushelnick *et al.*, 1998) and, in some cases, becomes extremely broad, such that the $\omega_0-\omega_p$ peak can no longer be distinguished. Raman sidescatter and backscatter can erode the back of a long pulse, $L>\lambda_p$, since energy is being transported out of the pulse. This erosion has been observed in fluid (Antonsen and Mora, 1993; Andreev *et al.*, 1995) and particle simulations (Bulanov *et al.*, 1995; Decker, Mori, Tzeng, *et al.*, 1996).

As the RBS mode grows to large amplitude, it can trap the background plasma electrons, thus heating the plasma and creating a fast tail on the electron distribution. The phase velocity of the RBS plasma wave is $v_p=\omega_e/k_e=\omega_p/2k_0\ll c$. Since $v_p/c\ll 1$, the plasma wave can trap the background thermal electrons. The resulting fast electrons can be subsequently trapped by Raman scattered modes propagating at smaller angles θ, which will accelerate the electrons to higher energies (Joshi *et al.*, 1981; Bertrand *et al.*, 1995; Esarey *et al.*, 1998). Eventually, these background electrons can be trapped and accelerated to very high energies by the plasma wave associated with the forward Raman instability or the self-modulation instability, which has $v_p\simeq c$. This mechanism may explain how background plasma electrons can be trapped and accelerated to high energies, as is observed in experiments (Coverdale *et al.*, 1995; Nakajima *et al.*, 1995; Ting *et al.*, 1997; Wagner *et al.*, 1997; Gordon *et al.*, 1998; Gahn *et al.*, 1999; Leemans *et al.*, 2001; Malka *et al.*, 2001) and simulations (Bulanov *et al.*, 1995; Decker, Mori, Tzeng, *et al.*, 1996) in the self-modulated or forward Raman scattering regimes. For sufficiently large relativistic plasma wave amplitudes, self-trapping of background plasma electrons can also occur in the absence of RBS (Modena *et al.*, 1995).

For high pump intensities ($a_0\gg\omega_p/\omega_0$), theory predicts that stimulated backscattering occurs in the strongly coupled or Compton regime (Leemans *et al.*, 1991; Antonsen and Mora 1993; Sakharov and Kirsanov, 1994; Everett, Lal, Gordon, *et al.*, 1995; Shvets *et al.*, 1997; Schroeder, Esarey, Shadwick, and Leemans, 2003), for which $\omega\sim\Gamma\gg\omega_p$ and the number of e-folds is $N_e=(\sqrt{3}/2)(\omega_p^2\omega_0a_0^2/4)^{1/3}|\zeta|/\gamma_\perp$. In addition, 1D nonlinear theory predicts that for a linearly polarized pump laser field, stimulated backscattered harmonic radiation can be generated (Esarey and Sprangle, 1992) at frequencies given approximately by $(2\ell+1)\omega_0$ (ℓ is an integer), i.e., odd harmonics. Although the growth rate for the higher harmonics can be significant when $a_0^2\gg 1$, thermal effects, i.e., trapping of the background plasma electrons, can severely limit the generation of higher harmonics (Esarey and Sprangle, 1992).

2. Raman forward scattering

In Raman forward scattering (RFS) (Kruer, 1988), the scattered waves propagate parallel (or nearly parallel) to the pump wave, and the associated plasma wave has a

phase velocity $v_p \simeq c$. Hence, the plasma wave can be used to accelerate electrons to high energies. The RFS instability can serve as the basis for an LWFA (Tajima and Dawson, 1979; Joshi *et al.*, 1981; Esarey *et al.*, 1996; Mori *et al.*, 1994), in which a single long ($L > \lambda_p$) laser pulse becomes modulated via RFS and drives a large amplitude plasma wave. An LWFA based on RFS can be viewed as the 1D analog to the self-modulated LWFA.

The physical mechanism of RFS can be understood by the following 1D description (Mori, 1997). Consider a long uniform laser pulse propagating in the presence of an initially small amplitude plasma wave of the form $\delta n = \delta n_0 \sin k_p \zeta$ with $\delta n_0 > 0$. Since the local group velocity v_g is given by $v_g/c \simeq 1 - \omega_p^2(\zeta)/2\omega_0^2$, the local group velocity decreases in regions where $\delta n > 0$ and increases in regions where $\delta n < 0$. This tends to modulate the laser pulse such that the intensity modulations are $\pi/2$ out of phase with the density wave, i.e., $a \simeq a_0 + \delta a$, where $\delta a = \delta a_0 \cos k_p \zeta$ and $\delta a_0 > 0$. This intensity modulation feeds back via $(\partial^2/\partial\zeta^2 + k_p^2)\delta n/n_0 = (\partial^2/\partial\zeta^2)a^2/2$ and drives the plasma wave to larger amplitudes, resulting in the RFS instability.

Several regimes of the RFS can be identified (McKinstrie and Bingham, 1992; Antonsen and Mori, 1993; Decker, Mori, Katsouleas, *et al.*, 1996; Schroeder, Esarey, Shadwick, and Leemans, 2003), such as a four-wave regime, in which both $\omega_0 \pm \omega_p$ modes are resonant, a three-wave regime, in which only $\omega_0 - \omega_p$ is resonant with the pump laser and the plasma wave, as well as an intermediate four-wave nonresonant regime. The temporal growth rate in the four-wave resonant regime is $\Gamma_4 = \omega_p^2 a_0/2\sqrt{2}\omega_0$, the temporal growth rate in the four-wave nonresonant regime is $\Gamma_{4\mathrm{nr}} = \sqrt{3}\omega_p (a_0\omega_p^2/4\omega_0^2)^{2/3}/2$, and the temporal growth rate in the three-wave regime is $\Gamma_3 = \omega_p a_0 (\omega_p/\omega_0)^{1/2}/4$. The spatiotemporal analysis (Antonsen and Mora, 1993; Decker, Mori, Katsouleas, *et al.*, 1996; Schroeder, Esarey, Shadwick, and Leemans, 2003) indicates, however, that as the RFS instability grows, it passes through these various regimes, depending on the relative value of $|\zeta|/c\tau$, where $\zeta = z - ct$ and $\tau = t$ are independent coordinates. The number of e-foldings for these three RFS modes and the corresponding spatiotemporal regimes are given by (Antonsen and Mora, 1993; Decker, Mori, Katsouleas, *et al.*, 1996; Schroeder, Esarey, Shadwick, and Leemans, 2003)

$$N_e \simeq 2\Gamma_4 (|\zeta|\tau/c)^{1/2} \quad \text{for } a_0^2 \frac{|\zeta|}{c\tau} \gg 2\frac{\omega_p^2}{\omega_0^2}, \tag{103}$$

$$N_e \simeq \frac{3}{2}\Gamma_{4nr}(2|\zeta|\tau^2/c)^{1/3} \quad \text{for } 8\frac{\omega_p^5}{\omega_0^5} \ll \frac{a_0^2}{2}\frac{|\zeta|}{c\tau} \ll \frac{\omega_p^2}{\omega_0^2}, \tag{104}$$

$$N_e \simeq 2\Gamma_3 (|\zeta|\tau/c)^{1/2} \quad \text{for } a_0^2 \frac{|\zeta|}{c\tau} \ll 16\frac{\omega_p^5}{\omega_0^5}, \tag{105}$$

where $a_0^2 \ll 1$ and $\omega_p^2/\omega_0^2 \ll 1$ are assumed. A similar analysis has been applied by Antonsen and Mora (1993) to describe small angle RFS, the resulting growth rate is proportional to Γ_3, similar to Eq. (105). Note that the paraxial approximation to the wave operator $(\nabla_\perp^2 + 2ik_0\partial/\partial c\tau)$ is not sufficient to describe direct ($\theta = 0$) RFS; retention of the term $2\partial^2/\partial\zeta\partial c\tau$ is necessary to describe on-axis RFS. This was done in the fluid simulation of the self-modulated LWFA presented in Sec. III.D, i.e., the effects of both the RFS and self-modulation instabilities are present. A nonparaxial theory (Esarey *et al.*, 2000), describing the coupling of RFS and self-modulation instabilities, is discussed in the next section.

In addition, it is also possible for a RFS mode to undergo multiple scattering, sometimes referred to as cascading (Joshi *et al.*, 1981; Gibbon and Bell, 1988), resulting in multiple waves with frequencies $\omega_0 \pm \ell\omega_p$ (ℓ is an integer). It is possible to interpret this as photon acceleration, or phase modulation by the plasma wave, of the scattered light wave (Mori *et al.*, 1994). Numerous high-order Stokes and anti-Stokes lines have been observed in simulations of RFS (Decker *et al.*, 1994). Multiple (Coverdale *et al.*, 1995; Moore *et al.*, 1997; Wagner *et al.*, 1997) [up to the fifth (Modena *et al.*, 1995)] anti-Stokes lines have been observed in RFS or self-modulated LWFA experiments.

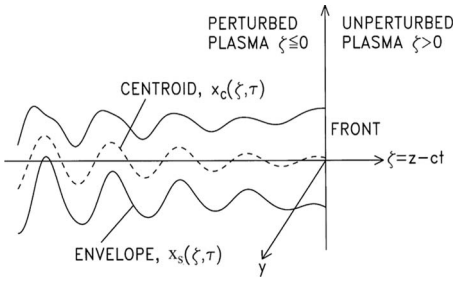

FIG. 35. Schematic of the hose-modulation instability showing the laser pulse centroid x_c and spot size x_s. From Sprangle *et al.*, 1994.

B. Self-modulation and laser-hose instabilities

A formalism has been developed (Esarey *et al.*, 1994, 2000; Sprangle *et al.*, 1994) to describe the 3D evolution of laser pulses in plasmas, including the effects of diffraction, relativistic and channel guiding, finite pulse duration, and coupling to the self-consistent plasma wave generated by the pulse structure. This formalism has been used to describe a class of "whole-beam" instabilities, which includes self-modulation (Esarey *et al.*, 1994; Sprangle *et al.*, 1994) and laser-hose (Sprangle *et al.*, 1994) instabilities. In this formalism, equations are derived to describe the evolution of the local laser pulse spot size $x_s(\zeta,t)$ and the local laser pulse centroid $x_c(\zeta,t)$, where the transverse profile of the laser field is assumed to be a Gaussian of the form $a \sim \exp[-(x-x_c)^2/x_s^2]$ (the y profile can be similarly defined). The self-modulation instability consists of a periodic "sausaging" of the laser spot size x_s and the laser hose consists of a periodic "kinking" of the laser centroid x_c, as show in Fig. 35. In

their most basic forms, the self-modulation and laser-hose instabilities are described by spot size and centroid perturbations of the forms $\delta x_{s,c} \sim \exp(\Gamma_{s,c} t + i k_p \zeta)$, i.e., having a period equal to the plasma wavelength $\lambda_p = 2\pi/k_p$ and a spatiotemporal growth rate $\Gamma_{s,c} = \Gamma_{s,c}(\zeta, t)$. Intrinsically, these instabilities involve a coupling to a plasma wave, and the dynamics of the instabilities are determined by the enhanced diffraction and focusing of the laser pulse owing to the presence of the plasma wave.

The physical mechanism underlying self-modulation has been described in Sec. III.D. The physical mechanism for laser hosing (Shvets and Wurtele, 1994; Sprangle *et al.*, 1994) is somewhat similar. Consider a long, $L > \lambda_p$, guided laser pulse $P/P_c = 1 - \Delta n/\Delta n_c$, with a centroid that is initially perturbed at the plasma wavelength $x_c \simeq x_{c0} \sin(k_p \zeta)$. This periodic centroid displacement will drive an asymmetric plasma wave. Notice that for $x_c^2/x_s^2 \ll 1$, the intensity profile is $a^2 \simeq a_0^2(1 + 4x x_c/x_s^2)\exp(-2x^2/x_s^2)$. At a fixed x position above the axis, $x = x_0$, the laser intensity modulation has the form $a^2(x_0)/a_0^2 \sim 1 + 4(x_0 x_{c0}/x_s^2)\sin(k_p \zeta)$, which drives a plasma wave. At a fixed x position below the axis, $x = -x_0$, the laser intensity is similarly modulated but π out of phase with respect to the $x = x_0$ modulation. Hence, the plasma wave driven below the axis is π out of phase with respect to the plasma wave driven above the axis, i.e., an asymmetric (with respect to x) plasma wave. Roughly speaking, the plasma wave has the form $\delta n \sim -(x/x_s)\cos(k_p \zeta)$. The laser pulse will tend to focus into the regions of reduced plasma density. For the asymmetric plasma wave, the laser pulse evolves in such a way as to enhance the initial centroid perturbation and the process proceeds in an unstable manner.

Equations describing the behavior of the spot size $x_s(\zeta, \tau)$ and centroid $x_c(\zeta, \tau)$ can be derived by analyzing the paraxial wave equation including the effects of a performed parabolic density channel and the self-consistent plasma response given by

$$\frac{\delta n}{n_0} = \int_0^\zeta d\zeta' \cos[k_p(\zeta - \zeta')] \frac{\partial}{\partial \zeta'} \frac{a^2(\zeta')}{2}. \tag{106}$$

In the limits $a^2 \ll 1$ and $k_p^2 r_0^2 \gg 1$, x_s and x_c obey equations of the form (Sprangle *et al.*, 1994)

$$\left(\frac{\partial^2}{\partial \hat{\tau}^2} + \frac{\Delta n}{\Delta n_c}\right)\hat{x}_c = -4k_p \int_0^\zeta d\zeta' \sin[k_p(\zeta' - \zeta)] \times [\hat{x}_c(\zeta') - \hat{x}_c(\zeta)] F_c(\zeta', \zeta) \frac{P(\zeta')}{P_c} \tag{107}$$

and

$$\frac{\partial^2 \hat{x}_s}{\partial \hat{\tau}^2} - \left(1 - \frac{\hat{x}_s P}{\hat{y}_s P_c} - \frac{\Delta n}{\Delta n_c}\hat{x}_s^4\right)\hat{x}_s^{-3} = 4\hat{x}_s \int_0^\zeta d\zeta' \cos[k_p(\zeta' - \zeta)] \frac{\partial}{\partial \zeta'}\left[F_s(\zeta', \zeta)\frac{P(\zeta')}{P_c}\right]. \tag{108}$$

Also, $\hat{y}_c$ and $\hat{y}_s$ obey equations similar to Eqs. (107) and (108), respectively. In the above, $\hat{x}_c = x_c/r_0$, $\hat{y}_c = y_c/r_0$, $\hat{x}_s = x_s/r_0$, $\hat{y}_s = y_s/r_0$, $\hat{\tau} = c\tau/Z_R$, $Z_R = k r_0^2/2$ is the Rayleigh length, $\Delta n_c = (\pi r_e r_0^2)^{-1}$ is the critical channel depth, $P(\zeta)/P_c = a^2 x_s y_s k_p^2/16$ is the laser power normalized to the critical power, and $F_{s,c}(\zeta', \zeta)$ are functions that depend on x_s, y_s, x_c, and y_c and couple the spot size dynamics to the centroid dynamics (Sprangle *et al.*, 1994).

The right-hand side of Eq. (107) indicates that if $x_c(\zeta) = x_c(\zeta')$ initially (i.e., a uniform centroid), $x_c(\zeta)$ will not increase. Hence, the laser-hose instability requires a nonuniform head-to-tail centroid displacement (Sprangle *et al.*, 1994), $\partial x_c/\partial \zeta \neq 0$. The right-hand side of Eq. (108) indicates that axial gradients in the laser power $\partial P/\partial \zeta \neq 0$ will lead to modulations in the laser envelopes (x_s, y_s), which can grow in an unstable manner as discussed in Sec. III.D. Both the self-modulation and laser-hose instabilities can occur either in a uniform plasma $(\Delta n = 0)$ or in a preformed density channel.

In the absence of a centroid perturbation, i.e., $x_c = 0$ (no hosing), self-modulation is described by Eq. (108). For an axisymmetric pulse $(x_s = y_s = r_s)$, $F_s = [R^2(\zeta) + R^2(\zeta')]^{-2}$ with $R = r_s/r_0$ (Esarey *et al.*, 1994). The second, third, and fourth terms on the left-hand side of Eq. (108) represent the effects of vacuum diffraction, relativistic focusing, and channel focusing, respectively, whereas the term on the right-hand side represents the nonlinear coupling of the laser envelope to the plasma wave. Equation (108) describes well-known laser pulse evolution, such as the inability of relativistic guiding to prevent the diffraction of short pulses $L < \lambda_p$ (Sprangle *et al.*, 1990a, 1990b, 1992; Ting *et al.*, 1990).

The evolution of a long axially uniform laser beam can be examined in the limit where the effect of the plasma wave is neglected, i.e., the nonlinear coupling term on the right-hand side of Eq. (108) is set equal to zero. This limit is discussed in Sec. V.C. In particular, a matched beam with $r_s = r_i = r_0$ requires $P = P_M$, where $P_M = P_c(1 - \Delta n/\Delta n_c)$ (Esarey *et al.*, 1994).

The effect of the plasma wave on the spot size evolution is described by the right-hand side of Eq. (108). The initial effect of the plasma wave can be estimated by approximating $R(\zeta') = R(\zeta)$ within the integral in Eq. (108), i.e., initially the spot size is uniform throughout the pulse. In this limit the right-hand side of Eq. (108) can be written as $(-\delta n/\Delta n_c)/(2R^3)$, where δn is the initial density perturbation given by Eq. (106). The rise associated with the front of the pulse gives a nonzero value of $\partial a^2/\partial \zeta$ that generates a finite amplitude density wake. Throughout the body of a long flat-top pulse, this density wake has the form $\delta n = \delta \hat{n} \cos(k_p \zeta)$. In particular,

for a flat-top pulse with a fast rise, $k_p^2 L_{\rm rise}^2 \ll 1$, Eq. (106) yields $\delta n/n_0 = -(a_0^2/2)\cos(k_p\zeta)$ and the right-hand side of Eq. (108) can be written as $(-\delta n/2\Delta n_c)R^{-3} = R^{-3}(P/P_c)\cos(k_p\zeta)$. Hence, at the phase regions where $\cos(k_p\zeta) = -1$, focusing requires $P \gg P_M/2$ (for $k_p^2 L_{\rm rise}^2 \gg 1$, the initial wake δn vanishes and focusing requires $P \gg P_M$). The effect of the initial density wake $\delta n(\zeta)$ is to produce ζ-periodic regions of enhanced focusing and diffraction. This causes the laser intensity to become modulated at λ_p, which subsequently enhances the density wake at later times. This is the basis of the self-modulation instability.

For sufficiently small perturbations, $x_s/r_0 \ll 1$ and $x_c/r_0 \ll 1$, Eqs. (107) and (108) decouple and self-modulation and the laser-hose instability can be analyzed independently. The growth of the instabilities for a long ($L \gg \lambda_p$) optically guided ($P = P_M$) laser pulse can be analyzed by perturbing Eq. (108) about the matched-beam equilibrium. Asymptotic growth rates can be obtained in various regimes using standard methods. A number of e-folds in the various regimes are given by the following (Esarey *et al.*, 1994; Sprangle *et al.*, 1994):

(i) Long pulse regime. $k_p|\zeta|Z_R/z \gg 4\alpha_1 P_c/P$,

$$N_e = \frac{3\sqrt{3}}{4}\left(\alpha_2 \frac{P}{P_c} k_p|\zeta| \frac{z^2}{Z_R^2}\right)^{1/3}, \tag{109}$$

(ii) Intermediate regime. $(\alpha_3/4)P/P_c \ll k_p|\zeta|Z_R/z \ll 4\alpha_1 P_c/P$,

$$N_e = \left(\alpha_3 \frac{P}{P_c} k_p|\zeta| \frac{z}{Z_R}\right)^{1/2}, \tag{110}$$

(iii) Short pulse regime. $k_p|\zeta|Z_R/z \ll (\alpha_3/4)(P/P_c)$,

$$N_e = \frac{3\sqrt{3}}{4}\left(\alpha_3 \frac{P}{P_c} k_p^2|\zeta|^2 \frac{z}{Z_R}\right)^{1/3}. \tag{111}$$

For the laser-hose instability, $\alpha_1 = \alpha_2 = \alpha_3 = 1$. For self-modulation, $\alpha_1 = \sqrt{2}(2 - P/P_c)^{3/2}$ ($\sqrt{2} \le \alpha_1 \le 4$), $\alpha_2 = 2$, and $\alpha_3 = \sqrt{2}(2 - P/P_c)^{-1/2}$ ($1 \le \alpha_3 \le \sqrt{2}$). Hence, the number of e-folds is a function of the dimensionless parameters P/P_c, $k_p|\zeta|$, and z/Z_R, where $z = c\tau$ in the underdense limit.

A nonparaxial theory of finite-radius pulses (Esarey *et al.*, 2000) can be used to describe the coupling of RFS and self-modulation instabilities. Linearizing about a matched, optically guided, laser yields the evolution of a laser spot size perturbation δr_s,

$$\mathcal{L}_1 \mathcal{L}_2 \delta r_s = (i/2)(k_p/k)\hat{P}^2 \delta r_s, \tag{112}$$

where $\mathcal{L}_1 = \partial_{\hat\zeta\hat z}^2 + (k_p/k)\hat{P} = (Z_R/k_p)[\partial_{\zeta z}^2 + (k_p^4/k^2)a_0^2/8]$ and $\mathcal{L}_2 = (\partial_{\hat z}^2 + \alpha_4^2)\partial_{\hat\zeta} + i\hat{P}$, with $\alpha_4 = (4 - 2\hat{P})^{1/2}$, $\hat{P} = P/P_c$, $\hat{z} = z/Z_R$, and $\hat{\zeta} = k_p\zeta$. The conventional 1D RFS instability is described by $\mathcal{L}_1 \delta r_s = 0$, and the conventional 2D self-modulational instability is described by $\mathcal{L}_2 \delta r_s = 0$. Asymptotic expressions for the number of e-folds N_e have been obtained in the appropriate spatial-temporal regimes. Two branches can be identified, and the coupling term on the right-hand side of Eq. (112) yields modified growth rates. For the self-modulational branch, $N_e = [2\hat{P}|\hat\zeta|\hat{z}/\alpha_4]^{1/2}$ in the regime $\hat{P}/(2\alpha_4) \ll |\hat\zeta|/\hat{z} \ll 2\alpha_4^3/\hat{P}$, $N_e = (3^{3/2}/4)[2\hat{P}|\hat\zeta|\hat{z}^2]^{1/3}$ in the regime $\alpha_4^3/2\hat{P} \ll |\hat\zeta|/\hat{z} \ll [2\hat{P}(k_p/k)^3]^{-1}$, and $N_e = (3^{3/2}/4)[\hat{P}|\hat\zeta|\hat{z}^2]^{1/3}$ in the regime $(k/k_p)^3/\hat{P} \ll |\hat\zeta|/\hat{z}$. For the RFS branch, $N_e = [4(k_p/k)\hat{P}|\hat\zeta|\hat{z}]^{1/2}$ in the regimes $(k_p/k)\hat{P} \ll |\hat\zeta|/\hat{z} \ll (k_p/k)\alpha_4^4/\hat{P}$ and $(k/k_p)^3/\hat{P} \ll |\hat\zeta|/\hat{z}$ and $N_e = [2(k_p/k)\hat{P}|\hat\zeta|\hat{z}]^{1/2}$ in the regime $(k_p/2k)\alpha_4^4/\hat{P} \ll |\hat\zeta|/\hat{z} \ll 8(k/k_p)^3/\hat{P}$. Note that the self-modulational instability dominates RFS in the above regimes (assuming $\alpha_4 k_p/k < 1/2$), except when $(k/k_p)^3/\hat{P} \ll |\hat\zeta|/\hat{z}$; however, here growth is significant only in the tail of a long pulse, i.e., $|k_p\zeta| \gg [2(k_p/k)^2 P/P_c]^{-1}$.

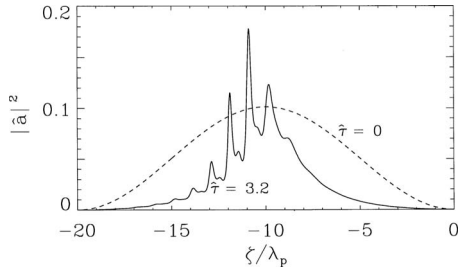

FIG. 36. Normalized laser intensity $|a|^2$ vs ζ/λ_p at $c\tau = 0$ (dashed curve) and $c\tau = 3.2Z_R$ (solid curve) for the parameters $\lambda_p = r_0/2 = 30$ μm. Laser is moving to the right. From Sprangle *et al.*, 1994.

To illustrate the behavior of the coupled self-modulation and laser-hose instabilities, Eqs. (107) and (108) are solved numerically (Sprangle *et al.*, 1994). Consider an initially uniform plasma with a 16 TW, 1 ps laser pulse with wavelength $\lambda = 1$ μm and initial spot size $r_0 = 60$ μm ($Z_R = 1.1$ cm) in a plasma of density $n_0 = 1.2 \times 10^{18}$ cm^{-3} ($\lambda_p = 30$ μm). For these parameters, $P(\zeta) = P_c$ at the center of the pulse. Initially, $\hat{x}_s = \hat{y}_s = 1$ and the centroid has a 1% random perturbation such that $|\partial \ln x_c/\partial\zeta| \ll 1/\lambda_0$.

As the laser propagates, the high-intensity center of the pulse remains guided ($\hat{x}_s \simeq 1$). However, the front and back portions of the pulse, with $P < P_c$, diffract, and the coupled hose and modulation instabilities grow within the guided portion of the pulse as illustrated in Figs. 36 and 37. Figure 36 shows the normalized laser intensity on axis $|\hat{a}|^2 = 16P(\zeta)/P_c\hat{x}_s\hat{y}_s k_p^2 r_0^2$ at $\hat{\tau} = 0$ and at $\hat{\tau} = 3.2$. Figure 37 plots $\hat{x}_s(\zeta)$ and $\hat{x}_c(\zeta)$ at $\hat{\tau} = 3.2$ and shows a significant level of hosing, with $|\hat{x}_c|$ as large as 0.5. In addition to the modulation of the envelope at λ_p, the second harmonic at $\lambda_p/2$ is present, indicating the coupling between the hose and self-modulation instabilities. The spatial modulation of the laser envelope at $\lambda_p/2$ is due to the dependence of the driving terms on the centroid motion. The second harmonic is not observed when the initial centroid perturbation is sufficiently small, 0.1% for the above parameters.

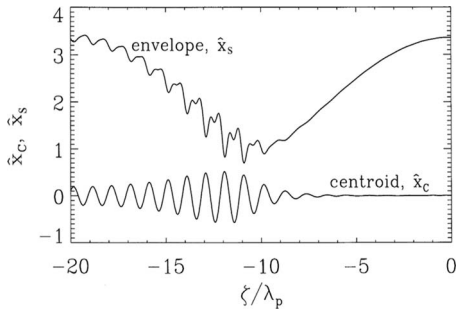

FIG. 37. Laser envelope x_s (upper curve) and centroid x_c (lower curve) vs ζ/λ_p at $c\tau=3.2Z_R$ for an initial perturbation of 1% in x_c. Perturbations grow at $\lambda_p=r_0/2=30$ μm. From Sprangle *et al.*, 1994.

The presence of the laser-hose instability can strongly modify the structure of the wakefield generated by the laser pulse. To illustrate this point, consider an initial centroid perturbation of 10% (Sprangle *et al.*, 1994). Here the centroid motion dominates both the development of the wakefield and the evolution of the envelope. The spot size modulations are dominated by the second harmonic component. Figure 38 shows the transverse profiles of both the longitudinal and transverse wakefields, at $\hat{\tau}=1.8$, near the back of the pulse. The transverse field E_x is nearly symmetric and peaked on axis while the longitudinal field E_z is nearly antisymmetric and vanishes on axis. This wakefield symmetry is opposite to that which occurs without hosing, i.e., in the absence of the hose instability, E_x is antisymmetric and vanishes on axis, while E_z is symmetric and peaked on axis.

Although the modulation instability can enhance the wakefield amplitude and acceleration in the LWFA, the laser-hose instability should generally be avoided. To avoid significant levels of hosing, the initial laser centroid must be sufficiently smooth. Equations (109)–(111) indicate that the growth of the hose instability can be reduced by decreasing the pulse length ($k_p|\zeta|$), the laser power (P/P_c), or the interaction distance (z/Z_R). Further simulations (Sprangle *et al.*, 1994) indicate that by appropriately varying (i.e., detuning) either the plasma density and/or the depth of the preformed plasma channel as a function of ζ in the laboratory frame, the laser-

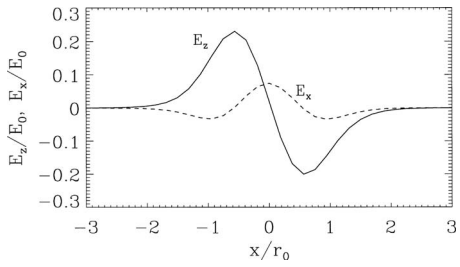

FIG. 38. Transverse profiles of the axial wakefield E_z/E_0 (solid curve) and the transverse wakefield E_x/E_0 (dashed curve) at $c\tau=1.8Z_R$ and $\zeta=-18\lambda_p$ for a hose-dominated case. From Sprangle *et al.*, 1994.

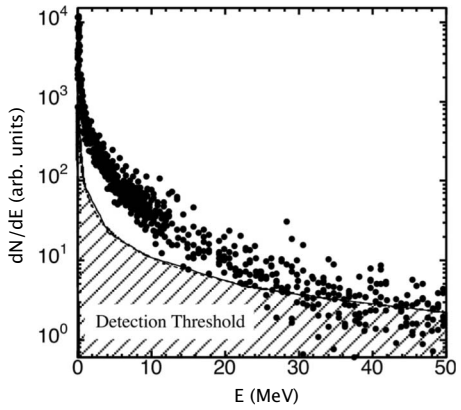

FIG. 39. Electron energy spectrum dN/dE measured using a magnetic spectrometer obtained by scanning the current in the magnet and measuring the intensity on a phosphor screen. Each data point represents ten shots. The spectrum is well approximated by a Boltzmann distribution with an effective temperature of 4.6 MeV. From Leemans *et al.*, 2004.

hose and self-modulation instability can be substantially reduced.

VII. HIGH-QUALITY BUNCH PRODUCTION

As described in the previous sections, a decade worth (1994–2004) of experiments by many groups demonstrated that, by focusing intense laser pulses onto a neutral gas, relativistic electron bunches can be produced. Typically, prior to 2004, the accelerated electron energy spectrum was characterized by an exponential or Boltzmann-like distribution, with the majority of electrons at modest energies (a few MeV). The total accelerated charge was large (up to several nC), but the number of electrons at high energy (tens of MeV) was an exponentially small fraction of the total charge. Figure 39 shows an example of a typical exponential energy spectrum (Leemans *et al.*, 2004). Although the bunches had large energy spread, they were typically well collimated with divergences <10 mrad (Leemans *et al.*, 2004). Furthermore, the normalized transverse emittance was measured and shown to be a few μm rad at 55 MeV (Fritzler *et al.*, 2004). Over the years, the properties of these bunches improved. For example, higher laser pulse energies led to more charge and higher observed maximum electron energies (up to a few hundred MeV) (Mangles *et al.*, 2005). Conversely, electron bunches were produced with "smaller" lasers, capable of operating at higher repetition rate (Malka *et al.*, 2002). Laser pulse shape effects were studied (Leemans *et al.*, 2002; Schroeder, Esarey, Geddes, *et al.*, 2003), and applications were explored such as radio-isotope production (Leemans *et al.*, 2001; Santala *et al.*, 2001; Ledingham *et al.*, 2003), terahertz radiation generation (Leemans *et al.*, 2003; Schroeder *et al.*, 2004; van Tilborg *et al.*, 2006, 2007), x-ray generation (Leemans *et al.*, 2000, 2005; Catravas *et al.*, 2001; Esarey *et al.*, 2002; Rousse *et al.*, 2004), and ultrafast chemistry (employing the ultrafast nature of the electron bunches) (Brozek-Pluskab *et al.*,

2005). Although steady progress was made, the broad electron beam energy distribution remained a major limitation.

A. High-quality bunches at the 100 MeV level

In 2004 a major milestone was achieved with the production and measurement of high-quality electron bunches. Three different groups [located at the Rutherford Appleton Laboratory (RAL) in the United Kingdom, Lawrence Berkeley National Laboratory (LBNL) in the United States, and the Laboratoire d'Optique Appliquée (LOA) in France] announced measurement of electron bunches with narrow energy spread containing a significant amount of charge in a bunch with a small divergence (Faure *et al.*, 2004; Geddes *et al.*, 2004; Mangles *et al.*, 2004). In the case of the LBNL experiments (Geddes *et al.*, 2004), this was accompanied by the achievement of another major milestone: the guiding of relativistically intense ($>10^{18}$ W/cm^2) laser pulses within preformed plasma channels (Geddes *et al.*, 2005a) and the self-trapping and acceleration of electrons within these channels (Geddes *et al.*, 2005b). Guiding of high-intensity laser pulses in plasma channels is necessary in order to extend the acceleration length and the energy gain up to the multi-GeV range with reasonable size laser systems that can operate at high repetition rates. Following 2004, several additional research groups (Hidding *et al.*, 2006; Hosokai *et al.*, 2006; Maksimchuk *et al.*, 2008; Osterhoff *et al.*, 2008) have reported monoenergetic beam production.

To obtain the monoenergetic bunches, the RAL and LOA groups used relatively large laser spot sizes. This effectively increases the diffraction (or Rayleigh range Z_R) of the laser pulse, thereby permitting propagation over distances on the order of the gas jet length. The RAL collaboration used a 0.5 J, 40 fs laser pulse focused (25 μm spot diameter, 2.5×10^{18} W/cm^2) on a plume of a 2 mm long gas jet with a plasma density of 2×10^{19} cm^{-3}. A narrow energy spread bunch was observed at 78 MeV with 3% FWHM energy spread, 22 pC of charge, and a divergence $<5°$ FWHM (Mangles *et al.*, 2004).

The LOA experiments used a 1 J, 33 fs laser pulse focused (21 μm FWHM diameter spot, 3.2×10^{18} W/cm^2) on a 3 mm gas jet with a plasma density of 6×10^{18} cm^{-3}. A narrow energy spread bunch was observed at 170 MeV bunch with a 24% energy spread, divergence of 10 mrad FWHM, and 500 pC of charge (Faure *et al.*, 2004). Plasma density scans indicated that there were optimal laser-plasma coupling parameters for production of high-charge monoenergetic electron beams, as predicted in the bubble regime and in agreement with 3D PIC simulations (Faure *et al.*, 2004; Malka *et al.*, 2005).

The LBNL experiments used a 9 TW, 55 fs laser pulse focused to a relatively tight spot size (8.5 μm FWHM, 10^{19} W/cm^2). To mitigate the short Z_R of the laser pulse, a preformed plasma channel (created using additional laser pulses, with an on-axis density of 2×10^{19} cm^{-3}) was used to guide the laser pulse through the 2 mm gas jet. With the preformed channels and laser input powers at the 8–10 TW level, electron bunches with narrow energy spread were observed (Geddes *et al.*, 2004). At 9 TW, using the 55° fine resolution magnetic spectrometer, bunches containing 2×10^9 electrons at 86 MeV with a 3.6 MeV FWHM energy spread were observed with a divergence near 3 mrad (see Fig. 40). Bunches containing 10^9 electrons at energies between 135 and 170 MeV were observed using the 5° port of the magnetic spectrometer. The normalized transverse emittance, estimated from assuming that the bunch comes from a source approximately the size of the laser spot, is $(1–2)\pi$ mm mrad, comparable to conventional radio-frequency sources.

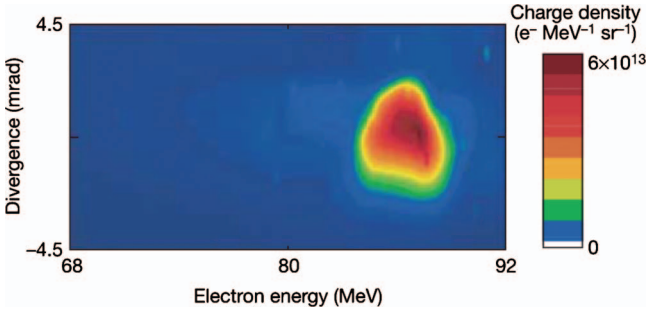

FIG. 40. (Color) Electron energy spectrum of a bunch produced by the channel-guided LWFA. The single-shot spectrum was obtained by dispersing the electron beam with a magnetic spectrometer and a charge-coupled device (CCD) imaged phosphor screen. Beam contains 2×10^9 electrons with energy spread of 3.6 MeV FWHM at 86 MeV. In the vertical (nondispersive) plane, the divergence was near 3 mrad FWHM for this bunch. From Geddes *et al.*, 2004.

Based on experiment, simulation, and theory, the production of monoenergetic bunches in an LPA requires the following four steps. Step 1 consists of exciting a wakefield. For a self-modulated LWFA, this typically occurs after the laser has propagated a sufficiently long distance within the plasma, such that the self-modulation instability (i.e., the feedback of the wake on the pulse and the self-consistent evolution of both the wake and the pulse) excites a large amplitude wakefield. Eventually, the laser pulse self-steepening and self-shortening can lead to a wake in the blow-out regime. Step 2 consists of a method for trapping and the initial injection of electrons into the wake. For a self-modulated LWFA, this can be the result of wake amplitudes approaching the wave breaking limit (i.e., sufficiently large plasma wave amplitude for self-trapping of background electrons). Step 3 consists of termination of the self-trapping or injection process. If trapping is not terminated, low energy electrons would continuously be injected into the wake over the entire length of acceleration, resulting in a large energy spread. One mechanism to accomplish this is by beam loading, i.e., the injected electron bunch is of sufficient charge so as to reduce the amplitude of the wake below the self-trapping threshold.

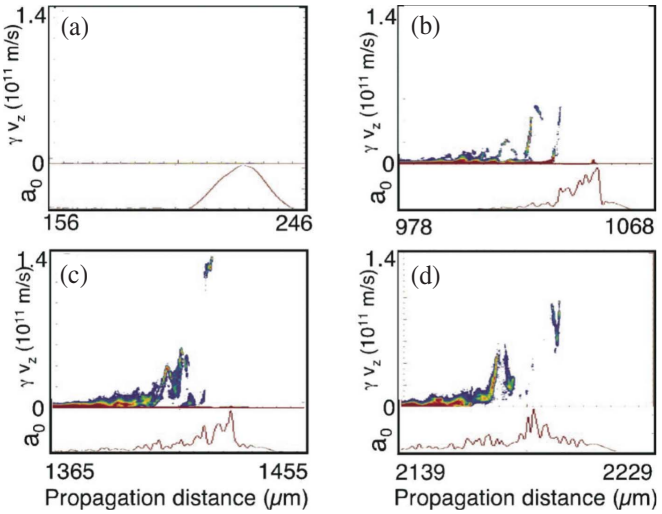

FIG. 41. (Color online) PIC simulation showing momentum phase space (top of each panel) and laser envelope (bottom of each panel) as a function of propagation distance. (a) The laser enters the plasma and (b) is modulated by the plasma response, exciting a wake and trapping electrons. Beam loading terminates trapping. (c) The trapped electrons are concentrated in energy at the dephasing length, forming a high-energy low-energy spread bunch, which (d) dissipates with further propagation. From Geddes *et al.*, 2005b.

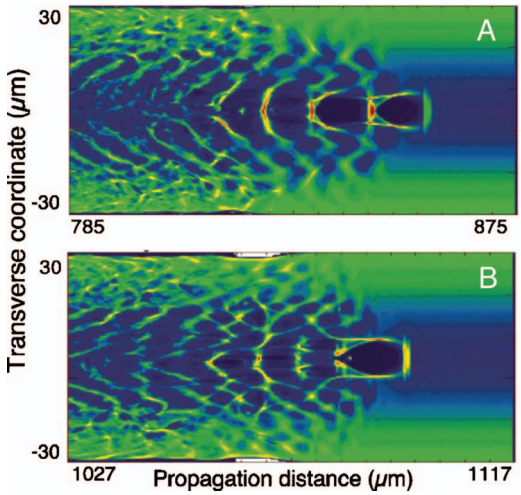

FIG. 42. (Color) PIC simulation of electron density after laser propagation of (a) 875 μm and (b) 1117 μm. (a) The density perturbation just prior to self-trapping in the first bucket behind the laser. (b) A trapped electron bunch is damping the wake and suppressing further trapping, isolating the initial bunch in phase space. From Geddes *et al.*, 2005b.

Step 4 is acceleration of the electron bunch over a distance equal to the dephasing length. If acceleration occurs over distances longer than the dephasing length, the trapped bunch will continue to circulate around the separatrix, losing energy and increasing its energy spread. Optimum acceleration would occur over a distance equal to the dephasing length, such that the trapped bunch exits the plasma near the top of the separatrix (i.e., the accelerating phase-space bucket), with maximum energy and minimum energy spread.

Simulations, using the PIC code VORPAL (Nieter and Cary, 2004), were performed in parameter regimes relevant to the LBNL experiments (Geddes *et al.*, 2004). The simulated laser envelope and particle phase space as a function of propagation distance are shown in Fig. 41, and the wake density is shown in Fig. 42. In these simulations (Geddes *et al.*, 2005b), it is observed that in the first few hundred microns of propagation of the laser pulse in the channel, the wake amplitudes (and hence the amount of trapped particles) are small. As the laser pulse envelope starts distorting through the self-modulation instability, developing features that have rise times on the order of or shorter than the plasma period, a highly nonlinear bubblelike plasma wake is excited that self-traps and accelerates particles. Once enough charge is accumulated in the accelerating bucket, the injection process is terminated due to beam loading, i.e., the field of the accelerated bunch modifies the wakefield and reduces its amplitude to below the trapping threshold. Pump depletion of the laser pulse energy (lost to wake excitation) also reduces the wake amplitude. If the trapped electrons propagate beyond a dephasing distance, the electrons lose energy, which leads to a broad energy distribution.

B. High-quality bunches at the 1 GeV level

In 2006, high-quality electron bunches at the 1 GeV level were demonstrated in channel-guided LWFA experiments at LBNL (Leemans, Nagler, *et al.*, 2006; Nakamura *et al.*, 2007). In these experiments, the energy gain was extended to the GeV range using higher laser powers (e.g., 40 TW), using longer plasma channels (e.g., 3.3 cm), and using lower plasma densities (e.g., 10^{18} cm^{-3}) so as to extend the dephasing length. Previous LBNL experiments at the 100 MeV level created plasma channels in a gas jet with a laser ionization and heating technique (Volfbeyn *et al.*, 1999; Geddes *et al.*, 2004, 2005b). Due to laser heating being inefficient at low densities, suitable plasma channels could only be produced in gas jets at densities $>10^{19}$ cm^{-3}, limiting the dephasing length and restricting electron energies to about 100 MeV.

To overcome the limitations of gas jets, a gas-filled capillary discharge waveguide (Spence and Hooker, 2000; Butler *et al.*, 2002) was used to produce centimeter scale lower density plasma channels. The experiments used a 10 Hz repetition rate Ti:sapphire laser system ($\lambda=810$ nm) delivering down to 40 fs FWHM pulses with up to 40 TW peak power. These pulses were focused by a 2 m focal length off-axis parabola ($f/25$) to $r_s=25$ μm at the capillary entrance (an input intensity $\sim 10^{18}$ W/cm^2). The capillaries (Spence and Hooker, 2000) were laser machined into 33 mm long sapphire blocks with diameters ranging from 190 to 310 μm. Hydrogen gas, introduced through two holes near the capillary ends, was ionized by striking a discharge between

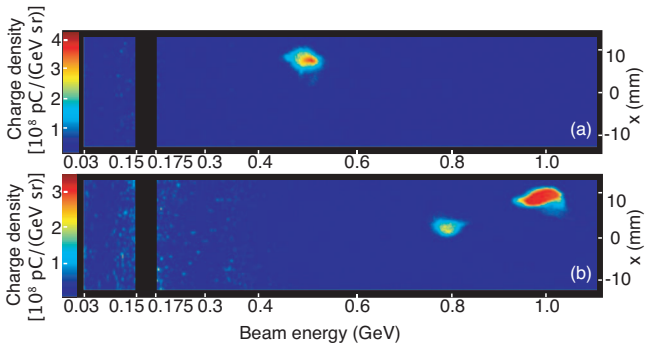

FIG. 43. (Color) Single-shot electron bunch spectra of the capillary-guided LWFA (Leemans, Nagler, *et al.*, 2006; Nakamura *et al.*, 2007). Examples are shown of bunches at (a) $0.50^{+0.02}_{-0.015}$ GeV (5.6% rms energy spread, 2.0 mrad divergence rms, ~50 pC charge) and (b) $1.0^{+0.08}_{-0.05}$ GeV (2.5% rms energy spread, 1.6 mrad divergence rms, ~30 pC). The 0.5 GeV (1.0 GeV) bunch was obtained in a 225 (310) μm capillary with a density of 3.5×10^{18} (4.3×10^{18}) cm^{-3} and input laser power of 12 TW (40 TW). The black stripe denotes the energy range not measured by the spectrometer. In (b) a second bunch at 0.8 GeV is also visible.

electrodes at the capillary ends, producing an approximately parabolic plasma channel. Accelerator performance was optimized by adjusting the initial gas density and the delay between onset of the discharge current and arrival of the laser pulse (from 1.0×10^{18} to 4.0×10^{18} cm^{-3} in an ~100 ns timing window). Electron bunch energy was measured by a 1.2 T single-shot magnetic spectrometer that deflected the electrons onto a 1.2 m long phosphor screen, covering energies from 0.03 up to 1.1 GeV.

Figure 43 shows energy spectra of electron bunches produced at (a) 0.5 GeV with ~50 pC charge and at (b) 1.0 GeV with ~30 pC charge, obtained using 12 TW (73 fs input) and 40 TW (38 fs input) laser pulses, respectively. In both cases the electron bunches had percent-level energy spread and an rms divergence of 1.2–2.0 mrad.

Bunches at ~0.5 GeV were obtained using a 225 μm diameter capillary for a density of $(3.2–3.8)\times10^{18}$ cm^{-3} and for laser power ranging from 12 TW (73 fs) to 18 TW (40 fs). The performance for the 225 μm diameter capillary-guided accelerator was found to be reproducible for delays of 80–110 ns and 12 TW laser peak power, with every laser shot resulting in an electron bunch at 0.48 GeV ±6% and an rms spread <5%. Fluctuations in electron bunch energy were directly correlated with those in laser power. For lower power (<12 TW), no electron bunches were observed suggesting that the wake amplitude was below the self-trapping threshold.

The GeV electron bunch was obtained in a 310 μm diameter channel capillary for $P=40$ TW and a density of 4.3×10^{18} cm^{-3}. In this larger diameter channel, transverse wakefields are reduced but the guiding properties are less ideal, as it requires a larger matched spot size than was injected. For lower laser power (<38 TW), no electron bunches were observed. For higher laser powers, the spectrum always showed structure with significant shot-to-shot fluctuations due in part to the self-trapping mechanism being sensitive to small variations in the laser and plasma parameters (Nakamura *et al.*, 2007).

PIC simulations in two and three dimensions confirm that the injection and acceleration mechanism is similar to that which occurs in the gas jet experiments at the 100 MeV level. The initial profile of the laser pulse injected into the channel produces a wake with an amplitude that is too low to produce self-trapping. Over the first few millimeters of propagation, the plasma wake feedbacks on the laser pulse, leading to self-modulation and self-steepening, which further increases the wake amplitude. A blow-out or cavitated wake is eventually produced of sufficient amplitude so as to allow self-trapping. Trapping continues until there is sufficient trapped charge to beam load the wake, reducing its amplitude and terminating the self-trapping process. Over the next ~1 cm of propagation, the bunch accelerates as the laser energy depletes. Laser depletion occurs after approximately a dephasing length, resulting in the production of narrow energy spread electron bunch with an energy near 1 GeV.

Using a similar experimental setup as described above, experiments (Karsch *et al.*, 2007) at the Max-Planck-Institut für Quantenoptik have demonstrated quasimonoenergetic electron beams as high as 500 MeV by focusing a 750 mJ, 42 fs laser pulse into a gas-filled capillary discharge waveguide (plasma density of 10^{18}–10^{19} cm^{-3}). Additional experiments with capillary discharge waveguides suggest that in certain operating regimes electron self-trapping may be assisted by laser ionization of atoms or ions within the capillary (Rowlands-Rees *et al.*, 2008).

C. High-quality bunches from colliding pulse injection

In addition to stable electron bunches generated at the 0.5 GeV level via self-trapping in the channel-guided LWFA experiments described in the previous section, stable electron bunches at the 100 MeV level were also generated in 2006 by colliding pulse injection within a gas jet in experiments at LOA (Faure, Rechatin, *et al.*, 2006). These experiments used a two pulse, collinear, counterpropagating geometry, in which injection results from the beat wave produced when the backward pulse overlaps the forward drive pulse that generates the wakefield (Fubiani *et al.*, 2004; Kotaki *et al.*, 2004). Specifically, two 30 fs laser pulses with linear polarization were focussed at the edge of a 2 mm supersonic helium gas jet. The pump pulse was focused to an intensity of $I_0=3.4\times10^{18}$ W/cm^2 (720 mJ, 20 μm FWHM spot, $a_0=1.3$) and the injection pulse intensity was $I_1=4.3\times10^{17}$ W/cm^2 (250 mJ, 31 μm FWHM spot, $a_1=0.4$). The electron bunch was passed through an electron spectrometer, which measured the electron bunch angu-

lar distribution, energy distribution, and charge.

For plasma densities at or below 7.5×10^{18} cm^{-3}, the nonlinear evolution of the pump laser pulse through self-focusing and self-steepening was not strong enough to cause significant injection of electrons into the wake-field. However, at a density of 7.5×10^{18} cm^{-3}, the addition of the injection pulse produced a monoenergetic electron bunch. The electron bunches obtained in this manner were stable: A series of 20 consecutive shots was carried out to estimate the statistical fluctuations of the bunch, giving a peak energy of 117±7 MeV, a FWHM energy spread of (11±2)%, a charge of 19±6.8 pC, a divergence of 5.8±2 mrad, and a pointing stability of 0±1.8 mrad (here the ± signifies the standard deviation about the mean). By varying the delay between the two pulses, the collision point, and hence the acceleration length, within the gas jet was varied. This allowed the electron bunch energy to be tuned from 50 (with 25% energy spread) to 250 MeV (with 5% energy spread). Furthermore, when the polarizations of the two laser pulses were orthogonal, no electron bunch was produced, which suggests that the injection mechanism depends on parallel polarization and the production of a beat wave.

Stable high-quality electron beam generation was also achieved by colliding a drive pulse with a counterpropagating pulse at 135° (Kotaki *et al.*, 2008). In this experiment a 0.2 J, 70 fs drive laser interacts with a 10 mJ, 70 fs injection laser (propagating at an angle of 135° with respect to the drive laser) in a 3.95×10^{19} cm^{-3} plasma to produce 14±0.7 MeV electron beams containing 22±3.8 pC of charge and (11±1.5)% of energy spread.

D. High-quality bunches from density transitions

Stable electron bunches at the 1 MeV level have been demonstrated experimentally at LBNL by focusing a 10 TW, 47 fs laser (2×10^{19} W/cm^2, 7.5 μm FWHM spot) on the downstream edge of a 750 μm wide gas jet of density 2.2×10^{19} cm^{-3} (Geddes *et al.*, 2008). The mechanism for self-trapping of electrons from the background plasma is the presence of a negative plasma density gradient (Bulanov *et al.* 1998), as discussed in Sec. IV.D. At the downstream edge of the gas jet, a decreasing plasma density causes λ_p to increase with propagation. Plasma wave fronts then fall further behind the laser as it propagates, decreasing the wake phase velocity to the point where background plasma electrons become trapped.

Using this method, stable (over hundreds of shots) electron bunches were produced with low absolute momentum spread. Electron bunches were generated with order 0.5 nC charge (15% charge stability), 0.76 MeV/c mean momenta with 20 keV/c rms momentum stability, 170 keV/c FWHM longitudinal momentum spread, 20 keV/c transverse momentum spread, and 2 mrad (2 keV/c) rms pointing stability. Examples of the momentum distribution of the bunch as obtained from a magnetic spectrometer are shown in Fig. 44. Furthermore, measurements of coherent terahertz emission imply a bunch duration on the order of 100 fs.

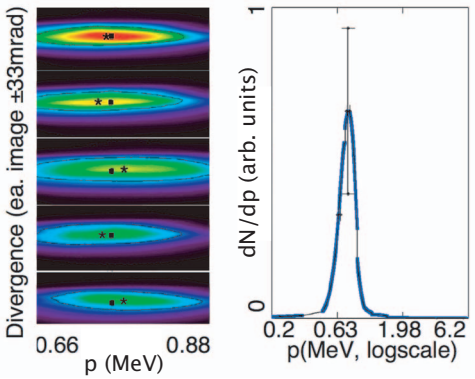

FIG. 44. (Color) Momentum distributions obtained from a magnetic spectrometer for electron bunches produced by a laser focused at the downstream edge of a gas jet, showing stable bunches at 0.76 MeV/c with ±10% momentum spread and ±3% momentum stability. Sequential single shot images are shown on the left with the centroid (*) indicated with respect to the average (square) over 45 shots. Integrated magnetic spectrum is shown on the right (vertical bar denotes the rms charge error) with the data points (blue) connected by a black line. From Geddes *et al.*, 2008.

One possible application of such a source would be as an electron injector into a second stage (dark current free) of an LWFA for acceleration to high energy. Simulations predict that postacceleration of a highly quality bunch can nearly preserve the absolute momentum spread and emittance (Tomassini *et al.*, 2003). Hence, postacceleration of bunches produced by density transitions could potentially lead to the generation of electron bunches at GeV (or greater) energies with 100 keV/c level momentum spread.

VIII. CONCLUSIONS

Perhaps the three most fundamental physics issues concerning LPAs are (i) can an ultrahigh accelerating field be generated, (ii) can this accelerating field be sustained over a sufficiently long propagation distance so as to provide a substantial single-stage electron energy gain, and (iii) can an ultrashort electron bunch be injected and accelerated while maintaining high bunch quality? Theory and simulation indicate that these requirements can be met. Experimental progress is proceeding at a rapid pace, and the generation of ultrahigh accelerating fields, the guiding of high-intensity laser pulses over many diffraction (Rayleigh) lengths, and the production of high-quality relativistic electron bunches have been demonstrated. Much of the experimental success can be attributed to the development of chirped-pulse amplification (Strickland and Mourou, 1985; Maine *et al.*, 1988; Mourou and Umstadter, 1992; Perry and Mourou, 1994), which has revolutionized laser technology by providing compact sources of 1–100 TW, 10–100 fs laser pulses. Numerous accelerator applica-

tions will benefit from high-average power sources of intense laser pulses, which require further technological advances.

The problem of generating a large amplitude plasma wave by an intense laser pulse, for the most part, is well understood. Theoretically, wakefield generation can be examined by assuming a nonevolving drive laser pulse and by calculating the plasma response to the ponderomotive force. This ponderomotive force can be associated with the envelope of a single laser pulse (e.g., a standard LWFA in the linear regime or a bubble wake in the highly nonlinear regime), a laser pulse train, envelope variations in an unstable laser pulse (e.g., self-modulated LWFA), or the beat wave produced by two copropagating laser pulses of different frequencies (e.g., PBWA). Wakefield generation is optimized when the laser envelope spatial gradients are on the order of the plasma wavelength λ_p. Analytical solutions or simple numerical models exist in the 3D linear regime ($a_0^2 \ll 1$) and in the 1D nonlinear ($a^2 \gtrsim 1$) regime. In the 3D nonlinear regime, wakefield generation can be examined with a variety of fluid and particle codes. Unresolved theoretical issues pertaining to wakefield generation include the detailed study of wave breaking in three dimensions, dynamics of the highly nonlinear blow-out regime, wakefield excitation and evolution in nonuniform plasmas, and electron self-trapping.

Laser pulse propagation in underdense plasma is affected by a variety of phenomena, including relativistic self-focusing, ponderomotive self-channeling, preformed density channels, plasma wave generation, pump depletion, and laser-plasma instabilities, as discussed in Secs. V and VI. In terms of fundamental limits to the energy gain in a single-stage LWFA, the most severe is typically diffraction, i.e., the Rayleigh length is usually much shorter than the dephasing length and pump depletion length. Hence, some form of optical guiding is required. Relativistic self-guiding, which occurs when $P \geq P_c \simeq 17\lambda_p^2/\lambda^2$ GW, strongly affects the body of a long ($L > \lambda_p$) laser pulse. The leading portion of the pulse ($\lesssim \lambda_p$), however, will diffractively erode due to the self-consistent response of the plasma density to the laser field. The self-focusing of a laser pulse can be enhanced by the ponderomotive blowout of the plasma electrons from the axis, i.e., electron cavitation. In addition, the body of long relativistically guided pulse is subject to instabilities (Raman scattering, self-modulation, and laser hosing). Preformed plasma density channels are effective in the guiding of short ($L < \lambda_p$) laser pulses when $\Delta n \geq \Delta n_c = 1/\pi r_e r_0^2$. For long pulses ($L > \lambda_p$), relativistic effects can reduce this criterion, i.e., $\Delta n/\Delta n_c \geq 1 - P/P_c$. In addition, if the pulse is sufficiently short ($L \lesssim \lambda_p$), the detrimental effects of various instabilities may be reduced, owing to the reduced growth of the unstable mode within the pulse.

Once diffraction is overcome and the laser pulse is guided by, for example, a plasma density channel, the propagation distance will be limited by a variety of nonlinear phenomena. For example, a laser pulse on the order of, or longer than, a plasma wavelength will undergo self-modulation, generally defined as the pulse evolution resulting from the feedback of the plasma wave (wakefield) on the laser pulse. For a long laser pulses, $L \gg \lambda_p$, self-modulation can lead to an unstable axial modulation of the pulse profile at λ_p, with the associated excitation of a large wakefield that can grow to the point of wave breaking, resulting in electron self-trapping and acceleration. For shorter pulses, $L \sim \lambda_p$, self-modulation can still play a dramatic role via pulse shortening and self-steepening. For example, as a pulse with $L \sim \lambda_p$ enters a plasma, the initial intensity profile may only drive a mildly nonlinear wake, but as this wake feed backs on the laser pulse, the intensity profile shortens and steepens, which can result in a highly nonlinear wake and the self-trapping of electrons. Hence, self-shortening and self-steeping can play an important role in the transition of a mildly nonlinear wake to a highly nonlinear blow-out regime. Furthermore, the physics of self-modulation is intrinsically coupled to that of pump depletion since as the laser pulse excites the plasma wave, it loses energy. Analytic studies of laser pulse evolution, for the most part, are limited to the linear regime in which, for example, analytic expressions for instability growth rates are readily obtained. The self-consistent problem of plasma wave generation by an evolving drive laser pulse is typically of sufficient complexity as to require numerical simulation. Self-consistent simulations of LPAs have been performed in the 2D and 3D nonlinear regimes using both fluid and PIC codes.

To generate a high-quality electron bunch, it is highly desirable that a bunch be injected with a length short compared to λ_p. Due to the shortness of λ_p ($\lesssim 100$ μm), this is not yet achievable using conventional photoinjectors, in which the production of femtosecond bunches is problematic. Alternatively, several novel laser-based methods for injecting electrons into a plasma wave have been proposed and studied. This includes self-trapping of background plasma electrons, which can occur as the plasma wave amplitude approaches the wave breaking amplitude for both long laser pulses, such as in the self-modulated regime, or for short laser pulses, as in the blow-out regime. In a plasma channel, curvature of the plasma wave fronts becomes more severe with distance behind the laser pulse and can lead to wave breaking. A density down ramp causes the phase velocity of the plasma wave to decrease, which can lead to self-trapping at a sufficiently far distance behind the pump laser pulse. Instead of relying on self-trapping, one or more additional ultrashort (short compared to λ_p) laser pulses can be used to inject electrons directly into the wakefield. This can be done using either the ponderomotive force of the injection pulse or the slow beat wave generated by two counterpropagating laser pulses. These laser injection methods show great promise since the injection process can be controlled in detail by adjusting the timing of the injection pulses with respect to the plasma wave phase, as well as by adjusting the injection pulse amplitude and duration. Once injected, it is important that the electron bunch be accelerated while

maintaining high quality, for example, maintaining a small energy spread and emittance. This may require controlling the transverse focusing forces of the wakefield by, for example, tailoring the transverse plasma density profile and/or the transverse laser intensity profile.

Experimentally, many groups have measured ultrahigh accelerating fields and accelerated electrons. Large accelerating fields (>200 GV/m) have been measured directly from optical probing techniques or inferred from the measurement of accelerated electrons. Large amounts of self-trapped electrons (up to several nanocoulambs) have been accelerated in the self-modulated LWFA regime, with maximum electron energies up to a few hundred MeV. Prior to 2004, however, the electron energy spectrum in the self-modulated regime was typically characterized by an exponential distribution with the majority of the electrons at low energy ($\sim$MeV) and a long tail extending out to high energies, e.g., >300 MeV when using PW-level Nd:glass laser system and a 2 mm diameter gas jet (Mangles *et al.*, 2005). Such an exponential energy distribution of accelerated electrons is typical of this first-generation of "brute force" experiments, in which a single high power (greater than few terawatts) laser pulse interacts with a gas jet plume of a couple of millimeter diameter and of relatively high density ($\sim 10^{19}$ cm^{-3}).

Two important experimental milestones toward the development of LPAs were achieved in 2004, guiding of relativistically intense ($a_0^2 \gtrsim 1$) laser pulses over many diffraction lengths (Geddes *et al.*, 2004) and the production of high-quality electron bunches at relativistic energies (~ 100 MeV), with high charge (up to 0.5 nC), low-energy spread (few percent), and small divergence (few milliradians) (Faure *et al.*, 2004; Geddes *et al.*, 2004; Mangles *et al.*, 2004). These results were obtained by a careful choice of laser and plasma parameters and/or a tailoring of the plasma density profile. In these experiments the electrons were self-trapped by the 10–100 TW laser pulse from the background plasma using millimeter-scale gas jet sources. High-quality bunches were obtained by controlling the acceleration length so that it was equal to the dephasing length. Matching of the acceleration length and the dephasing length was accomplished either by using a preformed plasma channel (Geddes *et al.*, 2004) or by using higher power laser pulses with larger laser spot sizes (which increases the propagation length) (Faure *et al.*, 2004; Mangles *et al.*, 2004) along with lower plasma densities (which increases the dephasing length).

In 2006, high-quality electron bunches were produced at the 1 GeV level using 100 TW class laser pulses in a centimeter-scale plasma channel. Again, the electrons were self-trapped from the background plasma (a gas-filled discharge capillary), and high-quality bunches were obtained by acceleration over a dephasing length (Leemans, Nagler, *et al.*, 2006). A capillary discharge plasma channel enabled operation at lower plasma densities and longer plasma lengths, thus allowing higher electron energies. Another important experimental milestone achieved in 2006 was demonstration of controlled injection and acceleration of electrons using the colliding pulse method (Faure, Rechatin, *et al.*, 2006). High-quality electron bunches at the 100 MeV level were generated with multi-10 TW laser pulses in a millimeter-scale gas jet using a two pulse, collinear, counterpropagating geometry. Production of stable electron bunches at the 1 MeV level using a plasma density transition has also been demonstrated (Geddes *et al.*, 2008).

Although not the focus of this review, an experimental milestone in the field of electron beam-driven plasma-based accelerators was achieved in 2007 (Blumenfeld *et al.*, 2007): the energy doubling of a fraction of electrons in a multi-10 GeV electron bunch using a meter-scale plasma. These experiments used the 50 fs, 42 GeV electron bunches from the 3 km long linear accelerator at the Stanford Linear Accelerator Center, propagating through a 85 cm plasma. In these single-bunch experiments, the front portion of the electron bunch generated a large amplitude plasma wakefield, which subsequently accelerated a fraction of electrons in the tail of the bunch to energies as high as 85 GeV. The majority of the bunch electrons lost energy, which represents the energy needed to drive the plasma wave.

Although much progress has been made, in many respects LPA experiments are still in their infancy. One important challenge is to stabilize the performance of the accelerator. Since the electron energy depends linearly on laser intensity in the linear wakefield regime [see, e.g., Eq. (56)], stable electron bunch energies to the few percent level requires control of the laser pulse energy, pulse length, and spot size at the few percent level. Novel methods for controlling laser pulse properties and pointing stability are being developed in industry for short pulse systems that may meet these requirements. Similarly, plasma densities must be controlled at the percent level to ensure that the wake amplitude ($\propto n^{1/2}$), dephasing length ($\propto n^{-3/2}$), and energy gain ($\propto 1/n$) remain constant. Novel time-resolved diagnostics need to be developed and implemented to allow, for example, measurement of the slice emittance and energy spread of femtosecond-duration electron bunches.

Perhaps the most severe fundamental limit to the single-stage energy gain in an LPA is pump depletion, i.e., energy is transferred out of the laser pulse and into the plasma wakefield as the laser propagates. In the nonlinear regime, theory and simulation indicate that the pump depletion length is on the order of the dephasing length. To extend the electron energy beyond the limits of pump depletion will require multiple stages. This requires additional challenges such as the synchronization of laser pulses with femtosecond accuracy, the alignment of plasma structures with micron accuracy, and the development of novel methods of laser coupling into subsequent stages.

One possible approach to the realization of an all-optical accelerator at the 10 GeV level is to use two stages. The first could be an injector at the 100 MeV level that utilized either self-trapping or a laser triggered

injection method such as colliding pulse. This electron bunch could then be injected into a second stage that would accelerate the bunch through a plasma channel in a mildly nonlinear wakefield regime without additional self-trapping (dark current free). Estimates based on linear wakefield theory predict a single-stage energy gain on the order of $\Delta W(\mathrm{GeV}) \simeq I_0(\mathrm{W/cm^2})/n_0(\mathrm{cm^{-3}})$. Hence, a second stage that used a few hundred femtosecond laser pulse with an intensity of 10^{18} W/cm^2 in a plasma of density 10^{17} cm^{-3} may provide a single-stage energy gain as high as 10 GeV. As can be seen from the basic scaling laws, reducing the density and lengthening the distance over which the plasma channel extends are essential to reach multi-GeV energies. Various numerical studies indicate that multi-GeV beams should be obtainable with laser powers in the range of 0.1–1 PW (Gordienko and Pukhov, 2005; Lifschitz *et al.*, 2005; Kalmykov *et al.*, 2006; Malka *et al.*, 2006; Lu *et al.*, 2007; Cormier-Michel *et al.*, 2009), where higher-energy gains can be achieved for a given laser power by the use of plasma channel guiding (Lu *et al.*, 2007; Cormier-Michel *et al.*, 2009).

The performance of LPAs, as well as essentially all applications of these accelerators, would benefit greatly from improvements in laser technology: higher peak powers, higher pulse energies, higher repetition rates, and the development of higher average power laser systems. Currently, 100 TW laser systems are limited to the 10 Hz regime (average powers on the order of 10 W). As a simple estimate of the type of laser pulses needed to drive a high-charge single-stage accelerator, consider producing a 10 GeV electron bunch containing 1 nC of charge. This represents 10 J worth of electron kinetic energy and, assuming a laser to particle beam efficiency between 1% and 10%, requires therefore 100–1000 J of laser energy per pulse. Hence, it is essential that plasma accelerator technology and laser technology be developed in parallel if the goal of all-optical accelerators is to be realized. Such an accelerator holds the promise of offering unique electron bunches, having femtosecond duration and containing hundreds of picocoulomb of charge, with an emittance that equals or surpasses conventional linacs. If the development continues to be successful, LPAs will serve as compact multi-GeV modules for high-energy physics applications, as well as drivers for novel radiation sources, including the next generation of femtosecond light sources.

ACKNOWLEDGMENTS

The authors acknowledge many contributions from past and present members of the LOASIS Program at Lawrence Berkeley National Laboratory, in particular, C. Geddes, E. Cormier-Michel, B. Shadwick, and Cs. Tóth, and many insightful conversations with the researchers in the plasma-based accelerator community. This work was supported by the Director, Office of Science, Office of High Energy Physics, of the U.S. Department of Energy under Contract No. DE-AC02-05CH11231.

REFERENCES

Akhiezer, A. I., and R. V. Polovin, 1956, Zh. Eksp. Teor. Fiz. **30**, 915 [Sov. Phys. JETP **3**, 696 (1956)].
Amiranoff, F., *et al.*, 1992, Phys. Rev. Lett. **68**, 3710.
Amiranoff, F., *et al.*, 1998, Phys. Rev. Lett. **81**, 995.
Amiranoff, F., D. Bernard, B. Cros, F. Jacquet, G. Matthieussent, P. Miné, P. Mora, J. Morillo, F. Moulin, A. E. Specka, and C. Stenz, 1995, Phys. Rev. Lett. **74**, 5220.
Andreev, N. E., L. M. Gorbunov, V. I. Kirsanov, K. Nakajima, and A. Ogata, 1997, Phys. Plasmas **4**, 1145.
Andreev, N. E., L. M. Gorbunov, V. I. Kirsanov, A. A. Pogosova, and R. R. Ramazashvili, 1992, Pis'ma Zh. Eksp. Teor. Fiz. **55**, 551.
Andreev, N. E., L. M. Gorbunov, V. I. Kirsanov, A. A. Pogosova, and R. R. Ramazashvili, 1994, Phys. Scr. **49**, 101.
Andreev, N. E., V. I. Kirsanov, and L. M. Gorbunov, 1995, Phys. Plasmas **2**, 2573.
Antonsen, T. M., Jr., and P. Mora, 1992, Phys. Rev. Lett. **69**, 2204.
Antonsen, T. M., Jr., and P. Mora, 1993, Phys. Fluids B **5**, 1440.
Antonsen, T. M., Jr., and P. Mora, 1995, Phys. Rev. Lett. **74**, 4440.
Berezhiani, V. I., and I. G. Murusidze, 1990, Phys. Lett. A **148**, 338.
Berezhiani, V. I., and I. G. Murusidze, 1992, Phys. Scr. **45**, 87.
Bernard, D., F. Amiranoff, W. P. Leemans, E. Esarey, and C. Joshi, 1999, Nucl. Instrum. Methods Phys. Res. A **432**, 227.
Bertrand, P., A. Ghizzo, S. J. Karttunen, T. J. H. Pattikangas, R. R. E. Salomaa, and M. Shoucri, 1995, Phys. Plasmas **2**, 3115.
Bian, Z., and T. M. Antonsen, Jr., 2001, Phys. Plasmas **8**, 3183.
Birdsall, C. K., A. B. Langdon, V. Vehedi, and J. P. Verboncoeur, 1991, *Plasma Physics via Computer Simulations* (Hilger, Bristol).
Blumenfeld, I., *et al.*, 2007, Nature (London) **445**, 741.
Bonnaud, G., D. Teychenné, and J. Bobin, 1994, Phys. Rev. E **50**, R36.
Borghesi, M., A. J. MacKinnon, L. Barringer, R. Gaillard, L. A. Gizzi, C. Meyer, O. Willi, A. Pukhov, and J. Meyer-ter-Vehn, 1997, Phys. Rev. Lett. **78**, 879.
Borisov, A. B., A. V. Borovskiy, V. V. Korobkin, A. M. Prokhorov, O. B. Shiryaev, X. M. Shi, T. S. Luk, A. McPherson, J. C. Solem, K. Boyer, and C. K. Rhodes, 1992, Phys. Rev. Lett. **68**, 2309.
Brantov, A. V., T. Z. Esirkepov, M. Kando, H. Kotaki, V. Y. Bychenkov, and S. V. Bulanov, 2008, Phys. Plasmas **15**, 073111.
Brozek-Pluskab, B., D. Gliger, A. Halloua, V. Malka, and Y. A. Gauduel, 2005, Radiat. Phys. Chem. **72**, 149.
Bulanov, S., N. Naumova, F. Pegoraro, and J. Sakai, 1998, Phys. Rev. E **58**, R5257.
Bulanov, S. V., I. N. Inovenkov, V. I. Kirsanov, N. M. Naumova, and A. S. Sakharov, 1992, Phys. Fluids B **4**, 1935.
Bulanov, S. V., V. I. Kirsanov, and A. S. Sakharov, 1989, JETP Lett. **50**, 198.
Bulanov, S. V., F. Pegoraro, and A. M. Pukhov, 1995, Phys. Rev. Lett. **74**, 710.
Bulanov, S. V., F. Pegoraro, A. M. Pukhov, and A. S. Sakharov, 1997, Phys. Rev. Lett. **78**, 4205.

Butler, A., D. J. Spence, and S. M. Hooker, 2002, Phys. Rev. Lett. **89**, 185003.
Catravas, P., E. Esarey, and W. P. Leemans, 2001, Meas. Sci. Technol. **12**, 1828.
Chen, W., T. Chien, C. Lee, J. Lin, J. Wang, and S. Chen, 2004, Phys. Rev. Lett. **92**, 075003.
Chen, X. L., and R. N. Sudan, 1993, Phys. Fluids B **5**, 1336.
Chien, T., C. Chang, C. Lee, J. Lin, J. Wang, and S. Chen, 2005, Phys. Rev. Lett. **94**, 115003.
Chiou, T. C., T. Katsouleas, C. Decker, W. B. Mori, G. Shvets, and J. S. Wurtele, 1995, Phys. Plasmas **2**, 310.
Chiron, A., G. Bonnaud, A. Dulieu, J. L. Miquel, G. Malka, M. Louis-Jacquet, and G. Mainfray, 1996, Phys. Plasmas **3**, 1373.
Clayton, C. E., C. Joshi, C. Darrow, and D. Umstadter, 1985, Phys. Rev. Lett. **54**, 2343.
Clayton, C. E., K. A. Marsh, A. Dyson, M. Everett, A. Lal, W. P. Leemans, R. Williams, and C. Joshi, 1993, Phys. Rev. Lett. **70**, 37.
Clayton, C. E., K. Tzeng, D. Gordon, P. Muggli, W. B. Mori, C. Joshi, V. Malka, Z. Najmudin, A. Modena, D. Neely, and A. E. Dangor, 1998, Phys. Rev. Lett. **81**, 100.
Coffey, T. P., 1971, Phys. Fluids **14**, 1402.
Cormier-Michel, E., C. G. R. Geddes, E. Esarey, C. B. Schroeder, D. L. Bruhwiler, K. Paul, B. Cowan, and W. P. Leemans, 2009, in *Advanced Accelerator Concepts: Thirteenth Workshop*, edited by C. B. Schroeder, W. Leemans, and E. Esarey (AIP, New York), Vol. 1089, pp. 315–320.
Coverdale, C. A., C. B. Darrow, C. D. Decker, W. B. Mori, K. Tzeng, K. A. Marsh, C. E. Clayton, and C. Joshi, 1995, Phys. Rev. Lett. **74**, 4659.
Dalla, S., and M. Lontano, 1994, Phys. Rev. E **49**, R1819.
Darrow, C., C. Coverdale, M. Perry, W. Mori, C. Clayton, K. Marsh, and C. Joshi, 1992, Phys. Rev. Lett. **69**, 442.
Dawson, J. M., 1959, Phys. Rev. **113**, 383.
Dawson, J. M., 1983, Rev. Mod. Phys. **55**, 403.
Decker, C. D., and W. B. Mori, 1994, Phys. Rev. Lett. **72**, 490.
Decker, C. D., W. B. Mori, and T. Katsouleas, 1994, Phys. Rev. E **50**, R3338.
Decker, C. D., W. B. Mori, T. Katsouleas, and D. E. Hinkel, 1996, Phys. Plasmas **3**, 1360.
Decker, C. D., W. B. Mori, K. Tzeng, and T. Katsouleas, 1996, Phys. Plasmas **3**, 2047.
Deutsch, M., B. Meerson, and J. E. Golub, 1991, Phys. Fluids B **3**, 1773.
Dewa, H., *et al.*, 1998, Nucl. Instrum. Methods Phys. Res. A **410**, 357.
Dorchies, F., J. R. Marquès, B. Cros, G. Matthieussent, C. Courtois, T. Vélikoroussov, P. Audebert, J. P. Geindre, S. Rebibo, G. Hamoniaux, and F. Amiranoff, 1999, Phys. Rev. Lett. **82**, 4655.
Durfee, C. G., III, J. Lynch, and H. M. Milchberg, 1995, Phys. Rev. E **51**, 2368.
Durfee, C. G., III, and H. M. Milchberg, 1993, Phys. Rev. Lett. **71**, 2409.
Ehrlich, Y., C. Cohen, D. Kaganovich, A. Zigler, R. F. Hubbard, P. Sprangle, and E. Esarey, 1998, J. Opt. Soc. Am. B **15**, 2416.
Ehrlich, Y., C. Cohen, A. Zigler, J. Krall, P. Sprangle, and E. Esarey, 1996, Phys. Rev. Lett. **77**, 4186.
Esarey, E., B. Hafizi, R. Hubbard, and A. Ting, 1998, Phys. Rev. Lett. **80**, 5552.
Esarey, E., R. F. Hubbard, W. P. Leemans, A. Ting, and P. Sprangle, 1997, Phys. Rev. Lett. **79**, 2682.
Esarey, E., J. Krall, and P. Sprangle, 1994, Phys. Rev. Lett. **72**, 2887.
Esarey, E., and W. P. Leemans, 1999, Phys. Rev. E **59**, 1082.
Esarey, E., and M. Pilloff, 1995, Phys. Plasmas **2**, 1432.
Esarey, E., C. B. Schroeder, E. Cormier-Michel, B. A. Shadwick, C. G. R. Geddes, and W. P. Leemans, 2007, Phys. Plasmas **14**, 056707.
Esarey, E., C. B. Schroeder, W. P. Leemans, and B. Hafizi, 1999, Phys. Plasmas **6**, 2262.
Esarey, E., C. B. Schroeder, B. A. Shadwick, J. S. Wurtele, and W. P. Leemans, 2000, Phys. Rev. Lett. **84**, 3081.
Esarey, E., B. A. Shadwick, P. Catravas, and W. P. Leemans, 2002, Phys. Rev. E **65**, 056505.
Esarey, E., B. A. Shadwick, C. B. Schroeder, and W. P. Leemans, 2004, in *Proceedings of the Advanced Accelerator Concepts Workshop*, edited by V. Yakimenko (AIP, New York), Vol. 737, pp. 578–584.
Esarey, E., and P. Sprangle, 1992, Phys. Rev. A **45**, 5872.
Esarey, E., P. Sprangle, and J. Krall, 1995, Phys. Rev. E **52**, 5443.
Esarey, E., P. Sprangle, J. Krall, and A. Ting, 1996, IEEE Trans. Plasma Sci. **24**, 252.
Esarey, E., P. Sprangle, J. Krall, and A. Ting, 1997, IEEE J. Quantum Electron. **33**, 1879.
Esarey, E., P. Sprangle, J. Krall, A. Ting, and G. Joyce, 1993, Phys. Fluids B **5**, 2690.
Esarey, E., and A. Ting, 1990, Phys. Rev. Lett. **65**, 1961.
Esarey, E., A. Ting, and P. Sprangle, 1988, Appl. Phys. Lett. **53**, 1266.
Esarey, E., A. Ting, and P. Sprangle, 1990, Phys. Rev. A **42**, 3526.
Esarey, E., A. Ting, P. Sprangle, and G. Joyce, 1989, Comments Plasma Phys. Controlled Fusion **12**, 191.
Esarey, E., A. Ting, P. Sprangle, D. Umstadter, and X. Liu, 1993, IEEE Trans. Plasma Sci. **21**, 95.
Everett, M., A. Lal, D. Gordon, C. E. Clayton, K. A. Marsh, and C. Joshi, 1994, Nature (London) **368**, 527.
Everett, M. J., A. Lal, C. E. Clayton, W. B. Mori, T. W. Johnston, and C. Joshi, 1995, Phys. Rev. Lett. **74**, 2236.
Everett, M. J., A. Lal, D. Gordon, K. Wharton, C. E. Clayton, W. B. Mori, and C. Joshi, 1995, Phys. Rev. Lett. **74**, 1355.
Faure, J., Y. Glinec, G. Gallot, and V. Malka, 2006, Phys. Plasmas **13**, 056706.
Faure, J., Y. Glinec, A. Pukhov, S. Kiselev, S. Gordienko, E. Lefebvre, J.-P. Rousseau, F. Burgy, and V. Malka, 2004, Nature (London) **431**, 541.
Faure, J., C. Rechatin, A. Norlin, A. Lifschitz, Y. Glinec, and V. Malka, 2006, Nature (London) **444**, 737.
Filip, C. V., R. Narang, S. Tochitsky, C. E. Clayton, P. Musumeci, R. B. Yoder, K. A. Marsh, J. B. Rosenzweig, C. Pellegrini, and C. Joshi, 2004, Phys. Rev. E **69**, 026404.
Fisher, D. L., and T. Tajima, 1996, Phys. Rev. E **53**, 1844.
Fisher, D. L., T. Tajima, M. C. Downer, and C. W. Siders, 1995, Phys. Rev. E **51**, 4860.
Fritzler, S., E. Lefebvre, V. Malka, F. Burgy, A. E. Dangor, K. Krushelnick, S. P. D. Mangles, Z. Najmudin, J.-P. Rousseau, and B. Walton, 2004, Phys. Rev. Lett. **92**, 165006.
Fubiani, G., E. Esarey, C. B. Schroeder, and W. P. Leemans, 2004, Phys. Rev. E **70**, 016402.
Fubiani, G., E. Esarey, C. B. Schroeder, and W. P. Leemans, 2006, Phys. Rev. E **73**, 026402.
Gahn, C., G. D. Tsakiris, A. Pukhov, J. Meyer-ter-Vehn, G.

Pretzler, P. Thirolf, D. Habs, and K. J. Witte, 1999, Phys. Rev. Lett. **83**, 4772.
Gaul, E. W., S. P. Le Blanc, A. R. Rundquist, R. Zgadzaj, H. Langhoff, and M. C. Downer, 2000, Appl. Phys. Lett. **77**, 4112.
Geddes, C. G. R., K. Nakamura, G. R. Plateau, C. Toth, E. Cormier-Michel, E. Esarey, C. B. Schroeder, J. R. Cary, and W. P. Leemans, 2008, Phys. Rev. Lett. **100**, 215004.
Geddes, C. G. R., C. Toth, J. van Tilborg, E. Esarey, C. B. Schroeder, D. Bruhwiler, C. Nieter, J. Cary, and W. P. Leemans, 2004, Nature (London) **431**, 538.
Geddes, C. G. R., C. Tóth, J. van Tilborg, E. Esarey, C. B. Schroeder, D. Bruhwiler, C. Nieter, J. Cary, and W. P. Leemans, 2005, Phys. Plasmas **12**, 056709.
Geddes, C. G. R., C. Toth, J. van Tilborg, E. Esarey, C. B. Schroeder, J. Cary, and W. P. Leemans, 2005, Phys. Rev. Lett. **95**, 145002.
Gibbon, P., and A. R. Bell, 1988, Phys. Rev. Lett. **61**, 1599.
Gonsalves, A. J., T. P. Rowlands-Rees, B. H. P. Broks, J. J. A. M. van der Mullen, and S. M. Hooker, 2007, Phys. Rev. Lett. **98**, 025002.
Gorbunov, L., P. Mora, and T. M. Antonsen, Jr., 1996, Phys. Rev. Lett. **76**, 2495.
Gorbunov, L. M., and V. I. Kirsanov, 1987, Sov. Phys. JETP **66**, 290.
Gorbunov, L. M., P. Mora, and T. M. Antonsen, Jr., 1997, Phys. Plasmas **4**, 4358.
Gordienko, S., and A. Pukhov, 2005, Phys. Plasmas **12**, 043109.
Gordon, D., *et al.*, 1998, Phys. Rev. Lett. **80**, 2133.
Gordon, D. F., B. Hafizi, P. Sprangle, R. F. Hubbard, J. R. Peñano, and W. B. Mori, 2001, Phys. Rev. E **64**, 046404.
Hafizi, B., E. Esarey, and P. Sprangle, 1997, Phys. Rev. E **55**, 3539.
Hafizi, B., A. Ting, P. Sprangle, and R. F. Hubbard, 2000, Phys. Rev. E **62**, 4120.
Hamster, H., A. Sullivan, S. Gordon, W. White, and R. W. Falcone, 1993, Phys. Rev. Lett. **71**, 2725.
Hemker, R. G., K.-C. Tzeng, W. B. Mori, C. E. Clayton, and T. Katsouleas, 1998, Phys. Rev. E **57**, 5920.
Hidding, B., *et al.*, 2006, Phys. Rev. Lett. **96**, 105004.
Hogan, M. J., *et al.*, 2000, Phys. Plasmas **7**, 2241.
Hogan, M. J., *et al.*, 2005, Phys. Rev. Lett. **95**, 054802.
Hooker, S. M., D. J. Spence, and R. A. Smith, 2000, J. Opt. Soc. Am. B **17**, 90.
Horton, W., and T. Tajima, 1986, Phys. Rev. A **34**, 4110.
Hosokai, T., M. Kando, H. Dewa, H. Kotaki, S. Kondo, N. Hasegawa, K. Nakajima, and K. Horioka, 2000, Opt. Lett. **25**, 10.
Hosokai, T., K. Kinoshita, A. Zhidkov, A. Maekawa, A. Yamazaki, and M. Uesaka, 2006, Phys. Rev. Lett. **97**, 075004.
Hosokai, T., K. Kinoshita, A. Zhidkov, K. Nakamura, T. Watanabe, T. Ueda, H. Kotaki, M. Kando, K. Nakajima, and M. Uesaka, 2003, Phys. Rev. E **67**, 036407.
Hosokai, T., *et al.*, 2006, Phys. Rev. E **73**, 036407.
Huang, Y. C., and R. L. Byer, 1996, Appl. Phys. Lett. **69**, 2175.
Irman, A., M. J. H. Luttikhof, A. G. Khachatryan, F. A. van Goor, J. W. J. Verschuur, H. M. J. Bastiaens, and K.-J. Boller, 2007, J. Appl. Phys. **102**, 024513.
Johnson, D. K., *et al.*, 2006, Phys. Rev. Lett. **97**, 175003.
Johnson, L. C., and T. K. Chu, 1974, Phys. Rev. Lett. **32**, 517.
Joshi, C., C. E. Clayton, and F. F. Chen, 1982, Phys. Rev. Lett. **48**, 874.
Joshi, C., W. B. Mori, T. Katsouleas, J. M. Dawson, J. M. Kindel, and D. W. Forslund, 1984, Nature (London) **311**, 525.
Joshi, C., T. Tajima, J. M. Dawson, H. A. Baldis, and N. A. Ebrahim, 1981, Phys. Rev. Lett. **47**, 1285.
Kalmykov, S. Y., L. M. Gorbunov, P. Mora, and G. Shvets, 2006, Phys. Plasmas **13**, 113102.
Karmakar, A., and A. Pukhov, 2007, Laser Part. Beams **25**, 371.
Karsch, S., *et al.*, 2007, New J. Phys. **9**, 415.
Katsouleas, T., 1986, Phys. Rev. A **33**, 2056.
Katsouleas, T., and J. M. Dawson, 1983, Phys. Rev. Lett. **51**, 392.
Katsouleas, T., and W. B. Mori, 1988, Phys. Rev. Lett. **61**, 90.
Katsouleas, T., S. Wilks, P. Chen, J. M. Dawson, and J. J. Su, 1987, Part. Accel. **22**, 81.
Keinigs, R., and M. E. Jones, 1987, Phys. Fluids **30**, 252.
Kim, J. U., N. Hafz, and H. Suk, 2004, Phys. Rev. E **69**, 026409.
Kimura, W. D., G. H. Kim, R. D. Romea, L. C. Steinhauer, I. V. Pogorelsky, K. P. Kusche, R. C. Fernow, X. Wang, and Y. Liu, 1995, Phys. Rev. Lett. **74**, 546.
Kimura, W. D., *et al.*, 2001, Phys. Rev. Lett. **86**, 4041.
Kimura, W. D., *et al.*, 2004, Phys. Rev. Lett. **92**, 054801.
Kimura, W. D., *et al.*, 2005, IEEE Trans. Plasma Sci. **33**, 3.
Kitagawa, Y., T. Matsumoto, T. Minamihata, K. Sawai, K. Matsuo, K. Mima, K. Nishihara, H. Azechi, K. A. Tanaka, H. Takabe, and S. Nakai, 1992, Phys. Rev. Lett. **68**, 48.
Kitagawa, Y., Y. Sentoku, S. Akamatsu, W. Sakamoto, R. Kodama, K. A. Tanaka, K. Azumi, T. Norimatsu, T. Matsuoka, H. Fujita, and H. Yoshida, 2004, Phys. Rev. Lett. **92**, 205002.
Kostyukov, I., S. Kiselev, and A. Pukhov, 2003, Phys. Plasmas **10**, 4818.
Kostyukov, I., A. Pukhov, and S. Kiselev, 2004, Phys. Plasmas **11**, 5256.
Kotaki, H., M. Kando, T. Oketa, S. Masuda, J. K. Koga, S. Kondo, S. Kanazawa, T. Yokoyama, T. Matoba, and K. Nakajima, 2002, Phys. Plasmas **9**, 1392.
Kotaki, H., S. Masuda, M. Kando, J. K. Koga, and K. Nakajima, 2004, Phys. Plasmas **11**, 3296.
Kotaki, H., *et al.*, 2008, IEEE Trans. Plasma Sci. **36**, 1760.
Krall, J., E. Esarey, P. Sprangle, and G. Joyce, 1994, Phys. Plasmas **1**, 1738.
Krall, J., A. Ting, E. Esarey, and P. Sprangle, 1993, Phys. Rev. E **48**, 2157.
Kruer, W. L., 1988, *The Physics of Laser Plasma Interactions* (Addison-Wesley, Redwood City).
Krushelnick, K., C. I. Moore, A. Ting, and H. R. Burris, 1998, Phys. Rev. E **58**, 4030.
Krushelnick, K., A. Ting, C. I. Moore, H. R. Burris, E. Esarey, P. Sprangle, and M. Baine, 1997, Phys. Rev. Lett. **78**, 4047.
Kumarappan, V., K. Y. Kim, and H. M. Milchberg, 2005, Phys. Rev. Lett. **94**, 205004.
Kurki-Suonio, T., P. J. Morrison, and T. Tajima, 1989, Phys. Rev. A **40**, 3230.
Lawson, J. D., 1979, IEEE Trans. Nucl. Sci. **NS-26**, 4217.
Le Blanc, S. P., M. C. Downer, R. Wagner, S. Y. Chen, A. Maksimchuk, G. Mourou, and D. Umstadter, 1996, Phys. Rev. Lett. **77**, 5381.
Ledingham, K., P. McKenna, and R. P. Singhal, 2003, Science **300**, 1107.
Leemans, W., S. Chattopadhyay, E. Esarey, A. Zholents, M. Zolotorev, A. Chin, R. Schoenlein, and C. Shank, 2000, C. R. Acad. Sci., Ser IV: Phys., Astrophys. **1**, 279.
Leemans, W., E. Esarey, C. Geddes, C. Schroeder, and C.

Toth, 2006, Philos. Trans. R. Soc. London, Ser. A **364**, 585.
Leemans, W. P., P. Catravas, E. Esarey, C. G. R. Geddes, C. Toth, R. Trines, C. B. Schroeder, B. A. Shadwick, J. van Tilborg, and J. Faure, 2002, Phys. Rev. Lett. **89**, 174802.
Leemans, W. P., C. E. Clayton, K. A. Marsh, and C. Joshi, 1991, Phys. Rev. Lett. **67**, 1434.
Leemans, W. P., C. E. Clayton, W. B. Mori, K. A. Marsh, A. Dyson, and C. Joshi, 1992a, Phys. Rev. Lett. **68**, 321.
Leemans, W. P., C. E. Clayton, W. B. Mori, K. A. Marsh, P. K. Kaw, A. Dyson, C. Joshi, and J. M. Wallace, 1992b, Phys. Rev. A **46**, 1091.
Leemans, W. P., E. Esarey, J. van Tilborg, P. A. Michel, C. B. Schroeder, C. Toth, C. G. R. Geddes, and B. A. Shadwick, 2005, IEEE Trans. Plasma Sci. **33**, 8.
Leemans, W. P., B. Nagler, A. J. Gonsalves, C. Tóth, K. Nakamura, C. G. R. Geddes, E. Esarey, C. B. Schroeder, and S. M. Hooker, 2006, Nat. Phys. **2**, 696.
Leemans, W. P., D. Rodgers, P. E. Catravas, C. G. R. Geddes, G. Fubiani, E. Esarey, B. A. Shadwick, R. Donahue, and A. Smith, 2001, Phys. Plasmas **8**, 2510.
Leemans, W. P., C. W. Siders, E. Esarey, N. E. Andreev, G. Shvets, and W. B. Mori, 1996, IEEE Trans. Plasma Sci. **24**, 331.
Leemans, W. P., J. van Tilborg, J. Faure, C. G. R. Geddes, C. Tóth, C. B. Schroeder, E. Esarey, and G. Fubiani, 2004, Phys. Plasmas **11**, 2899.
Leemans, W. P., P. Volfbeyn, K. Z. Guo, S. Chattopadhyay, C. B. Schroeder, B. A. Shadwick, P. B. Lee, J. S. Wurtele, and E. Esarey, 1998, Phys. Plasmas **5**, 1615.
Leemans, W. P., *et al.*, 2003, Phys. Rev. Lett. **91**, 074802.
Lifschitz, A. F., J. Faure, V. Malka, and P. Mora, 2005, Phys. Plasmas **12**, 093104.
Lindberg, R. R., A. E. Charman, J. S. Wurtele, and L. Friedland, 2004, Phys. Rev. Lett. **93**, 055001.
Lindberg, R. R., A. E. Charman, J. S. Wurtele, L. Friedland, and B. A. Shadwick, 2006, Phys. Plasmas **13**, 123103.
Litvak, A. G., 1969, Zh. Eksp. Teor. Fiz. **57**, 629.
Liu, Y., X. J. Wang, D. B. Cline, M. Babzien, J. M. Fang, J. Gallardo, K. Kusche, I. Pogorelsky, J. Skaritka, and A. van Steenbergen, 1998, Phys. Rev. Lett. **80**, 4418.
Lu, W., C. Huang, M. M. Zhou, W. B. Mori, and T. Katsouleas, 2005, Phys. Plasmas **12**, 063101.
Lu, W., C. Huang, M. Zhou, W. B. Mori, and T. Katsouleas, 2006, Phys. Rev. Lett. **96**, 165002.
Lu, W., C. Huang, M. Zhou, M. Tzoufras, F. S. Tsung, W. B. Mori, and T. Katsouleas, 2006, Phys. Plasmas **13**, 056709.
Lu, W., M. Tzoufras, C. Joshi, F. S. Tsung, W. B. Mori, J. Vieira, R. A. Fonseca, and L. O. Silva, 2007, Phys. Rev. ST Accel. Beams **10**, 061301.
Luther, B. M., Y. Wang, M. C. Marconi, J. L. A. Chilla, M. A. Larotonda, and J. J. Rocca, 2004, Phys. Rev. Lett. **92**, 235002.
Maine, P., D. Strickland, P. Bado, M. Pessot, and G. Mourou, 1988, IEEE J. Quantum Electron. **QE-24**, 398.
Maksimchuk, A., *et al.*, 2008, Phys. Plasmas **15**, 056703.
Malka, G., E. Lefebvre, and J. L. Miquel, 1997, Phys. Rev. Lett. **78**, 3314.
Malka, V., J. Faure, Y. Glinec, A. Pukhov, and J. Rousseau, 2005, Phys. Plasmas **12**, 056702.
Malka, V., J. Faure, J. R. Marquès, F. Amiranoff, J. P. Rousseau, S. Ranc, J. P. Chambaret, Z. Najmudin, B. Walton, P. Mora, and A. Solodov, 2001, Phys. Plasmas **8**, 2605.
Malka, V., A. Lifschitz, J. Faure, and Y. Glinec, 2006, Phys. Rev. ST Accel. Beams **9**, 091301.
Malka, V., *et al.*, 2002, Science **298**, 1596.
Mangles, S. P. D., *et al.*, 2004, Nature (London) **431**, 535.
Mangles, S. P. D., *et al.*, 2005, Phys. Rev. Lett. **94**, 245001.
Mangles, S. P. D., *et al.*, 2006, Plasma Phys. Controlled Fusion **48**, B83.
Marquès, J. R., J. P. Geindre, F. Amiranoff, P. Audebert, J. C. Gauthier, A. Antonetti, and G. Grillon, 1996, Phys. Rev. Lett. **76**, 3566.
Matlis, N. H., S. Reed, S. S. Bulanov, V. Chvykov, G. Kalintchenko, T. Matsuoka, P. Rousseau, V. Yanovsky, A. Maksimchuk, S. Kalmykov, G. Shvets, and M. C. Downer, 2006, Nat. Phys. **2**, 749.
Max, C., J. Arons, and A. B. Langdon, 1974, Phys. Rev. Lett. **33**, 209.
McKinstrie, C. J., and R. Bingham, 1992, Phys. Fluids B **4**, 2626.
McKinstrie, C. J., and D. W. Forslund, 1987, Phys. Fluids **30**, 904.
Michel, P., E. Esarey, C. B. Schroeder, B. A. Shadwick, and W. P. Leemans, 2006, Phys. Plasmas **13**, 113112.
Michel, P., C. B. Schroeder, B. A. Shadwick, E. Esarey, and W. P. Leemans, 2006, Phys. Rev. E **74**, 026501.
Milchberg, H. M., T. R. Clark, C. G. Durfee III, and T. M. Antonsen, Jr., 1996, Phys. Plasmas **3**, 2149.
Modena, A., Z. Najmudin, A. E. Dangor, C. E. Clayton, K. A. Marsh, C. Joshi, V. Malka, C. B. Darrow, C. Danson, D. Neely, and F. N. Walsh, 1995, Nature (London) **377**, 606.
Monot, P., T. Auguste, P. Gibbon, F. Jakober, G. Mainfray, A. Dulieu, M. Louis-Jacquet, G. Malka, and J. L. Miquel, 1995, Phys. Rev. Lett. **74**, 2953.
Moore, C. I., A. Ting, K. Krushelnick, E. Esarey, R. F. Hubbard, B. Hafizi, H. R. Burris, C. Manka, and P. Sprangle, 1997, Phys. Rev. Lett. **79**, 3909.
Moore, C. I., A. Ting, S. J. McNaught, J. Qiu, H. R. Burris, and P. Sprangle, 1999, Phys. Rev. Lett. **82**, 1688.
Mora, P., 1992, Phys. Fluids B **4**, 1630.
Mora, P., and T. M. Antonsen, Jr., 1996, Phys. Rev. E **53**, R2068.
Mora, P., and T. M. Antonsen, Jr., 1997, Phys. Plasmas **4**, 217.
Mori, W. B., 1997, IEEE J. Quantum Electron. **33**, 1942.
Mori, W. B., C. D. Decker, D. E. Hinkel, and T. Katsouleas, 1994, Phys. Rev. Lett. **72**, 1482.
Mori, W. B., C. Joshi, J. M. Dawson, D. W. Forslund, and J. M. Kindel, 1988, Phys. Rev. Lett. **60**, 1298.
Mori, W. B., and T. Katsouleas, 1992, Phys. Rev. Lett. **69**, 3495.
Mourou, G., and D. Umstadter, 1992, Phys. Fluids B **4**, 2315.
Murphy, C. D., *et al.*, 2006, Phys. Plasmas **13**, 033108.
Musumeci, P., *et al.*, 2005, Phys. Rev. Lett. **94**, 154801.
Nakajima, K., 1992, Phys. Rev. A **45**, 1149.
Nakajima, K., *et al.*, 1995, Phys. Rev. Lett. **74**, 4428.
Nakamura, K., G. Fubiani, C. G. R. Geddes, P. Michel, J. van Tilborg, C. Tóth, E. Esarey, C. B. Schroeder, and W. P. Leemans, 2004, in *Proceedings of the Advanced Accelerator Concepts Workshop*, edited by V. Yakimenko (AIP, New York), Vol. 737, pp. 901–906.
Nakamura, K., B. Nagler, C. Tóth, C. G. R. Geddes, C. B. Schroeder, E. Esarey, W. P. Leemans, A. J. Gonsalves, and S. M. Hooker, 2007, Phys. Plasmas **14**, 056708.
Nieter, C., and J. Cary, 2004, J. Comput. Phys. **196**, 448.
Osterhoff, J., *et al.*, 2008, Phys. Rev. Lett. **101**, 085002.
Palmer, R. B., 1980, Part. Accel. **11**, 81.
Pang, J., Y. K. Ho, X. Q. Yuan, N. Cao, Q. Kong, P. X. Wang, L. Shao, E. H. Esarey, and A. M. Sessler, 2002, Phys. Rev. E

66, 066501.
Panofsky, W. K. H., and W. A. Wenzel, 1956, Rev. Sci. Instrum. **27**, 967.
Perry, M. D., and G. Mourou, 1994, Science **264**, 917.
Plettner, T., R. L. Byer, E. Colby, B. Cowan, C. M. S. Sears, J. E. Spencer, and R. H. Siemann, 2005, Phys. Rev. Lett. **95**, 134801.
Popov, K. I., V. Y. Bychenkov, W. Rozmus, and R. D. Sydora, 2008, Phys. Plasmas **15**, 013108.
Pukhov, A., and J. Meyer-ter-Vehn, 1996, Phys. Rev. Lett. **76**, 3975.
Pukhov, A., and J. Meyer-ter-Vehn, 2002, Appl. Phys. B: Lasers Opt. **74**, 355.
Pukhov, A., Z.-M. Sheng, and J. Meyer-ter-Vehn, 1999, Phys. Plasmas **6**, 2847.
Quesnel, B., and P. Mora, 1998, Phys. Rev. E **58**, 3719.
Rankin, R., C. E. Capjack, N. H. Burnett, and P. B. Corkum, 1991, Opt. Lett. **16**, 835.
Rechatin, C., J. Faure, A. Lifschitz, V. Malka, and E. Lefebvre, 2007, Phys. Plasmas **14**, 060702.
Reitsma, A. J. W., W. P. Leemans, E. Esarey, C. B. Schroeder, L. P. J. Kamp, and T. J. Schep, 2002, Phys. Rev. ST Accel. Beams **5**, 051301.
Ren, C., R. G. Hemker, R. A. Fonseca, B. J. Duda, and W. B. Mori, 2000, Phys. Rev. Lett. **85**, 2124.
Rosenbluth, M. N., and C. S. Liu, 1972, Phys. Rev. Lett. **29**, 701.
Rosenzweig, J. B., 1988, Phys. Rev. A **38**, 3634.
Rosenzweig, J. B., B. Breizman, T. Katsouleas, and J. J. Su, 1991, Phys. Rev. A **44**, R6189.
Rousse, A., K. Phuoc, R. Shah, A. Pukhov, E. Lefebvre, V. Malka, S. Kiselev, F. Burgy, J. Rousseau, D. Umstadter, and D. Hulin, 2004, Phys. Rev. Lett. **93**, 135005.
Rousseaux, C., G. Malka, J. L. Miquel, F. Amiranoff, S. D. Baton, and P. Mounaix, 1995, Phys. Rev. Lett. **74**, 4655.
Rowlands-Rees, T. P., *et al.*, 2008, Phys. Rev. Lett. **100**, 105005.
Ruhl, H., 2000, *Collective Super-Intense Laser-Plasma Interactions* (Technische Universität Darmstadt, Darmstadt).
Sakharov, A. S., and V. I. Kirsanov, 1994, Phys. Rev. E **49**, 3274.
Santala, M. I. K., Z. Najmudin, E. L. Clark, M. Tatarakis, K. Krushelnick, A. E. Dangor, V. Malka, J. Faure, R. Allott, and R. J. Clarke, 2001, Phys. Rev. Lett. **86**, 1227.
Santala, M. I. K., *et al.*, 2001, Appl. Phys. Lett. **78**, 19.
Schroeder, C. B., E. Esarey, C. G. R. Geddes, C. Tóth, B. A. Shadwick, J. van Tilborg, J. Faure, and W. P. Leemans, 2003, Phys. Plasmas **10**, 2039.
Schroeder, C. B., E. Esarey, and B. A. Shadwick, 2005, Phys. Rev. E **72**, 055401.
Schroeder, C. B., E. Esarey, B. A. Shadwick, and W. P. Leemans, 2003, Phys. Plasmas **10**, 285.
Schroeder, C. B., E. Esarey, B. A. Shadwick, and W. P. Leemans, 2006, Phys. Plasmas **13**, 033103.
Schroeder, C. B., E. Esarey, J. van Tilborg, and W. P. Leemans, 2004, Phys. Rev. E **69**, 016501.
Schroeder, C. B., P. B. Lee, J. S. Wurtele, E. Esarey, and W. P. Leemans, 1999, Phys. Rev. E **59**, 6037.
Schroeder, C. B., W. Leemans, and E. Esarey, 2009, Eds., *Proceedings of the Advanced Accelerator Concepts Workshop* (AIP, New York), Vol. 1086.
Schroeder, C. B., J. S. Wurtele, and D. H. Whittum, 1999, Phys. Rev. Lett. **82**, 1177.
Shadwick, B. A., C. B. Schroeder, and E. Esarey, 2009, Phys. Plasmas **16**, 056704.
Shadwick, B. A., G. M. Tarkenton, and E. H. Esarey, 2004, Phys. Rev. Lett. **93**, 175002.
Shadwick, B. A., G. M. Tarkenton, E. H. Esarey, and W. P. Leemans, 2002, IEEE Trans. Plasma Sci. **30**, 38.
Shadwick, B. A., G. M. Tarkenton, E. H. Esarey, and C. B. Schroeder, 2005, Phys. Plasmas **12**, 056710.
Sheng, Z.-M., K. Mima, J. Zhang, and J. M. ter Vehn, 2004, Phys. Rev. E **69**, 016407.
Shvets, G., N. J. Fisch, and A. Pukhov, 2002, Phys. Plasmas **9**, 2383.
Shvets, G., N. J. Fisch, A. Pukhov, and J. Meyer-ter Vehn, 1999, Phys. Rev. E **60**, 2218.
Shvets, G., and X. Li, 1999, Phys. Plasmas **6**, 591.
Shvets, G., and J. S. Wurtele, 1994, Phys. Rev. Lett. **73**, 3540.
Shvets, G., J. S. Wurtele, T. C. Chiou, and T. C. Katsouleas, 1996, IEEE Trans. Plasma Sci. **24**, 351.
Shvets, G., J. S. Wurtele, and B. A. Shadwick, 1997, Phys. Plasmas **4**, 1872.
Siders, C. W., S. P. Le Blanc, D. Fisher, T. Tajima, M. C. Downer, A. Babine, A. Stepanov, and A. Sergeev, 1996, Phys. Rev. Lett. **76**, 3570.
Spence, D. J., and S. M. Hooker, 2000, Phys. Rev. E **63**, 015401.
Sprangle, P., and E. Esarey, 1992, Phys. Fluids B **4**, 2241.
Sprangle, P., E. Esarey, and J. Krall, 1996a, Phys. Plasmas **3**, 2183.
Sprangle, P., E. Esarey, and J. Krall, 1996b, Phys. Rev. E **54**, 4211.
Sprangle, P., E. Esarey, J. Krall, and G. Joyce, 1992, Phys. Rev. Lett. **69**, 2200.
Sprangle, P., E. Esarey, and A. Ting, 1990a, Phys. Rev. A **41**, 4463.
Sprangle, P., E. Esarey, and A. Ting, 1990b, Phys. Rev. Lett. **64**, 2011.
Sprangle, P., E. Esarey, A. Ting, and G. Joyce, 1988, Appl. Phys. Lett. **53**, 2146.
Sprangle, P., B. Hafizi, J. R. Peñano, R. F. Hubbard, A. Ting, C. I. Moore, D. F. Gordon, A. Zigler, D. Kaganovich, and T. M. Antonsen, Jr., 2001, Phys. Rev. E **63**, 056405.
Sprangle, P., J. Krall, and E. Esarey, 1994, Phys. Rev. Lett. **73**, 3544.
Sprangle, P., C. M. Tang, and E. Esarey, 1987, IEEE Trans. Plasma Sci. **PS-15**, 145.
Sprangle, P., A. Ting, and C. M. Tang, 1987, Phys. Rev. A **36**, 2773.
Sprangle, P., A. Zigler, and E. Esarey, 1991, Appl. Phys. Lett. **58**, 346.
Steinhauer, L. C., and H. G. Ahlstrom, 1971, Phys. Fluids **14**, 1109.
Strickland, D., and G. Mourou, 1985, Opt. Commun. **56**, 219.
Stupakov, G. V., and M. S. Zolotorev, 2001, Phys. Rev. Lett. **86**, 5274.
Suk, H., N. Barov, J. B. Rosenzweig, and E. Esarey, 2001, Phys. Rev. Lett. **86**, 1011.
Sun, G. Z., E. Ott, Y. C. Lee, and P. Guzdar, 1987, Phys. Fluids **30**, 526.
Tajima, T., and J. M. Dawson, 1979, Phys. Rev. Lett. **43**, 267.
Tang, C. M., P. Sprangle, and R. N. Sudan, 1985, Phys. Fluids **28**, 1974.
Ta Phuoc, K., S. Corde, R. Shah, F. Albert, R. Fitour, J.-P. Rousseau, F. Burgy, B. Mercier, and A. Rousse, 2006, Phys. Rev. Lett. **97**, 225002.

Teychenné, D., G. Bonnaud, and J. Bobin, 1993, Phys. Rev. E **48**, R3248.
Teychenné, D., G. Bonnaud, and J.-L. Bobin, 1994a, Phys. Plasmas **1**, 1771.
Teychenné, D., G. Bonnaud, and J.-L. Bobin, 1994b, Phys. Rev. E **49**, 3253.
Ting, A., E. Esarey, and P. Sprangle, 1990, Phys. Fluids B **2**, 1390.
Ting, A., D. Kaganovich, D. F. Gordon, R. F. Hubbard, and P. Sprangle, 2005, Phys. Plasmas **12**, 010701.
Ting, A., K. Krushelnick, C. I. Moore, H. R. Burris, E. Esarey, J. Krall, and P. Sprangle, 1996, Phys. Rev. Lett. **77**, 5377.
Ting, A., C. I. Moore, K. Krushelnick, C. Manka, E. Esarey, P. Sprangle, R. Hubbard, H. R. Burris, R. Fischer, and M. Baine, 1997, Phys. Plasmas **4**, 1889.
Tochitsky, S., R. Narang, C. V. Filip, P. Musumeci, C. E. Clayton, R. B. Yoder, K. A. Marsh, J. B. Rosenzweig, C. Pellegrini, and C. Joshi, 2004, Phys. Rev. Lett. **92**, 095004.
Tomassini, P., M. Galimberti, A. Giulietti, D. Giulietti, L. A. Gizzi, L. Labate, and F. Pegoraro, 2003, Phys. Rev. ST Accel. Beams **6**, 121301.
Tsung, F. S., R. Narang, W. B. Mori, C. Joshi, R. A. Fonseca, and L. O. Silva, 2004, Phys. Rev. Lett. **93**, 185002.
Tzeng, K.-C., W. B. Mori, and C. D. Decker, 1996, Phys. Rev. Lett. **76**, 3332.
Tzeng, K.-C., W. B. Mori, and T. Katsouleas, 1997, Phys. Rev. Lett. **79**, 5258.
Umstadter, D., S.-Y. Chen, A. Maksimchuk, G. Mourou, and R. Wagner, 1996, Science **273**, 472.
Umstadter, D., E. Esarey, and J. Kim, 1994, Phys. Rev. Lett. **72**, 1224.
Umstadter, D., J. Kim, E. Esarey, E. Dodd, and T. Neubert, 1995, Phys. Rev. E **51**, 3484.
Umstadter, D., J. K. Kim, and E. Dodd, 1996, Phys. Rev. Lett. **76**, 2073.
van Tilborg, J., C. B. Schroeder, C. V. Filip, C. Tóth, C. G. R. Geddes, G. Fubiani, R. Huber, R. A. Kaindl, E. Esarey, and W. P. Leemans, 2006, Phys. Rev. Lett. **96**, 014801.
van Tilborg, J., C. B. Schroeder, C. Tóth, C. G. R. Geddes, E. Esarey, and W. P. Leemans, 2007, Opt. Lett. **32**, 313.
Varin, C., and M. Piché, 2002, Appl. Phys. B: Lasers Opt. **74**, S83.
Volfbeyn, P., E. Esarey, and W. Leemans, 1999, Phys. Plasmas **6**, 2269.
Wagner, R., S.-Y. Chen, A. Maksimchuk, and D. Umstadter, 1997, Phys. Rev. Lett. **78**, 3125.
Wang, S., *et al.*, 2002, Phys. Rev. Lett. **88**, 135004.
Whittum, D. H., A. M. Sessler, and J. M. Dawson, 1990, Phys. Rev. Lett. **64**, 2511.
Wilks, S. C., J. M. Dawson, W. B. Mori, T. Katsouleas, and M. E. Jones, 1989, Phys. Rev. Lett. **62**, 2600.
Woodward, P. M., 1947, J. Inst. Electr. Eng., Part 3 **93**, 1554.
Wu, J., and T. M. Antonsen, Jr., 2003, Phys. Plasmas **10**, 2254.
York, A. G., H. M. Milchberg, J. P. Palastro, and T. M. Antonsen, 2008, Phys. Rev. Lett. **100**, 195001.
Young, P. E., M. E. Foord, J. H. Hammer, W. L. Kruer, M. Tabak, and S. C. Wilks, 1995, Phys. Rev. Lett. **75**, 1082.
Zigler, A., Y. Ehrlich, C. Cohen, J. Krall, and P. Sprangle, 1996, J. Opt. Soc. Am. B **13**, 68.